MONITORING NEUROTRANSMITTER AMINO ACIDS IN VIVO BY MICRODIALYSIS WITH ON-LINE FLOW GATED CAPILLARY ELECTROPHORESIS

By

STEVEN RICHARD WITOWSKI

A DISSERTATION PRESENTED TO THE GRADUATE SCHOOL
OF THE UNIVERSITY OF FLORIDA IN PARTIAL FULFILLMENT
OF THE REQUIREMENTS FOR THE DEGREE OF
DOCTOR OF PHILOSOPHY

UNIVERSITY OF FLORIDA

2000

ACKNOWLEDGMENTS

I would like to thank my research advisor, Dr. Robert T. Kennedy, for his scientific support. I also acknowledge Dr. Thomas Vickroy for his help with the *in vivo* aspects of this work, both procedure and design. In addition I would like to thank the Kennedy research group, both past and present, for informal discussions that solved more problems than could be counted.

TABLE OF CONTENTS

page

ACKNOWLEDGMENTS.....ii

LIST OF ABBREVIATIONS.....vi

ABSTRACT.....ix

CHAPTERS

1 INTRODUCTION.....1

Microdialysis.....2
Analysis of Dialysate.....5
On-Line Analysis.....6
Glutatmate and Aspartate in the Brain.....8

2 TEMPORAL RESOLUTION IN MICRODIALYSIS.....14

Introduction.....14
Experimental.....15
Results.....19
Discussion.....22

3 IN VIVO MONITORING OF GLUTAMATE: THE ROLE OF ASCORBIC ACID IN THE BRAIN.....34

Introduction.....34
Experimental.....35
Results.....39
Discussion.....41

4 CHARACTERIZATION OF METABOTROPIC RECEPTOR CONTROL AND UPTAKE ON GLUTAMATE AND ASPARTATE IN THE HIPPOCAMPUS.....46

Introduction.....46
Experimental.....48

Results.....50
Discussion.....54

5 REGIONAL DIFFERENCES IN THE STRIATUM AND HIPPOCAMPUS: EVIDENCE FOR VOLUME TRANSMISSION.....69

Introduction.....69
Experimental.....70
Results.....73
Discussion.....76

6 THE ROLE OF GLUTAMATE IN THE PILOCARPINE MODEL OF SEIZURE.....87

Introduction.....87
Experimental.....91
Results.....95
Discussion.....101

7 DEVELOPMENT STRATEGIES FOR THE HIGH SPEED CHROMATOGRAPHIC SEPARATIONS.....118

Theory.....119
Non-Porous Particles.....120
Capillary Columns.....126
Monoliths.....128
Temperature.....130
Electrochromatography.....133

8 COMPARISON OF PRESSURE AND ELECTROOSMOTICALLY DRIVEN FLOW IN CAPILLARIES PACKED WITH NON-POROUS PARTICLES FOR HIGH-SPEED SEPARATIONS.....137

Introduction.....137
Experimental.....138
Results.....142
Discussion.....146

9 SUMMARY AND FUTURE DIRECTIONS.....152

Summary.....152
Future Directions.....156

APPENDICES

A TROUBLESHOOTING THE INSTRUMENT.....160

B MICRODIALYSIS PROBE CONSTRUCTION.....162

REFERENCES.....167

BIOGRAPHICAL SKETCH.....182

LIST OF ABBREVIATIONS

AA	ascorbic acid
AChE	acetylcholinesterase
ACPD	(1S, 3R)-1-aminocyclopentane-trans-1,3-dicarboxylic acid
aCSF	artificial cerebral spinal fluid
ALS	amyotrophic lateral sclerosis
AMPD	2-amino-2-methyl-1,3-propanediol
AP	anterior-posterior
Asp	aspartate
BME	β-mercaptoethanol
CE	capillary electrophoresis
CEC	capillary electrochromatography
D	diffusion coefficient
D_{eff}	effective diffusion coefficient
d_p	particle diameter
DV	dorsal-ventral
EAA	excitatory amino acid
EAAC	excitatory amino acid carrier
EAAT	excitatory amino acid transporter
EEG	electroencephalography

EGTA	bis-(aminoethyl)glycoether-N,N,N',N'-tetraacetic acid
EOF	electroosmotic flow
GABA	γ-aminobutyric acid
GLAST	glutamtae –aspartate transporter
GLT	glutamate transporter
Glu	glutamate
h	reduced plate height
HV	high voltage
IAA	iso-ascorbic acid
i.d.	inner-diameter
iGluR	ionotropic glutamate receptor
i.v.	intravenous
k'	capacity factor
λ	tortuosity factor
LC	liquid chromatography
LIF	laser induced fluorescence
LSOP	l-serine-o-phosphate
MCPG	(RS)-α-methyl-4-carboxyphenylglycine
mGluR	metabotropic glutamate receptor
ML	medial-lateral
ν	reduced velocity
NDA	naphthalene dicarboxyaldehyde
NT	neurotransmitter

o.d.	outer diameter
ODS	octadecylsilane
OPA	ortho-phthaldialdehyde
PDC	L-trans-pyrrolidine-2,4-dicarboxylic acid
PI	polyphosphorinositide
PILO	pilocarpine
PMT	photomultiplier tube
ρ	column to particle diameter ratio
TAPS	N-tris[hydroxymethyl]methyl-3-amino propane sulfonic acid
TTX	tetrodotoxin
u	linear velocity
UV	ultraviolet

Abstract of Dissertation Presented to the Graduate School
Of the University of Florida in Partial Fulfillment of the
Requirements for the Degree of the Doctor of Philosophy

MONITORING NEUROTRANSMITTER AMINO ACIDS IN VIVO BY MICRODIALYSIS WITH ON LINE FLOW GATED CAPILLARY ELECTROPHORESIS

By

Steven Richard Witowski

December 2000

Chairman: Robert T. Kennedy
Major Department: Chemistry

Microdialysis is a sampling technique based on the diffusion of analyte molecules across a semipermeable membrane and has been widely used to probe brain chemistry. This method has previously been coupled to on-line flow gated capillary electrophoresis for the analysis of the excitatory amino acid neurotransmitters glutamate and aspartate in the rat striatum with temporal resolution of 7 to 14 s. By eliminating system dead volumes, resolution has improved to 3.5 s and is in fact limited by the microdialysis probe itself. These improvements have allowed the study of smaller, more complex brain regions while maintaining similar or improved performance characteristics.

Electrical stimulation of neuronal paths was used to elicit extracellular changes in glutamate and aspartate to study their regulation in both the striatum and hippocampus. A possible role for ascorbic acid in the brain is to heteroexchange with glutamate during reuptake by glutamate transporters. In heteroexchange, as glutamate is uptaken into a

cell, ascorbic acid is released into the extracellular space. Electrical stimulation of the prefrontal cortex with monitoring in the striatum shows that when ascorbic acid is added to the extracellular space via reversed dialysis both basal and stimulated release of glutamate increase. This effect is not seen with the addition of iso-ascorbic acid, which has the same anti-oxidant activity but is not transportable.

A characterization of metabotropic glutamate receptors and uptake in the hippocampus by electrical stimulation of the perforant path shows that there is weak tonic autoreceptor control and strong uptake. These results are in contrast to previous results in the striatum where there was strong autoreceptor control that is normally inactive with less uptake. To determine the relative overall clearance rates in striatum and hippocampus, exogenous D-aspartate was introduced into each region. It was found that diffusion played a greater role in clearance in the striatum as compared to hippocampus. Taken together with the data on receptor activity, it was concluded that volume transmission was more likely in the striatum than hippocampus.

The role of glutamate in seizure generation and maintenance is unclear. The effects of the seizure agent pilocarpine on both glutamate and aspartate in the hippocampus in chloral hydrate anesthetized rats were studied. Different treatments with pilocarpine (intravenous injection or direct infusion) produced different effects on glutamate and aspartate. Direct infusion with a lithium pretreatment consistently resulted in a decrease in both transmitters. The infusion of pilocarpine during electrical stimulation inhibited the immediate change in glutamate seen in control stimulations but produced a delayed and prolonged change after 20 min of infusion. A change in extracellular Glu is not seizurogenic, but pilocarpine does affect Glu neurons.

CHAPTER 1
INTRODUCTION

Early analyses in the brain involved dissection of the region of interest followed by time consuming extraction and purification steps. These measurements offer snapshots of the overall analyte concentration in the tissue sampled. The source of the chemical change can be unclear and may be from any number of processes including intracellular stores, metabolic processes, trauma from the dissection, or a direct result of the process of interest. Additionally, the analyte may be diluted or lost during the extraction and purification steps.

With the advent of small carbon paste electrodes, it became possible to monitor a chemical in the brain of a living animal (KIS73). The first of such experiments monitored ascorbic acid which is easily oxidized and at a high concentration in the brain (and therefore easily measured). As the analytical methods improved, it became possible to measure different and more varied compounds via electrochemistry. Addition of a negatively charged polymer (nafion) coating allowed for the analysis of catacholamines (GER84). Fast scan voltammetry with carbon fiber microelectrodes can measure changes in dopamine on the ms time scale (EWI82, WIG76). Additionally, the use of selective enzyme coatings allows the measurement of non-electroactive compounds such as glutamate (Glu), glucose, lactic acid, ethanol, proteins, and drugs and their metabolites (see RUZ96, TRO95, VAD92 for reviews).

The main advantages of electrodes are that they are small, and can therefore monitor specific brain locations, and that they offer very high temporal resolution, how often a measurement can be made. Glu sensitive electrodes have anywhere from 1 min (KUL99) to 1 s (HU94) temporal resolution while carbon fiber microelectrodes have millisecond resolution.

Unfortunately these electrodes have several drawbacks. The first is that there is a background signal associated with the measurements. Because of this background it is difficult to measure a basal concentration of the analyte and low levels or small changes may be obscured. Another disadvantage of electrodes is that one is never sure if only the analyte of interest is being measured. A change in signal may be the result of a change in background current or a change in the concentration of a similar chemical. For example, with Glu selective electrodes, there are small peptides such as Glu-Glu or glutathione (Glu-Cys-Gly) that may interact with the electrode; in addition, the total amino acid concentration (mM range) in the extracellular space of the brain may affect the response of the electrode. Also, an electrode can monitor only one chemical even though several may be changing and interacting with each other.

Microdialysis

An alternative to electrodes is microdialysis (ROB91). Microdialysis is a sampling technique in which small molecules diffuse across a semipermeable membrane (typically regenerated cellulose or polycarbonate) based on concentration gradients into a continuously refreshed medium called the perfusion fluid; see Figure 1-1. Probes can be implanted into virtually any part of the body including skin, internal organs, veins, and of

interest here, the brain. Because microdialysis is only a sampling technique, any detection scheme can be employed to monitor a single compound or several compounds.

The type of molecule that can be sampled depends on the membrane, usually regenerated cellulose or polycarbonate. Typical probes have molecular cutoff ranges of anywhere from a few thousand to one hundred thousand Daltons, meaning that molecules with a molecular weight below the cutoff will be able to diffuse across the membrane. One distinct advantage of the technique is that dialysate is considered to be a clean sample. The technique provides samples free of tissue or blood cells that often require significant steps to remove. As the molecular weight cutoff decreases, more molecules will be excluded. A low molecular weight cutoff membrane will provide a sample free of enzymes and proteins that may interfere with or degrade the analyte of interest. A rule of thumb is the molecular weight cutoff should be at least 10 times greater than the molecular weight of the analyte.

The amount of analyte that will diffuse across the dialysis membrane is dependent on tip length of the probe, flow rate of the perfusion fluid, diffusion coefficient of analyte in tissue, and type of membrane (BUN90). The most common measurement of this process is relative recovery, which is defined as the concentration of analyte in the dialysate divided by the true concentration of analyte in the sample and is usually expressed as a percentage. For example, with a 30% recovery a 10 μM analyte in the brain would be 3 μM in dialysate. Just as a molecule can diffuse into the probe, it can also diffuse out of the probe. This technique, called reversed dialysis, is used commonly to deliver a drug or other chemical directly to the brain. In this case instead of recovery, the term extraction is used. Under steady state conditions recovery and extraction are

equal. The absolute, or mass, recovery is defined as the total mass of analyte collected over a set period of time (for example: 20 pmol/μL/20 min). As flow rate increases, absolute recovery increases while relative recovery decreases. A shorter tip length will decrease both absolute and relative recovery.

Microdialysis probes come in three general shapes. The first, termed in-line or a dialysis tube (Figure 1-2A), is in the shape of a tube with a section replaced by the hollow fiber. This type of probe is used to sample large areas typically under the skin or in an internal organ. The probe is implanted in the region with a needle and passed completely through the skin or organ. The second style of probe, a loop probe (Figure 1-2B), is similar to the in-line probe described above, but in this case instead of passing through a region, the probe is folded so that the inlet and outlet are side by side. The sampling region is smaller than the first type of probe described; these probes are generally used in the brain. The last type of probe is called a side-by-side probe (Figure 1-2C). Here, two smaller capillaries are sleeved inside the dialysis fiber. One end of the fiber is sealed. Perfusion fluid enters the membrane at the bottom of the probe and leaves through the other capillary. The side-by-side probe is a simple version of the concentric probe (Figure 1-2D) in which the inlet line is sleeved inside the outlet. The ends are constructed so that the inlet and outlet are separate. The concentric probe is difficult to construct and is therefore often replaced by the side-by-side probe.

Each of the three types has its advantages. The dialysis tube, as mentioned above, is useful for sampling of large areas such as skin and offers recoveries close to 100% because of its size. The loop probe is smaller than the in-line probe and therefore is used to sample smaller regions. Its drawback is that while its length is smaller, its diameter is

double that of the others and may cause more damage to the surrounding tissue. The side by side probe is the smallest of the three and should cause the least amount of damage. The drawback to this probe is that because of its size, it has poorer recoveries than the other two. The selection of a probe should be based on the specific experimental parameters accounting for all the factors discussed above.

The advantage of microdialysis is that because of the associated separation, multiple analytes can be measured, possible interferent problems are removed, and basal levels can be determined. Additionally, extremely sensitive detectors can be utilized to monitor very low levels of analyte. The major disadvantage of microdialysis is that because of requirements of the separation or detection method, temporal resolution is poor. It will be the focus of this dissertation to achieve electrode-like response with microdialysis and to use the technique to monitor brain activity.

Analysis of Dialysate

The most common method to analyze dialysate is by liquid chromatography with either electrochemical or UV detection (see DAV99, TON99, DAV97, VAN95 for reviews). Liquid chromatography is used most often because of the variety of developed separation methods and its ruggedness. Unfortunately it is not selected because it is highly amenable to microdialysis. Conventional LC columns of 4.6 mm inner diameter (i.d.) typically require 20 to 30 μL of sample for injection which corresponds to a sampling time of 20 to 30 min with a dialysis flow rate of 1 μL/min. While this sampling rate is adequate for monitoring slow changes such as drug effects or diurnal fluctuations, it is unacceptable if processes that change in a few minutes or seconds, such as

neurological transmission, are to be measured.

An obvious way to improve the sampling time, or temporal resolution, in this case is to increase the perfusion flow rate. If the flow rate is increased to 10 μL/min from the original 1 μL/min 30 μL will be collected in 3 minutes. The drawback to this approach is that the relative recovery decreases with increasing flow rate. The 10 fold improvement will result in a 10 fold decrease in the concentration of the analyte. In some analyses, this loss may be acceptable; however, when monitoring analytes at low concentrations, the decrease in recovery may interfere with the measurement. In these cases the sensitivity of the detector will limit how often a measurement can be made. For this reason high sensitivity detection methods such as electrochemistry and laser-induced fluorescence have become popular. By coupling micro and capillary LC columns that require less volume to these ultra-sensitive detection techniques low level analytes and short sampling times can be obtained. For example, with a capillary column, electrochemical detection, and special handling methods it was possible to monitor the 16 amino acids present in the brain with 10 s sampling (BOY00). The drawback to high sampling rates is that a large number of samples are generated. In the example given above, 100 s of monitoring generated 10 samples. With an analysis time of 30 min per sample, 100 s of monitoring required 5 h to analyze.

On-Line Analysis

Manually collecting samples is labor intensive, can be difficult depending on the sampling rate, and is less precise than automated collection. Additionally, because analysis can be time consuming, samples are usually frozen and stored for a considerable

length of time. The freeze-thaw process can cause loss of analyte due to degradation and adsorbtion. A way to avoid these problems is on-line analysis where the dialysis stream is loaded directly into a sample loop or is discretely sampled and injected onto a separation column.

One potential drawback of on-line microdialysis is that the separation time of the analysis is the limit to temporal resolution as opposed to sample volume or mass sensitivity of the detection scheme. A separation time of 30 minutes would only allow 30 minute temporal resolution and would offset most of the advantages of the on-line analysis. As the speed of the separation is increased, the benefits of an on-line instrument become greater. The use of microbore columns and small injection volumes have allowed for sampling times as short as 30 s with microdialysis with on-line LC (CHU87, CHE95, NEW94).

On-line capillary electrophoresis (DAV97 for review) is not as straightforward as on-line liquid chromatography but offers unique advantages. Sample loops and injection valves do not lend themselves to CE because of the very small volumes injected onto the capillary and the high voltage required for the separation. One method developed for on-line CE is the gap-junction method developed in the Lunte group (HOG94). Here, dialysate flows into a 60 nL internal loop injection valve which can be switched to introduce as little as 10 nL into the system to be derivatized and injected onto the CE column. The actual injection is performed by aligning the transfer line with the separation capillary with a small gap in between. The gap junction is grounded to complete the electrical circuit. With this method Glu and aspartate (Asp) have been monitored in 2 min intervals (ZHO95B).

An on-line flow gated capillary electrophoresis instrument with laser-induced fluorescence instrument has been previously developed in this lab for the analysis of the neurotransmitter amino acids Glu and Asp capable of 5 s sampling intervals (LAD98). The flow-gated interface is based on one introduced by Lemmo and Jorgenson (LEM91). Briefly, the dialysis outlet and inlet of the separation capillary are placed a small distance apart (from 30 to 300 μm, depending on flow rates). A perpendicular cross flow of electrophoresis buffer sweeps the dialysis away from the separation capillary so that only buffer is introduced onto the column. For injection, the cross flow is stopped for a short period of time (from a few milliseconds to a few seconds) which allows the dialysis to reach the separation capillary. The applied potential injects a plug of dialysate. The injection is terminated when the cross flow is resumed.

Glutamate and Aspartate in the Brain

We have chosen to use the microdialysis flow-gated capillary electrophoresis instrument described above to study glutamate and aspartate in the rat brain. These two amino acids are the two major excitatory neurotransmitter amino acids in the mammalian central nervous system (ORR93). It is generally accepted that Glu functions in this manner and there is a wealth of data to support this idea. Asp is also believed to be a neurotransmitter but its evidence is less convincing (PAL89). Previous work in this lab in the striatum provides evidence for Asp's neurotransmitter role (LAD98).

A glutamatergic synapse is diagrammed in Figure 1-3. The signal propagates through a cell by a change in action potential and is dependent on the opening and closing of sodium/potassium ion channels. This action potential then causes the opening of gated

calcium channels. The influx of calcium into the cell allows the vesicular release of neurotransmitters into the synaptic cleft to continue the signal at the next neuron (JES93). Once in the cleft the neurotransmitter can interact with 1) autoreceptors that will either promote or inhibit further Glu signaling or 2) Glu transporters on either glia or neuron to clear Glu from the cleft. The neurotransmitter may also diffuse out of the cleft and interact with receptors and transporters on other cells. It is what happens in and around the synaptic cleft that is the focus of this work.

The major signal mediators of the glutamatergic system are ionotropic and metabotropic glutamate autoreceptors (iGluR and mGluR). This work will focus on the mGluR only. There are currently 8 known mGluRs divided into three sub groups; all of which are differentially located throughout the brain and have been mapped by immunostaining (SHI97). Group I mGluRs (subtypes 1 and 5) are coupled to polyphosphoinositide (PI) hydrolysis and serve to amplify post synaptic responses (CON94). They are located both pre- and post-synaptically and are typically at the periphery of the post synaptic densities (ABE92). Both subtypes are also differentially located throughout the brain with group 5 primarily located in the hippocampus, neostriatum, and cerebral cortex. Additionally group 5 has also been found on cultured astrocytes. Group II (subtypes 2 and 3) and group III (subtypes 4, 6, 7, and 8) are negatively coupled to cAMP and are considered to be inhibitory in nature (CON94). All subtypes are predominately located in the nerve terminals but mGluR3 is also found in astrocytes (BRU94).

A set of five glutamate transporters (GLAST, GLT, EAAC, EAAT4, and EAAT5) are responsible for removing Glu and Asp from the synaptic cleft and extracellular space

(DIE97). GLT is the most prevalent of the transporters, located mostly on astrocytes (CHA95), and is in fact one of the most prevalent of all brain membrane proteins at approximately 1 % of all proteins (DAN90). The hippocampus and cerebral cortex have the highest levels of GLT (PIN92). GLAST is found exclusively on glial cells and has its highest concentration in the cerebellum. EAAC is located primarily on neurons, but away from the nerve terminals, and is found throughout the brain (COC97). EAAT4 is located in the hippocampus and neocortex at very low concentrations (FUR97) while EAAT5 is primarily in the retina (ARR97).

For normal brain function, it is required that both receptors and transporters work properly. Because of their excitatory nature, increased levels of group I mGluR have been associated with several neurological diseases from ALS to Parkinson's to epilepsy (see BOR99 for review); conversely, group II and III mGluR activity has been shown to be neuroprotective because of its inhibitory effects (BRU98). High extracellular Glu has been shown to be excitotoxic and may be due to inactive or reversed transporters, especially in an energy deprived system (SAN99). In addition to elevated group I mGluR, decreased transport has also been found in patients with ALS (ROT92). Because of their neurodegenerative or neuroprotective characteristics, mGluR and Glu transporters are drug candidates for a variety of neurological diseases.

By using the analytical methods for the high-speed *in vivo* analysis of Glu and Asp developed previously and in the work presented here, the interactions between Glu, mGluR, and Glu transporters are studied. Once the normal and stressed activity of the glutamatergic system is known it will be possible to guide the development of treatments for a variety of neurological diseases.

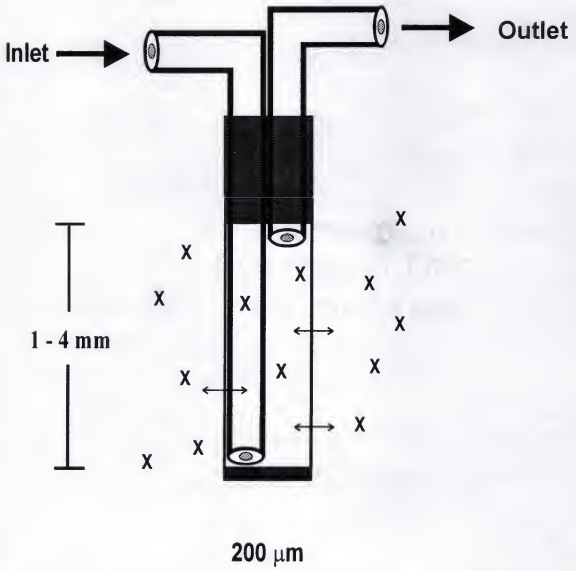

Figure 1-1. Microdialysis probe. Perfusion fluid enters the inlet, passes through a semipermeable membrane and to the outlet. A concentration gradient across the membrane allows analytes to pass into the probe.

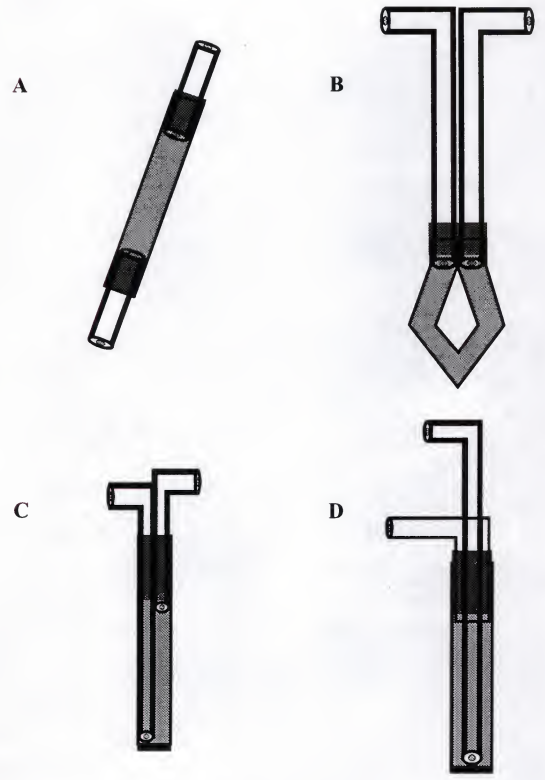

Figure 1-2. Types of microdialysis probes. A) In-line. B). Loop. C) Concentric. D) Side-by-side.

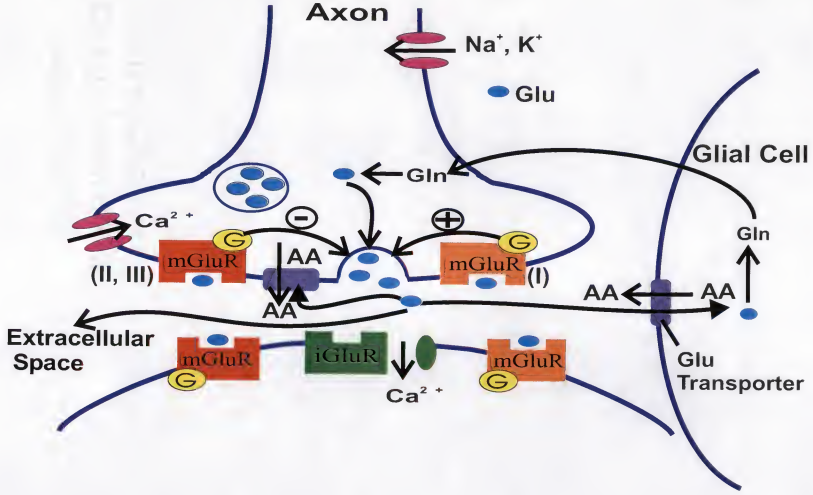

Figure 1-3. Action of glutamate at a neuron.

CHAPTER 2
TEMPORAL RESOLUTION IN MICRODIALYSIS

Introduction

Temporal resolution in microdialysis with conventional analysis methods, such as LC, is limited by volume or mass requirements for detection in an off-line analysis or separation time in an on-line analysis. The best temporal resolution reported in microdialysis coupled to a LC separation is 10 s (BOY00). This measurement utilized capillary columns with electrochemical detection and preconcentration to load the highest possible mass onto the column. Coupled to a flow-gated interface, on-line capillary electrophoresis with laser-induced fluorescence detection is capable of monitoring Glu and Asp with 7 to 14 s temporal resolution (LAD96) and has been used to monitor the two neurotransmitters *in vivo* with 5 s sampling (LAD98). In that study temporal resolution was assumed to be limited by the separation time but no studies were performed to confirm it.

With such high sampling rates, it now becomes important to know the limits to temporal resolution of the microdialysis probe itself. The time the perfusion fluid remains in contact with the dialysis membrane, diffusion across the membrane, and diffusion in transfer lines may all play a role in the lower limit to temporal resolution. As discussed in Chapter 1, decreasing probe length and increasing flow rates will improve temporal resolution at the expense of relative recovery.

In order to determine the limit to temporal resolution associated with microdialysis, the temporal characteristics of probes constructed by the method of Church and Justice (CHU87) are rigorously studied with respect to tip length and flow rate. The effects of these parameters on relative recovery are also studied. Additionally, the sources of temporal broadening of the on-line flow-gated capillary electrophoresis instrument discussed above will be determined and eliminated to obtain the best possible temporal resolution with microdialysis.

Finally, an advantage of microdialysis probes most often stated by the manufacturer is that probes can be reused for chronic measurements or to reduce inter-animal variability and cost. Here, the effects of probe reuse in different animals on both relative recovery and basal levels of Glu are examined.

Experimental

Probe Construction and Equilibration

Side by side microdialysis probes 1, 2, 3, and 4 mm long were constructed following the methods developed by Church and Justice (CHU87) as detailed in Appendix 2. Probes consisted of 9 cm of 20 μm i.d. and 100 μm o.d. fused silica capillary as the inlet and 8 cm of 20 μm i.d. and 100 μm o.d. as the outlet. The dialysis membrane was regenerated cellulose (Spectrum, Houston, TX, USA) with 18 kD cutoff and the tip sealed with polyimide sealing resin (Alltech Associates, Deerfield, IL, USA). Active areas were 200 μm o.d. Before use, all probes were perfused with 70% ethanol in water for 30 min at 1.2 μL/min followed by perfusion with artificial cerebrospinal fluid (aCSF) that consisted of 145 mM NaCl, 2.68 mM KCl, 1.01 mM $MgSO_4$, and 1.22 mM $CaCl_2$,

for a minimum of 30 min.

Measurement of Temporal Resolution and Relative Recovery of the Probe

For experiments determining the temporal resolution and relative recovery of side by side microdialysis probes, the setup depicted in Figure 2-1A was used. aCSF was perfused through the probe via a mechanical syringe pump (Harvard, Holliston, MA, USA) at flow rates of 0.22, 0.60, 1.17, or 2.29 μl/min. The active area of the probe was immersed in 10 ml of stirred aCSF at 37 °C and the outlet connected to a 50 μm i.d. 360 μm o.d. fused silica capillary with a variable wavelength UV detector (Spectraphysics, Anaheim, CA, USA) set at 261 nm 16 cm down column.

One hundred μL of 10 mM ascorbic acid in aCSF was injected with a 500 μL Hamilton gas tight syringe into the stirred CSF. The temporal resolution was calculated by the time for the absorbance to rise from 10% to 90% of the maximum value. Five repetitions were performed for each probe at each flow rate and 3 probes of each length were used. Relative recovery for a probe was determined using the average absorbance at each flow rate divided by the absorbance of an aliquot of solution taken from the 10 mL stirred CSF solution pumped directly into the 50 μm i.d. capillary.

Measurement of Temporal Resolution of the On-Line System

A schematic of the on-line system is shown in Figure 2-1B. The outlet of the probe was 8 cm, the mixing tee was either from Valco (Figure 2-2A) (Houston, TX, USA) or a zero dead volume tee constructed in house (for dimensions, see Figure 2-2B) as follows. Approximately 5 cm lengths of 50 μm i.d. by 360 μm o.d. fused silica capillaries were cut so that the end was straight and flat. Under a stereomicroscope (Nikon, Japan) the ends were ground to 45°. The tee itself consisted of a standard Valco

housing with the center made of Lucite and constructed by the University of Florida Chemistry Department Machine Shop. The ground capillaries were sleeved into 1/16" o.d. Teflon tubing and inserted into the tee so that the ends fit together flush. If one capillary did not fit flush, it was removed and remade. Once in place the capillary ends were cut to be flush with the holding nut. The dialysis and derivatization lines were connected by Teflon sleeves. The reaction capillary was 16 cm by 75 μm i.d., 360 μm o.d. The "derivatization fluid" was aCSF at the same flow rate as the dialysis fluid. Experiments were performed in the same manner as above.

Capillary Electrophoresis with Laser-Induced Fluorescence

The CE-LIF system for monitoring dialysate was similar to that described previously (LAD96, LAD97) and is diagrammed in Figure 2-3. Dialysate was derivatized on-line by pumping 10 mM *o*-phthaldialdehyde/40 mM β-mercaptoethanol (OPA/BME) in 35 mM borate at pH 10.5 at 0.60 μL/min via a syringe pump (Harvard apparatus, Holliston, MA, USA) into a tee attached to the outlet of the dialysis probe. The dialysate and OPA/BME were allowed to mix and react for 50 s as they flowed out of the tee and through a 16 cm long by 75 μm i.d. fused silica reactor capillary. Derivatized dialysate was pumped from the reactor capillary to a flow-gated interface which allowed automatic injection onto the electrophoresis capillary. Dialysate was electrokinetically injected for 40 ms at the separation voltage every 3.5 s. Electrophoresis was carried out inside a 5 cm long (3.5 cm from injection point to detector) by 10 μm i.d. capillary. Voltage was applied by grounding the flow-gated interface and applying –14.5 kV to a buffer reservoir that was connected to the outlet of the separation capillary by 20 cm long by 150 μm i.d. linker capillary. The

electrophoresis buffer was 40 mM carbonate adjusted to pH 9.5 with NaOH.

Fluorescence detection was performed on the electrophoresis column with an epillumination fluorescence microscope (Carl Zeiss, Hanover, MD, USA) as described in detail elsewhere (HER90, SHU93). Fluorescence was excited with 1.3 mW of the 354 nm line of a He-Cd laser (Liconix, Carlsbad CA, USA). Emission over 400 nm was collected with a 40x oil immersion objective and detected by a PMT (CRG Instruments, Austin, TX, USA). Data was collected via a personal computer (Gateway, Sioux City, SD, USA) and data acquisition board (AT-MIO-16F-5, National Instruments, Austin, TX, USA) at 1 kHz and low-pass filtered at 200 Hz. All collection and analysis software was written in house in Lab Windows (National Instruments).

Surgical Procedures

Male Sprague-Dawley rats (250-350 g) were anesthetized with chloral hydrate by an initial subcutaneous injection of 100 mg/ml H_2O at a dose of 400 mg/kg followed by booster injections of 100 mg/kg at 30 min intervals until the rat no longer exhibited a withdrawal reflex to limb pinch. Additional injections were given as needed to maintain no withdrawal reflex. Microdialysis probes were stereotaxically implanted in the dorsal striatum at AP +0.2 mm, ML -3.0 mm, DV -6.5 mm relative to bregma (SWA98). Probes were implanted over a period of 15 to 20 min in 200 μm steps in order to minimize tissue damage. Recordings were made at least 1 h post implantation and after basal levels were found to stabilize.

For repetitive implantations of the same probe, a single 2 mm tip probe was conditioned as above and used in a single rat for approximately 4 to 6 h on four consecutive days. During experiments the flow rate was 0.60 μl/min. After use, the

outside of the probe was rinsed thoroughly with aCSF and then perfused with aCSF at a low flow rate overnight. The probe was perfused with EtOH/H_20 only prior to initial use.

All experimental uses of laboratory rats in the present study were reviewed and approved by the University of Florida Institutional Animal Care and Use Committee and conform with policies and procedures set forth by U.S. Public Health Service Policy on Humane Care and Use of Laboratory Animals.

Results

Temporal Resolution of Microdialysis Probes

The response time of the probe is defined as the time for the signal to rise from 10 to 90% of the height of the step (see inset in Figure 2-1). The expected trend in response time is that as flow rate increases or tip length decreases, response time will decrease but is not seen over the entire range as expected. A plot of response time vs. tip length (Figure 2-4) shows that for the two slowest flow rates (0.22 and 0.60 µl/min) or longest tip lengths tip lengths (3 and 4 mm) the effect is linear. Response time reaches a minimum between 1-1.5 s with 1 mm tip lengths at flow rates of 1.17 and 2.29 µL/min and 2 mm tip lengths at 2.29 µL/min. The measurement is likely limited by the mixing time after the injection of ascorbic acid and not a real limit due to the probe. In fact, in initial experiments ascorbic acid was introduced via a Brinkmann pipette and the lower limit of temporal resolution was more than 2 s. By using the Hamilton syringe, the sample could be introduced faster and hence decreased the lower limit.

Relative Recovery of Microdialysis Probes

Overall flow rates and tip lengths the relative recovery changed as expected, doubling the flow rate or halving the tip length resulted in halving the recovery (see

Figure 2-5). The recovery ranged from nearly 100% at 0.22 μl/min with a 4 mm tip probe down to approximately 6% at 2.29 μl/min with a 1 mm tip probe.

Temporal Response of the On-Line Instrument

The temporal resolution measured in the configuration used for on-line CE was much worse than the microdialysis probe by itself. There are two possible sources for broadening in the system, diffusion in the capillaries and dead volume. The calculated broadening due to diffusion in the capillaries was insignificant indicating that dead volume was the problem. Dead volume can be considered a region where fluid becomes stagnant due to eddies in flow or a region where fluid can pool and mix. The system has one such region, the Valco reaction tee (see Figure 2-2A). Fluid enters via a 40 μm i.d. capillary and exits via a 75 μm i.d. capillary, both sleeved in a $1/16^{th}$ in. o.d. Teflon holder. Additionally, the internal volume of the 150 μm i.d. tee is 42 nL, seemingly small but virtually identical to the volume inside the active region of a 2mm long probe (45 nL). The capillary to tee interface may provide an unswept region because of the sudden change in diameter and the additional volume will cause extra mixing. These two factors make the Valco reaction tee a likely source of temporal broadening.

In order to confirm the tee as a broadening source, a zero dead volume tee (see Figure 2-2B) was constructed using fused silica capillaries ground at 45° angles and held flush inside a Lucite housing. With this configuration there is virtually no dead volume throughout the system. Figure 2-6 compares the temporal resolution of the system with the Valco tee to the zero dead volume tee. As can be seen, the Valco tee was responsible for a significant amount of temporal broadening. With a 3 mm tip at 1.2 ml/min, the response time with the Valco tee was nearly 250% (9.7 vs. 4.0 s) greater than that with a

zero dead volume tee. Response time of the system with the zero dead volume tee was equal to that of a microdialysis probe only.

Possible Broadening Inside the Probe

Even though the system after the microdialysis probe does not contribute any significant broadening, it is possible that the microdialysis probe has an unswept volume or that there is broadening due to diffusion across the membrane itself. If rapid diffusion across the dialysis membrane can be assumed, the theoretical temporal resolution should be the time it takes to replace all of the perfusion fluid in the active area of the probe. Figure 2-7 compares the temporal resolution at a single flow rate to the calculated time to clear the active area, represented by the solid line. As can be seen, the experimentally determined resolution agrees extremely well with the calculated value.

Finally, to determine any temporal broadening associated with the on-line derivatization reaction or glow-gated interface, the *in vitro* resolution with a Glu and Asp standard was determined. A typical electropherogram of a standard solution of 2.5 μM Glu and 1.4 μM Asp is shown in Figure 2-8. The probe size and flow rate used in this experiment were 2 mm and 0.60 μl/min, which should correspond to a temporal resolution of approximately 5 s. As seen in Figure 2-9, both Glu and Asp reach maximum height in 2 injections at 3.5 s per injection. This time frame corresponds to a temporal resolution between 3.5 and 7.0 s, exactly what was determined for the microdialysis probe only.

Reuse of the Microdialysis Probe

The effect of multiple uses of a single probe is shown in Figure 2-10. As expected the relative recovery of the probe decreases with each consecutive day. The

initial relative recovery of this particular probe was 35.6 % and decreased to 21.7 % by the fourth day. Brain concentration of Glu on the first day was 670 nM, by the fourth day, the measured basal Glu increased over ten fold to 7.6 μM. In brain concentrations are used here to account for the change in relative recovery.

Discussion

The results presented here show that microdialysis is a sampling method that is highly amenable to and capable of high-speed analyses. Temporal resolution of the microdialysis probe itself was shown to be as low as 1 s, depending on the flow rate and probe size. It is likely that a better testing method will result in a more accurate and lower limit to temporal resolution. With a tip length that was not apparently limited by mixing time, temporal resolution was equal to the time for the active area of the probe to be completely swept by perfusion media. Based on this result, a 1 mm tip probe and a flow rate of 2.4 μl/min should provide a temporal resolution of 500 ms. Such resolution does however have its drawbacks. With improvement in temporal resolution there is a corresponding loss in relative recovery. The same 1 mm tip probe at 2.4 μl/min and 500 ms temporal resolution has a relative recovery of just 6%. This means that a 1.0 μM analyte in the brain is only 60 nM in dialysate.

The CE system used here has a limit of detection for dialysate of approximately 30 nM and can reproducibly inject every 3.5 s, so therefore would barely be able to detect the analyte and would not be capable of taking advantage of this temporal resolution. It again becomes necessary to improve the analysis system. With proper instrument design it should be possible to obtain sub-second temporal resolution with microdialysis and on-

line flow gated capillary electrophoresis.

Even though the lower limits of temporal resolution can not be taken advantage of in the work carried out here; the knowledge of the limitations of both the system and microdialysis will make better designed experiments possible. For example, probe lengths and flow rates can be chosen to maximize both temporal and spatial resolution as well as relative recovery. The same as one minute sampling does not take advantage of 5 s temporal resolution due to high flow rates and small tip lengths, a 1 s separation is unnecessary with 5 s temporal resolution.

With these particular probes, it appears that reuse will result in decreased performance of the probe as well as an increase in measured basal levels. It may be possible to explain both phenomena by a layer of gliosis that develops on the probe after implantation in the brain. This layer of cells in fact forms on any object implanted in the brain for a length of time, including metal electrodes and fused silica capillary. The layer of cells could serve as an added diffusion barrier that retards Glu from crossing the membrane. The increase in basal concentrations may be the result of additional damage caused by a thicker probe or some sort of interaction between the gliosis and the brain.

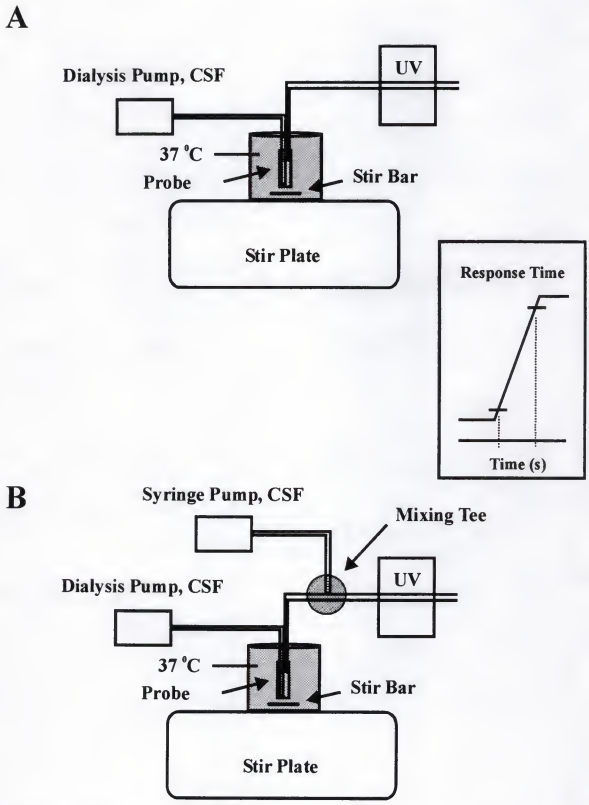

Figure 2-1. Schematics for temporal resolution studies. A) Set up for probe only B) Set up for on-line analysis .

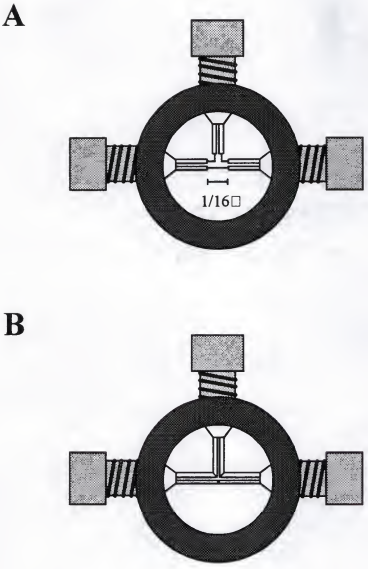

Figure 2-2. Diagram of mixing tees. A) Valco tee. The volume inside is 42 nl. B) Zero dead volume tee. 50 μm i.d. x 360 μm o.d. capillaries are ground to 45 degree angles and butted against each other inside the tee. Once secured in place capillaries are cut to be flush with the nut.

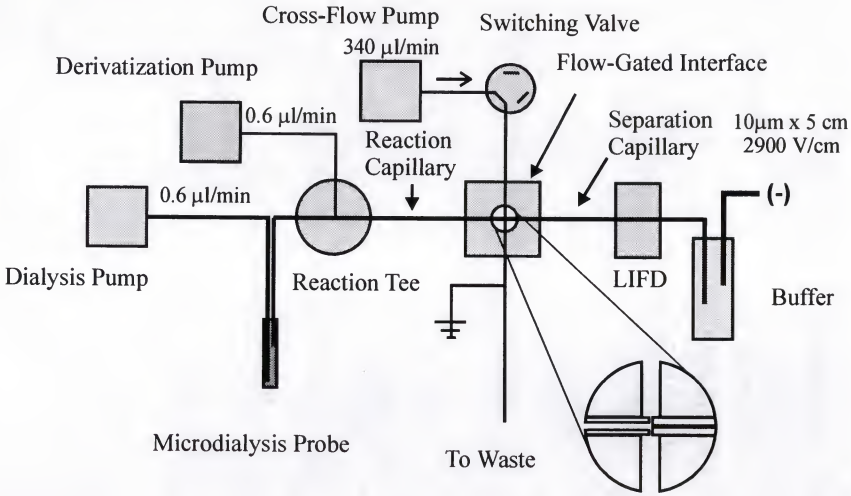

Figure 2-3. Microdialysis with on-line flow gated capillary electrophoresis

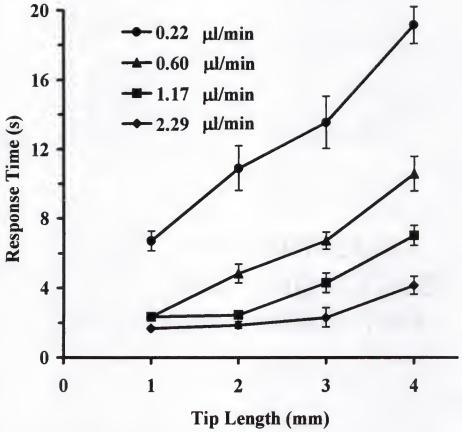

Figure 2-4. Effect of tip length and flow rate on temporal resolution. At high flow rates and smal tip lengths resolution levels off around 1 s. This limit is likely due to the mixing time of the solution. Error bars represent one S. E. M. (n = 3)

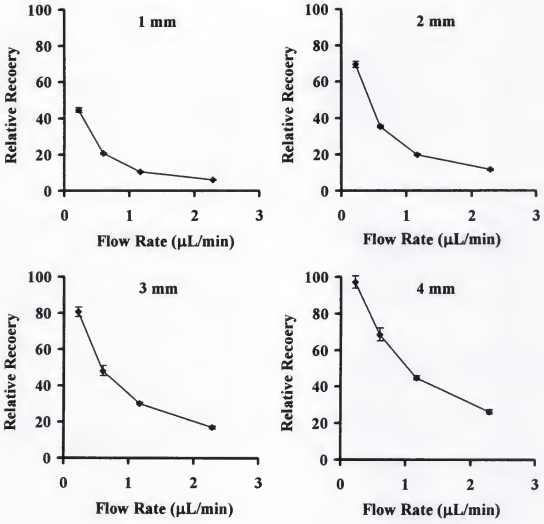

Figure 2-5. Effect of flow rate and probe tip length on relative recovery. Recovery decreases as flow rate increases and tip length decreases over the range tested. Error bars represent one S. E. M. (n = 3).

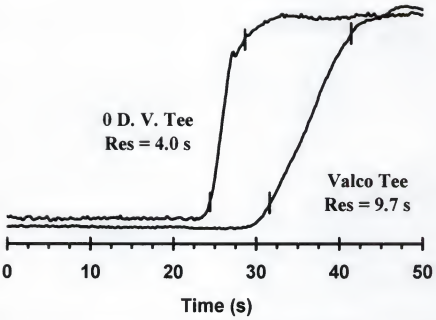

Figure 2-6. Temporal resolution of the on-line system, Comparison of Tees. As seen here the dead volume due to the Valco tee more than doubles temporal resolution. Conditions: 3 mm tip probe, flow rate 1.17 µl/min, 100 µl injection of 10 mM ascorbic acid into 10 ml of CSF at 37 ^{0}C. The calculated time in the active area of the probe is 3.7 s.

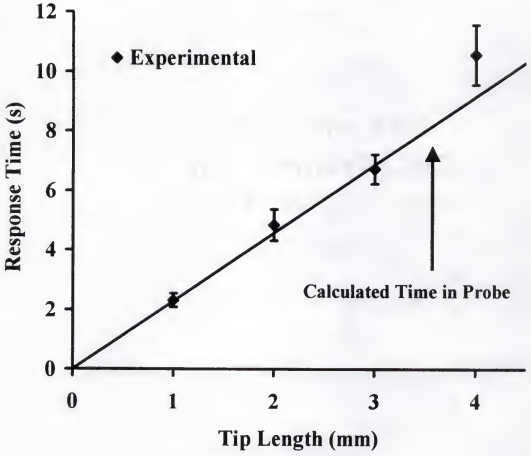

Figure 2-7. System temporal resolution compared to calculated resolution. At 0.60 μL/min the temporal resolution of the system with a zero dead volume tee is equivalent to the calculated dwell time in the active area of the microdialysis probe. Error bars represent one S. E. M. (n = 5)

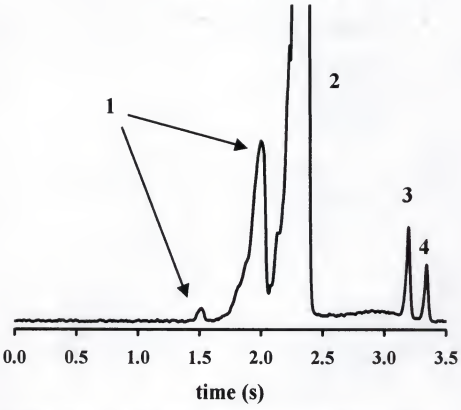

Figure 2-8. *In vitro* electropherogram of 2.5 μM Glu and 1.4 μM Asp. Labelled peaks are as follows 1) reagent peaks, 2) 200 μM glycine, 3) glutamate, 4) aspartate. Figures of merit: Glu: N = 34,600, S/N = 160, Asp: N = 44,000, S/N = 100. Microdialysis probe: 2 mm tip, Flow Rate: 0.6 μl/min. See text for separation conditions.

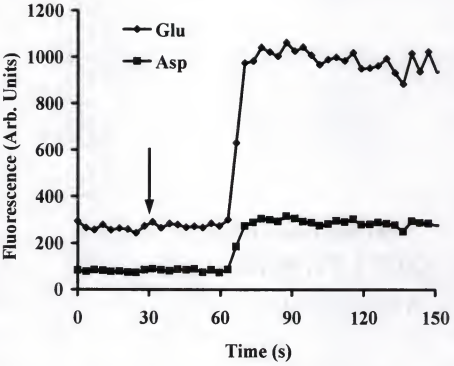

Figure 2-9. Response of CE-LIF to step change in Glu and Asp. Points represent the peak height of analyte and are from electropherograms collected every 3.5 s. With 2 mm tip probes at 0.60 μl/min, temporal resolution is between 3.5 and 7.0 s. Arrow indicates change, the delay in response is due to the dwell time of the system. See text for separation conditions.

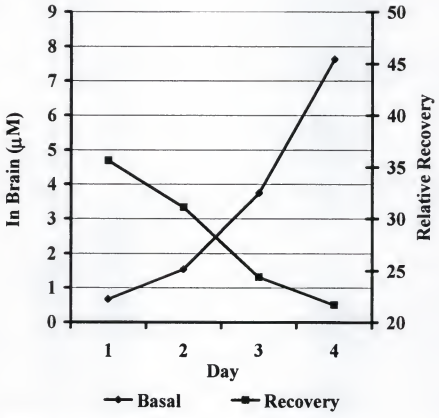

Figure 2-10. Reuse of a single microdialysis probe in 4 rats on consecutive days. Tip length was 2 mm with a flow rate of 0.6 μL/min. Note concentration is given as in brain to correct for recovery changes.

CHAPTER 3
IN VIVO MONITORING OF GLUTAMATE: THE ROLE OF ASCORBIC ACID IN THE BRAIN

Introduction

Ascorbic acid (AA), present as the anion ascorbate *in vivo*, is a ubiquitous substance throughout the body with a wide range of functions. Its most widely recognized role is as an antioxidant, reducing free radicals formed during oxidative metabolism (BEY94, ROS93). This role seems to be especially important in the brain where a high level of oxidative activity is required for the metabolism and release of neurotransmitters (GOT94). Concentrations of AA in the extracellular fluid are between 200 and 500 μM (GON81, ONE82, SCH82) and are unevenly distributed throughout the brain (MIL82, STA84). Regions of highest concentration are the hippocampus, hypothalamus and cerebral cortex. Both the striatum and hippocampus have concentration gradients in the individual region (BAS91, MIL82). Intracellular concentrations can be up to 10 mM and also vary by region and cell type (neuron vs. glia) (RIC97).

An additional role for AA has recently been proposed in which it heteroexchanges with Glu during reuptake at Glu transporters (GRU93, REB97). In this scenario, AA would act as a charge carrier to preserve the cell potential (neuron or glia) as Glu is removed from the extracellular space. The majority of the evidence is indirect and involves the effect of Glu on AA. This first line of evidence for heteroexchange is that direct infusion of Glu will cause an increase in extracellular AA measured by

voltammetry (ONE84). This effect is transient, with AA returning to basal levels within 3 to 5 min (PIE93) and can be blocked by Glu uptake inhibitors (CAM91). Additionally, electrical stimulation of the glutamatergic pathway in the hippocampus causes an increase in AA (ONE84, CAM91). Glu uptake inhibitors have also been shown to attenuate the release of AA (GRU93, CAM91).

In this chapter we study the direct effect of adding 500 μM AA to the brain via reverse dialysis on basal Glu and how it affects the electrically stimulated release of Glu by stimulation of the prefrontal cortex. Electrical stimulation will be used because it provides a neuronal source of Glu (LAD98) which will then be uptaken into the surrounding cells. If heteroexchange occurs, the excess AA in the extracellular space should retard uptake due to an altered equilibrium. This effect may result in an increase in basal Glu and/or stimulated overflow because of reduced uptake. To differentiate between heteroexchange and oxidative metabolism, the effects of 500 μM iso-ascorbic acid (IAA) on basal and stimulated levels are also studied. IAA is the D-isomer of AA and has the same antioxidant properties as AA but is not transportable.

Experimental

Chemicals and Reagents

All chemicals were purchased from Sigma Chemical (St. Louis, MO USA). All fused silica capillary tubing was from Polymicro Technologies (Phoenix, AZ, USA) and had a 360 μm outer diameter (o.d.) unless noted otherwise.

Capillary Electrophoresis and Laser-Induced Fluorescence Detection

The CE-LIF system for monitoring dialysate was the same as that described in

Chapter 2. Dialysate was derivatized on-line by pumping 10 mM *o*-phthaldialdehyde/40 mM β-mercaptoethanol (OPA/BME) in 35 mM borate at pH 10.5 at 1.2 μL/min via a syringe pump (Harvard Apparatus, Holliston, MA, USA) into a tee (Valco, Houston, TX, USA) attached to the outlet of the dialysis probe. The dialysate and OPA/BME were allowed to mix and react for 18 s as they flowed out of the tee and through a 16 cm long by 75 μm i.d. fused silica reactor capillary. Derivatized dialysate was pumped from the reactor capillary into a flow-gated interface which allowed automatic injection onto the electrophoresis capillary. The distance between the reaction and separation capillaries was approximately 60 μm. Dialysate was electokinetically injected for 40 ms at the separation voltage every 5 s. Electrophoresis was carried out inside a 5 cm long (3.5 cm from injection point to detector) by 10 μm i.d. capillary. Voltage was applied by grounding the flow-gated interface and applying –13 kV to a buffer reservoir that was connected to the outlet of the separation capillary by 20 cm long by 150 μm i.d. linker capillary. The electrophoresis buffer was 40 mM carbonate adjusted to pH 9.5 with NaOH.

Fluorescence detection was performed on the electrophoresis column with an epillumination fluorescence microscope (Carl Zeiss, Hanover, MD, USA). Fluorescence was excited with 1.3 mW of the 354 nm line of a He-Cd laser (Liconix, Carlsbad CA, USA). Emission over 400 nm was collected with a 40x objective and detected by a PMT (CRG Instruments, Austin, TX, USA). Data was collected via a personal computer (Gateway, Sioux City, SD, USA) and data acquisition board (AT-MIO-16F-5, National Instruments, Austin, TX, USA) at 1 kHz and low-pass filtered at 200 Hz. All collection and analysis software was written in house in Lab Windows (National Instruments).

Microdialysis

Side by side microdialysis probes were constructed as described in Appendix 2. Probes consisted of 9 cm of 20 μm i.d. and 100 μm o.d. fused silica capillary as the inlet and 8 cm of 20 μm i.d. and 100 μm o.d. as the outlet. The dialysis membrane was regenerated cellulose (Spectrum, Houston, TX, USA) with 18 kD cutoff and the tip sealed with polyimide sealing resin (Alltech Associates, Deerfield, IL, USA). Active areas were 200 μm o.d. and 4 mm long. Before use, all probes were perfused with 70% ethanol in water for 30 min at 1.2 μL/min followed by perfusion with artificial cerebrospinal fluid (aCSF) that consisted of 145 mM NaCl, 2.68 mM KCl, 1.01 mM $MgSO_4$, and 1.22 mM $CaCl_2$, for a minimum of 30 min. Perfusion flow rate was 1.2 μL/min and was driven by a syringe pump (Harvard apparatus, Holliston, MA, USA) for all experiments. Calibration and *in vitro* recovery was performed before implantation by placing the probe in Glu and Asp standards dissolved in aCSF held at 37 °C. For calibration and *in vivo* experiments, the outlet capillary of the probe was connected to the reactor tee described above for on-line CE-LIF analysis.

Surgical Procedures

Male Sprague-Dawley rats (250-350 g) were anesthetized with chloral hydrate by an initial subcutaneous injection of 100 mg/ml H_2O at a dose of 400 mg/kg followed by booster injections of 100 mg/kg at 30 min intervals until the rat no longer exhibited a withdrawal reflex to limb pinch. Additional injections were given as needed to maintain no withdrawal reflex. Microdialysis probes were stereotaxically implanted in the dorsal striatum at AP +0.2 mm, ML -3.0 mm, DV -6.5 mm relative to bregma (SWA98). Electrical stimulations were performed by placing a single platinum electrode (1 mm

diameter) in direct contact with the surface of the prefrontal cortex (AP +3.5 mm, ML +1.5 mm). Probes were implanted over a period of 15 to 20 min in 200 μm steps in order to minimize tissue damage. Recordings were made at least 1 h post implantation and after basal levels were found to stabilize.

All experimental uses of laboratory rats in the present study were reviewed and approved by the University of Florida Institutional Animal Care and Use Committee and conform with policies and procedures set forth by U.S. Public Health Service Policy on Humane Care and Use of Laboratory Animals.

Electrical Stimulation and Pharmacological Treatments

Electrical stimulation of the perforant path consisted of application of a 10 s train of 0.5 ms, 20 Hz, 80 V square wave pulses (Grass Medical Instruments, Quincy, MA). To evaluate the effects of pharmacological treatment on the signal from electrical stimulation, 500 μM AA or IAA in aCSF was administered by reverse dialysis. Prior to treatment, at least 2 control stimulations were recorded in each rat, with 30 min between each stimulation. After control stimulations, the dialysis media was switched to the additive media. 60 min after initiation of perfusion with either AA or IAA, a set of 2-3 identical electrical stimulations was again performed at 30 min intervals.

Data Analysis

Electropherograms were analyzed using a statistical moments program written in house (Lab Windows). Glu and Asp peaks were marked manually and dialysate concentration determined by *in vitro* calibration. The 100 % basal level was measured as the average concentration of analyte in 10 electropherograms immediately prior to stimulation. Elevated concentrations due to AA were determined by comparison to the

analyte concentration before application of the additive. Stimulated overflow was calculated as the total mass of analyte collected by the microdialysis probe above the average pre-stimulus level. A two-tailed student's t-test was used to determine all statistical differences. All values are reported as mean ± one standard error, n is given as the number of rats for basal concentrations or number of stimulations for overflow.

Results

Basal Conditions

Basal levels in dialysate determined by the 4 mm side-by-side probes were 250 ± 85 nM for Glu and 95 ± 10 nM for Asp (n = 7) respectively. Relative recoveries were 40 ± 2% and 43 ± 2% for Glu and Asp respectively. In the basal electropherogram shown in Figure 3-1, it can be seen that several peaks besides Glu and Asp are present. Several of them have been identified by comparison to the migration time of amino acid standards. From left to right, they are o-phosphoserine a mGluR agonist (from the previous injection), arginine, glycine an inhibitory amino acid (partially resolved from the large neutral peak) glutathione an antioxidant, and o-phosphoethanolamine an osmo-regulator, glutamate, and aspartate. The other peaks could not be conclusively identified. These peaks do not occur in a 40 amino acid standard (Sigma Chemical) and may be small peptides (2-3 amino acids) or degradation products from larger peptides.

Effects of Ascorbic Acid

Control basal levels of Glu in the dialysate were 250 ± 80 nM (n = 7). One hour after infusion of 500 μM AA the extracellular concentration of Glu in dialysate was 910 ± 140 nM (n = 4), a 360 % increase over control ($p < 0.001$). It must be noted that the

effect of AA on extracellular Glu was not an immediate effect but increased over approximately 40 min. While this effect was observed there were no attempts made to monitor the time course of the change. The addition of 500 mM IAA to the perfusion medium resulted in no change in basal Glu (n = 3).

The application of an electrical stimulus to the prefrontal cortex resulted in an immediate increase in extracellular Glu and return to basal upon termination of stimulus within the resolution of the instrument and can be seen in Figure 3-2. The peak increase in Glu was 76 ± 13 % (n = 17) over basal and returned to within 10% of original basal levels within 40 s after termination of stimulus. The total mass of Glu collected over basal level was 328 ± 31 fmol (n = 17). In the presence of 500 μM AA, the peak increase of Glu was 201 ± 31 % (n = 11) and returned to within 10 % of basal 160 s after cessation of stimulus. The total mass collected over the elevated basal level was 1650 ± 144 fmol (n = 11), or a 503 % increase over control ($p < 0.0001$). In contrast 500 μM IAA added to the perfusion medium resulted in a 92 ± 21 % (n = 7) increase over basal and returned to within 10 % of basal levels 60 s after cessation of stimulus. The total mass of Glu collected over basal was 355 ± 37 fmol (n = 7). Neither the maximum stimulated increase nor total mass collected was statistically different from control.

To quantify the change in overall clearance rate due to addition of 500 μM AA to the perfusion medium, the concentration dependent decay rates of the stimulation curves were determined (see Figure 3-3). The slope of the line indicates the overall clearance rate, including uptake, diffusion, and recovery by the probe. Assuming that diffusion and probe recovery are constant, the change in slope will be due to the change in uptake. The decay rates are: aCSF only = 0.143 ± 0.010 s^{-1}, IAA = 0.136 ± 0.010 s^{-1}, and AA = 0.109

$\pm$ 0.010 s^{-1} (different from aCSF $p < 0.01$, from IAA $p < 0.05$). The difference between aCSF and IAA was not statistically significant.

Discussion

As seen in Figure 3-2, addition of AA to the perfusion medium resulted in both a 360% increase in basal levels and 500% increase in stimulated overflow of Glu in the striatum. The addition of IAA to the perfusion medium lead to no change in basal Glu and a small but statistically insignificant increase in stimulated overflow. The combination of these two pieces of data is consistent with Glu and AA heteroexchange. The small change with IAA may indicate a minor role for oxidative loss of Glu from the extracellular space. But, because this change is not significant no reliable conclusions can be made. Higher concentrations of IAA should be infused to determine any role of oxidative loss of extracellular Glu.

The gradual increase in basal Glu does not immediately suggest a direct action of AA on the transporters when compared to the action of drugs that directly inhibit the Glu transporter. The direct infusion of an uptake inhibitor such as L-trans-pyrrolidine-2,4-dicarboxylic acid (PDC) results in an immediate increase in Glu basal levels. However, because there already is a high level of AA in the extracellular fluid and the added AA is not much higher than the natural level it may take quite some time for the added AA to have an effect. It has been previously suggested that the Glu-AA interaction is not direct (GRU93) and may be associated with carrier proteins not involved with Glu transport (FIL86) although no such proteins have been found.

This relatively small addition of AA leads to an interesting possibility. When

aCSF without AA is perfused, extracellular AA will actually be depleted due to reverse dialysis. Therefore, control experiments may not be representative of true physiological conditions. It may be that in this case, the amount of AA added only returns the concentration to near normal levels. If this holds true, it would appear that uptake in the brain is not as strong as previously believed. It is not an uncommon practice to add AA to the perfusion medium but is most often used to protect against oxidation of the analyte, not to specifically add it back to the brain.

The results from the work here demonstrate for the first time direct evidence for the modulation of Glu by AA which is consistent with heteroexchange. However, this is not a complete picture, additional studies to confirm these results should be carried out. These studies include concentration dependent studies as well as a rigorous study of the time course of the effect of AA on both basal and stimulated levels of Glu.

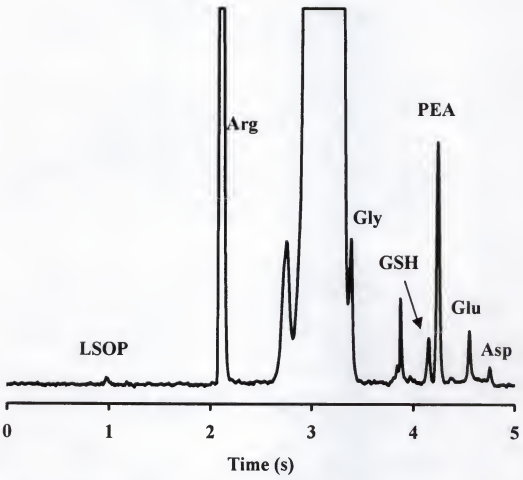

Figure 3-1. Basal electropherogram. The peaks are identified as follows: LSOP = o-phosphoserine (overlapped from previous run), Arg = arginine, Gly = glycine (partially resolved), GSH = glutathione, PEA = o-phospho-ethanolamine, Glu = glutamate, Asp = aspartate. The remaining peaks were not conclusively identified. See text for conditions.

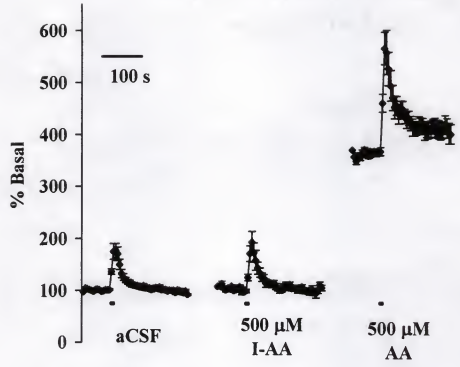

Figure 3-2. Evidence for ascorbic acid heteroexchange with Glu. 500 µM of AA added to the perfusion medium resulted in an increase in basal and stimulated overflow of Glu by 360% and 500% respectively. IAA had no effect on basal or stimulated overflow. See text for separation conditions. Error bars represent one S. E. M.

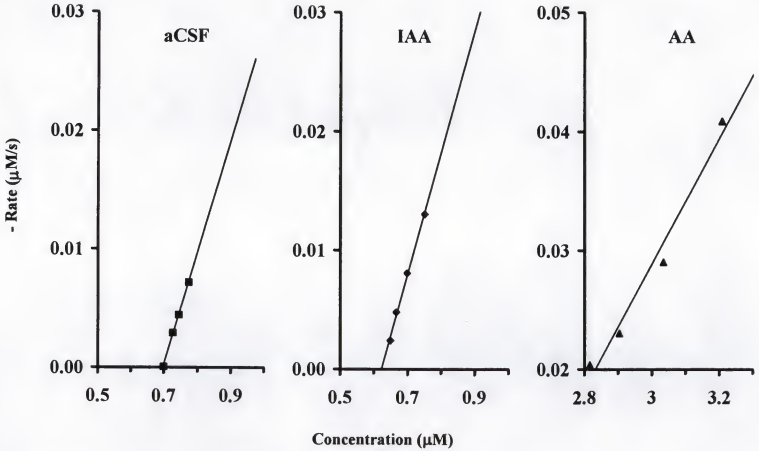

Figure 3-3. Caculated decay rates for aCSF, IAA, and AA. Points were taken from data in Figure 3-2. Slopes: aCSF = 0.143 +/- 0.010, IAA = 0.136 +/- 0.010, AA = 0.1093 +/- 0.010.

CHAPTER 4
CHARACTERIZATION OF METABOTROPIC RECEPTOR CONTROL AND UPTAKE OF GLUTAMATE AND ASPARTATE IN THE RAT HIPPOCAMPUS

Introduction

Glutamate has been well established as the major excitatory neurotransmitter in the CNS. Despite overwhelming evidence for the role of glutamate as a neurotransmitter, direct measurement of its extracellular level *in vivo* by microdialysis sampling or sensors has not provided convincing evidence of a neuronal origin for glutamate in the extracellular space. Rather, extracellular glutamate level appears to have an atypical regulation that suggests a more complex level of control than that encountered with amine neurotransmitters or acetylcholine.

Particular problems with glutamate measurements include that the basal levels are not sensitive to Na^+ channel blockage by local administration of TTX or to local depletion of Ca^{2+} as summarized in several recent reviews and papers (FIL95, TIM97, HER96). TTX-sensitivity and Ca^{2+}-dependency are taken as minimal requirements for considering extracellular measurements to reflect neuronal activity. Thus, the exact source of the basal levels of glutamate in the extracellular space sampled by sensors and microdialysis is unclear. Several hypotheses have been advanced to explain the source of the basal glutamate level detected by microdialysis including carrier mediated release (LEV93) or transport from the plasma (FIL95).

Additionally, physiological events such as stress (MOG93) or seizure generation (MIL93) have been shown to increase Glu in a partially TTX-dependent fashion. These changes have been interpreted as illustration of measurement of synaptic overflow of Glu released from neurons. An alternative interpretation however is the increased level, while dependent upon neuronal activity is actually a secondary change (TIM97) perhaps reflective of changes in metabolism. This view acknowledges the fact that inclusion of TTX will stop all neuronal firing, including non-glutamatergic neurons thus causing cessation of any process that depends upon neuronal electrical activity. Because of these limitations, it seems useful to utilize selective stimulus of glutamatergic cell bodies combined with measurement in the terminal fields of these neurons in order to attempt to characterize neuronal release of glutamate *in vivo*. One approach to avoiding the confusion over the basal levels of glutamate is to characterize the extracellular level changes during stimuli as has been shown in the previous chapter.

In the hippocampus, stimulation of the perforant pathway has allowed detection of glutamate increases in two different reports. In one report, an amperometric glutamate sensor placed in the dentate gyrus detected increases over ~45 s that peaked at a 21 μM increase over basal following a 5 s stimulation (HU94). Such an observation is consistent with the notion of detection of electrically stimulated overflow; however, the TTX-sensitivity and Ca^{2+} dependency of this change was not studied. In another report, 20 s stimulations allowed detection of 20% increases over basal glutamate over a 15 s period (WAL95). Again however, the TTX sensitivity and Ca^{2+}-dependency were not assessed.

In this chapter, the influence of EAA transporters and presynaptic metabotropic Glu autoreceptors (effects of utilized drugs are summarized in Table 4-1) on extracellular

levels of Glu and Asp in rat hippocampus under basal (steady-state) conditions as well as under dynamic conditions associated with perforant pathway stimulation are evaluated. Our results provide novel evidence that synaptic overflow of neuronally-released Glu occurs *in vivo* within hippocampal circuits following afferent stimulation.

Experimental

Drugs and Reagents

All chemicals were purchased from Sigma Chemical (St. Louis, MO, USA) unless otherwise indicated. All drugs were administered by reverse microdialysis. Fused silica capillary was purchased from Polymicro Technologies (Phoenix, AZ, USA) and was 360 μm o.d. unless otherwise stated.

Capillary Electrophoresis and Laser-Induced Fluorescence Detection

The instrument is the same as was described in Chapter 2. aCSF is perfused (0.60 μl/min) through the microdialysis probe and mixed with 10 mM o-phthaldialdehyde/40 mM β-mercaptoethanol in 35 mM borate at pH 10.5 (0.60 μl/min) in a zero dead volume tee described in chapter 4. The mixture reacts for 50 s in a 16 cm x 75 μm i.d. fused silica capillary and is carried to a flow-gated interface. Cross flow is 340 μl/min and the distance between reaction and separation capillaries is 30 μm. For injection, the cross-flow is stopped for 40 ms via a pneumatically actuated valve with a high-speed switching assembly. For better injection reproducibility (1-2% improvement) 1-2 mm of polyimide was removed from the tip of each capillary. The separation capillary was 5 cm x 10 μm i.d. x 360 μm o.d. and connected to voltage via a 20 cm x 150 μm i.d. x 360 μm o.d. linker capillary. A 5 mm detection window was burned by electric arc 3.5 cm from the

injection end. The separation buffer was 40 mM carbonate adjusted to pH 9.5 with saturated NaOH. The applied potential was – 13,000 V with the interface held at ground. Injections were made every 5 s.

Fluorescence detection was performed by excitation with the 354 nm line of a He-Cd laser (Liconix, Carlsbad, CA, USA). Emission over 400 nm was detected with a PMT and associated components (CRG Instruments, Austin, TX, USA) and low pass filtered at 200 Hz. Data was collected via a personal computer (Gateway, Sioux City, SD, USA) and data acquisition board (AT-MIO-16F-5, National Instruments, Austin,TX, USA) at 1000 Hz. All software was written in house in Lab Windows (National Instruments).

Microdialysis and Electrical Stimulation

Side by side microdialysis probes were constructed as described in Appendix 2. Probes consisted of 9 cm of 20 i.d. and 100 o.d. fused silica capillary as the inlet and 7 cm of 20 i.d. and 100 o.d. as the outlet. The dialysis membrane was regenerated cellulose (Spectrum, Houston, TX, USA) with 18 kD cutoff and the tip sealed with polyimide sealing resin (Alltech Associates, Deerfield, IL, USA). Active areas were 200 μm o.d. and 2 mm in length. Before use, all probes were perfused with 70% ethanol in water for 30 min at 1.2 μL/min followed by perfusion with artificial cerebrospinal fluid (aCSF) that consisted of 145 mM NaCl, 2.68 mM KCl, 1.01 mM $MgSO_4$, and 1.22 mM $CaCl_2$, for a minimum of 30 min. Unless otherwise stated, perfusion flow rate was 0.60 μL/min and was driven by a syringe pump (Harvard apparatus, Holliston, MA, USA) for all experiments. Calibration and *in vitro* recovery was performed before implantation by placing the probe in Glu and Asp standards dissolved in aCSF held at 37 °C.

Probes were stereotaxicly implanted in the dentate gyrus of chloral hydrate

anesthetized rat (coordinates: AP – 3.8 mm, ML –3.0 mm, DV = -4.7 mm (from dura) from bregma). Bipolar stimulating electrodes (Rhodes Medical Equipment, Woodland Hills, CA, USA) were stereotaxicly implanted in the lateral perforant path (coordinates: AP: 0.0 mm, ML –4.4 mm, DV –3.5 mm (from dura) from lambda). Both probe and electrode were implanted over a period of 15 to 20 min in order to minimize tissue damage. No experiments were performed for at least 1 hr post implantation to allow stabilization of basal levels.

The perforant path was stimulated by application of a 20 s train of 0.1 ms, 20 Hz, 10 V square wave pulses (Grass Instruments, Quincy, MA, USA). Stimulations were applied at least 20 min apart. Four stimulations were performed for each treatment per rat and only one drug treatment was given per rat.

Pharmacological Treatments

All treatments were administered by reverse dialysis with at least 30 min allowed before stimulation. Treatments were as follows: Na^+ channel blockage, 2 μM tetrodotoxin (TTX); Ca^{2+} blockage, 2 mM EGTA in Ca^{2+} free CSF (same as regular CSF, without $CaCl_2$ added); uptake inhibition, 200 μM L-trans-pyrrolidine-2,4-dicarboxylic acid (PDC); mGluR blockage, 200 μM (RS)-α-methyl-4-carboxyphenylglycine (MCPG) (Tocris Cookson, Ballwin, MO, USA); mGluR activation, 200 μM (1S,3R)-1-aminocyclopentane-trans-1,3-dicarboxylic acid (ACPD) (Tocris Cookson) or 20 μM o-phosphoserine (LSOP).

Results

Basal levels of Glu and Asp in dialysates obtained from the hippocampus were

310 ± 40 nM and 87 ± 11 nM (n = 21) respectively. Average *in vitro* relative recoveries at 37 °C were 36.5 ± 1.2 % and 39.4 ± 1.6 % for Glu and Asp respectively.

As shown in Figure 4-1, we observed that with the onset of electrical pulses, Glu level rose instantaneously, within the limits of our temporal resolution, and continued to increase during the entire stimulation. As soon as the stimulus was ended, Glu level began to decline and returned to pre-stimulus basal levels within 20 s. Interestingly, the level after stimulus was often slightly lower than the prestimulus level. The amount of Glu collected by the dialysis probe over basal level as a result of the stimulation averaged 66.5 ± 7.3 fmol (n = 80 stimulations in total of 21 rats). The maximal level achieved during the stimulation was 112 ± 3% of the basal level. The response of Glu to successive stimulations was highly reproducible as shown by the traces in Figure 4-1A and C with no significant difference in maximum Glu increase, duration, or peak area after 4 stimulations. The high reproducibility of successive stimulations allowed changes in stimulated Glu levels to be precisely monitored by this approach. Asp showed a small change correlated with the stimulation that is only apparent after averaging all stimulations together (Figure 4-1B). In view of the difficulty of measuring changes in Asp level, it was not quantified in further studies.

Effect of Na^+-Channel Blockade with TTX and Ca^{2+} Depletion

To ascertain if the observed Glu concentration changes were related to neuronal events, we tested the TTX-sensitivity and Ca^{2+}-dependency of the signals. Infusion of 2 μM TTX through the probe in the hippocampus did not significantly affect basal Glu or Asp levels (summary of basal data are given in Table 4-2). TTX infusion completely eliminated electrically-stimulated increases in Glu concentration in the hippocampus, as

seen in Figures 4-2A and Table 4-3. Removal of Ca^{2+} from the dialysis medium with addition of 2.0 mM of the Ca^{2+}-chelator EGTA, resulted in no change in the basal level for Glu or Asp in the hippocampus as shown in Table 4-2; however, this manipulation significantly ($p < 0.005$) reduced the stimulated overflow of Glu in the hippocampus to $17 \pm 4\%$ of the stimulated overflow in control conditions ($n = 12$ stimulations in 3 rats) as shown in Figures 4-2B and Table 4-3. The observation that EGTA did not completely halt electrical stimulation is likely due to ineffective removal of extracellular Ca^{2+}.

mGluR Regulation of Glu

mGluR autoreceptors are reported to have significant effects on glutamate release in the hippocampus. We therefore examined the effect of infusion of different mGluR antagonists and agonists on the basal and stimulated level of Glu in the hippocampus. Infusion with 200 μM MCPG, a broad spectrum mGluR antagonist, increased the basal level of Glu to $116 \pm 5\%$ ($p < 0.05$) of the control value and increased the stimulated overflow (measured as the area under the peak) to $190 \pm 11\%$ of the control ($p < 0.02$, $n = 12$ stimulations in 4 rats) as shown in Figures 4-3 and Table 4-2. This result indicates significant autoreceptor control over release during electrical stimulations. Asp basal levels increased dramatically with MCPG (Table 4-2), but substantial stimulated release was not observed. Addition of the group I and II agonist ACPD (200 μM) to the dialysis perfusion medium decreased the basal Glu level to $87 \pm 5\%$ of control ($p < 0.05$) but did not significantly affect the stimulated overflow (overflow was $102 \pm 21\%$ of control, $n = 16$ stimulations in 4 rats) as shown in Figure 4-4A. As ACPD is only effective at group I and II mGluR, we also examined the effect of L-SOP, a group III agonist. At 20 μM L-SOP did not significantly affect either the basal (Figure 4-4B and Table 4-2) or

stimulated overflow of Glu in the hippocampus (Table 4-3). These results indicated that the blockade of autoinhibition apparent with MCPG was achieved at basal concentrations of Glu and further addition of agonist had no additional inhibitory effect. Interestingly, when a higher concentration of LSOP (200 μM) was added, the opposite effect as expected was seen. 200 μM LSOP increased Glu to 166 +/- 19% and Asp to 152 +/-10% above basal (Figure 4-4C and Table 4-2). Stimulated overflow of Glu was also increased by 162 +/- 21% of control values (Table 4-3).

Effect of Uptake Inhibition

Infusion of the transportable Glu uptake inhibitor PDC (200 μM) into the hippocampus caused a dramatic increase in both Glu and Asp to 614 ± 81% and 540 ± 74% (n = 4) of basal levels which may reflect both decreased uptake and increased efflux of these amino acids by reverse transport. (see Figure 4-5 and Table 4-2) This result is in agreement with previous studies on the effect of PDC on basal Glu level in the hippocampus (ZUI96, OBR96). PDC also caused a dramatic increase in the electrically stimulated overflow of Glu to 987 ± 146% of control stimulations ($p < 0.0001$, n = 16 stimulations in 4 rats). (Figure 4-5 and Table 4-3) In the presence of PDC, changes in Asp were still not observed aside from small change after the end of the stimulus. Since PDC raised basal levels and affected the endogenous agonist of the mGluR, the effect of MCPG was re-tested under these elevated basal conditions. Addition of 200 μM MCPG to the perfusion fluid after 40 min of PDC treatment reduced the basal level of Glu and Asp to 431 ± 90% and 397 ± 65% (n = 4) of control basal levels. This was a statistically significant decrease from the PDC induced basal level ($p < 0.05$). Electrically stimulated overflow of Glu was reduced to 583 ± 146% of control (n = 14 stimulations in 4 rats)

which was significantly smaller ($p < 0.05$) than the overflow that occurred with only PDC present. Traces illustrating the effect of PDC and PDC with MCPG on the stimulated overflow are shown in Figure 4-5 and a summary the effects on basal and stimulated overflow are shown in Tables 4-2 and 4-3 respectively. Reversal of the order of addition of MCPG and PDC did not affect the final result (data not shown).

Discussion

The measurement of electrical stimulation of the perforant path proved to be an analytically challenging task. Because the average change in Glu was only 12% over basal, the instrument reproducibility became the limiting factor in being able to measure a change. It was necessary to use great care in maintaining and setting up the instrument. For example, mechanical factors such as keeping the syringe pumps well oiled and the injection valve and rotor clean were crucial in minimizing variability. Additionally any misalignment in the flow gated interface contributed significantly to injection irreproducibility.

Another factor to consider in the measurement of such small changes is the sensitivity of the detector. An average change of 12% in dialysate of Glu corresponds to a concentration change of 36 nM. For Asp, this change would be only 10 nM. It is likely that this small a change in Asp was below the sensitivity of the instrument, supported by the fact that a change in Asp could only be seen after averaging all stimulations. The response of Asp is discussed below.

Evidence for Synaptic Glu Overflow in Hippocampus Following Perforant Path Stimulation.

In these experiments we evaluated glutamate level under basal, i.e., steady state, conditions and dynamically during electrical stimulation. In the absence of an applied stimulus, basal levels of Glu and Asp are insensitive to either pharmacological blockade of voltage-activated sodium channels or a marked reduction in the concentration of extracellular free calcium ions (Table 4-2). The insensitivity of extracellular EAA levels to these experimental manipulations have been reported widely by other investigators and have been used as supportive evidence for the hypothesis that extracellular EAA levels *in vivo* do not provide an accurate measure of neurogenically-derived EAA release (FIL95; TIM97; HER96). In this regard, the fast (5 s) sampling intervals with on-line measurement of EAA level used in this study have provided data that parallel results from studies that employ much longer (up to 15 min) sampling intervals. However, the clear advantage of fast on-line measurements is apparent when this approach is used to monitor rapid changes in extracellular EAA levels initiated by a brief electrical stimulus. Similar to previous reports that utilized sensors (HU94; WAL95), extracellular Glu concentration in the hippocampal formation exhibits close temporal coupling with perforant path stimulation insofar as Glu level undergoes a sharp rise and fall that coincides closely with the onset and termination, respectively, of a 20-s stimulus period (Fig. 4-1). In view of the modest size and duration of the stimulated rise in hippocampal extracellular Glu, it is likely that conventional microdialysis sampling methods would not detect such brief elevations of extracellular Glu owing to the extensive loss of signal caused by protracted temporal averaging. For the first time, we demonstrate that these changes exhibit complete TTX-sensitivity as well as a nearly total reliance upon extracellular free Ca^{2+} (Fig. 4-2). From the temporal relationship, TTX-sensitivity, and

Ca^{2+}-dependence, it appears that impulse-dependent neuronal release is the major contributor for this increased extracellular Glu level following perforant path stimulation. In light of these observations, we conclude that, following exocytotic release from hippocampal nerve terminals, a significant amount of Glu can diffuse from synapses into the surrounding extracellular fluid. As a consequence of this synaptic overflow, it is likely that a rapidly dissipating wave of Glu diffuses into the surrounding tissues wherein it could elicit non-synaptic excitatory effects.

The detected overflow was greatly increased in the presence of PDC, a competitive and transportable inhibitor of glutamate uptake. These results support the hypothesis that uptake plays a strong role in preventing spread of the glutamate signal and cross-talk among neurons in the hippocampus. This idea has previously been advanced based on theoretical and electrophysiological studies of Glu spread in the hippocampus (RUS98, ASZ97, CLE92).

mGluR Control

While uptake plays an obviously strong role in regulating the spread of a Glu signal, the role of mGluR is less clear from our results. Metabotropic glutamate receptors have been implicated as autoreceptors in regulation of Glu release with both facilatory and inhibitory effects having been observed (LIU95, SCA97). In our experiments we observed a fairly weak autoreceptor regulation of stimulated overflow. For example, addition of ACPD (agonist for group I and II mGluR) or 20 μM L-SOP (agonist for group III mGluR) had no effect on stimulated release and MCPG (broad spectrum antagonist) caused a small increase in stimulated overflow. These results are consistent with the notion of autoinhibition of release mediated by mGluR that is maximally

activated under basal conditions so that addition of agonist does not inhibit release but antagonist can block the endogenous ligand and give rise to enhanced release. Interestingly, in the presence of PDC, where endogenous ligand level was enhanced 914%, MCPG actually had the opposite effect on overflow and substantially reduced it as well as the basal level. These results are consistent with a feed-forward mechanism of glutamate release mediated by mGluR under conditions of high agonist availability (HER92, TIZ95, LIU95). Thus, it appears that when Glu levels are low, autoreceptors are active that mediate an inhibition of release so that antagonists increase the stimulated release of Glu; however, when glutamate levels are high, mGluR mediate positive feedback thus giving rise to a decrease in release with antagonist. A previous *in vivo* microdialysis study of the hippocampus of freely moving rats revealed a similar regulation of Glu level in that mGluR mediated tonic inhibitory and phasic excitatory control over Glu release (LIU95). A detailed explanation of this observation would require considerably further study. It should be recognized that the dialysis probes are relatively large and sample Glu release from multiple sub-regions of the hippocampus and many neurons and glia. Since multiple sub-types of mGluR with opposite effects are co-localized and heterogeneously distributed throughout the hippocampus (SHI97), this lack of spatial resolution available with microdialysis makes interpretation of the results difficult. Probes with better spatial resolution and more selective drugs would be required to better address this unusual effect.

Regulation of Extracellular Asp

While the major focus of this investigation has centered on changes in hippocampal extracellular Glu levels during perforant path stimulation, it remains unclear

whether or to what degree Asp may contribute to the synaptic or extra-synaptic effects of EAA within the hippocampal formation. Our previous study of stimulated changes in striatal EAA levels revealed large parallel increases in both Glu and Asp following electrical stimulation of the prefrontal cortex (LAD98). Results from that study provided compelling and novel evidence for exocytotic Asp release insofar as the stimulated rise in Asp occurred simultaneously with the rise in extracellular Glu and was completely attenuated by calcium depletion or TTX treatment. In light of these earlier results, we believe that Asp could exhibit a similar profile in hippocampus and potentially play a role in synaptic or non-synaptic excitatory communication. Indeed, following perforant path stimulation a small increase in hippocampal extracellular Asp levels is detectable (Fig. 4-1B). The low signal to noise ratio of the Asp signal required extensive signal averaging to detect this change; therefore further characterization of the Asp signal was not performed; however, in view of the basal levels of Glu (310 nM) and Asp (87 nM) in dialysate samples, the average peak rise in Asp following perforant path stimulation represents approximately 20 percent of the net stimulated rise in extracellular Glu concentration. This result agrees closely with studies in hippocampal tissues *in vivo* wherein depolarizing stimuli have been reported to release Glu and Asp in a 5:1 ratio (SZE87, BUR88, ZHO95). In view of this data and the close temporal coupling between perforant path stimulation and the rise in extracellular Asp, we suggest that the stimulated increase in Asp level may derive from neuronal exocytotic release. While it remains to be determined whether Asp exhibits the expected requirement for calcium and TTX sensitivity, several lines of evidence support our premise that Asp undergoes exocytotic release in the hippocampus. Studies *in vivo* reveal that a variety of depolarizing stimuli

can elicit calcium-dependent release of Glu and Asp from hippocampal synaptosomes (ZHO95) as well as hippocampal slices (SZE87; BUR88, NAD90, ROI91, KLA92). In addition, a recent report by Gundersen and coworkers (1998) indicates that Glu and Asp are co-stored in hippocampal synaptic vesicles and that both amino acids are depleted from vesicles through a tetanus toxin-sensitive process following depolarization of hippocampal slices (GUN98). Taken together, these results provide compelling evidence for exocytotic Asp release from hippocampal neurons. In view of our *in vivo* evidence for exocytotic Asp release in striatum (LAD98), the approach of Gundersen and coworkers (1998) may prove useful in order to determine whether Asp and Glu are co-stored in synaptic vesicles of the striatum or other forebrain regions. Although evidence regarding vesicular localization and calcium-dependent release are just two of several criteria that must be satisfied in order to validate Asp as an excitatory neurotransmitter, it is important to note that this issue remains unresolved. Previous failures to detect Asp within synaptic vesicles have been used to discount a possible transmitter role for Asp within forebrain pathways (FIL95). However, we have noted that nearly all studies that have reported a lack of vesicular Asp uptake/storage have been carried out in homogenates or purified subcellular fractions from the cerebral cortex. (BUR89, CAR89, VIL90, TAB92). In view of the convincing results of Gundersen and coworkers (1998) in hippocampal slices, it seems plausible that vesicular pools of Asp may be extremely labile or factor(s) that are required for vesicular Asp uptake may be depleted during subcellular fractionation procedures. Alternatively, neurons within the cerebral cortex may differ from excitatory neurons in other brain regions with respect to the capacity for Asp uptake or storage. In any event, we conclude that current evidence regarding a

possible role of Asp as a neurotransmitter or neuromodulator in the hippocampal formation is inconclusive and warrants more careful consideration.

In conclusion, electrical stimulation of the perforant yields an increase in extracellular Glu that is susceptible to Na^+ channel blockage and Ca^{2+} depletion, indicating a neuronal origin. Additionally, application of mGluR agonists and antagonists indicate that the receptors are activated under normal conditions.

Table 4-1. Additives Used for Glu Characterization.

Additive	Abbreviation	Action	Reference
(1S,3R)-1-aminocyclopentane-trans-1,3-dicarboxylic acid	ACPD	Group I and II metabotropic receptor agonist	KAH93 BRO95 PIN95
l-serine-o-phosphate	LSOP	Group III metabotropic receptor agonist	NAK92 SAU94
(RS)-a-methyl-4-carboxyphenylglycine	MCPG	Group I, II, and III metabotropic receptor antagonist	CHO96
L-trans-pyrrolidine-2,4-dicarboxylic acid	PDC	Glu uptake inhibitor	BRI91 GRI94
Bis-(aminoethyl)glycoether-N,N,N',N'-tetraacetic acid	EGTA	Ca2+ chelator, disrupts Ca2+ channels	IMP84
Tetrodotoxin	TTX	Na+ channel blocker	WES87

Table 4-2. Effects of Chemical Additives on Basal Levels of Glutamate and Aspartate

Treatment	Glu (% of Control)	Asp (% of Control)
Control	100 +/- 12	100 +/- 8
2 μM TTX	97.8 +/- 1.2	100 +/- 4
2 mM EGTA/Ca2+ Free	96.7 +/- 11.5	98.7 +/- 9.5
200 μM ACPD	87.4 +/- 5.5*	73.5 +/- 16.1*
20 μM LSOP	103 +/- 3	86.2 +/- 7.4*
200 μM LSOP	166 +/- 19	152 +/- 10*
200 μM MCPG	116 +/- 5*	328 +/- 130*
200 μM PDC	614 +/- 81*	540 +/- 117*
200 μM PDC/MCPG	431 +/- 90.1*	397 +/- 65*

Basal Levels of glutamate and aspartate were 310 +/- 40 and 87 +/- 11 nM respectively ($n = 21$). Values in the table are expressed as percent of control levels, mean +/- SEM following a 30 min infusion of the drug ($n = 4$ for additives).
* indicates significantly different from control ($p < 0.01$)

Table 4-3. Effects of Chemical Additives on Electrically Stimulated Levels Glutamate

Treatment	Glu (% of Control)
Control	100 +/- 11
2 μM TTX	3.0 +/- 1.0*
2 mM EGTA/Ca2+ Free	17.1 +/- 4.3*
200 μM ACPD	95.8 +/- 21.5
20 μM LSOP	103 +/- 17
200 μM LSOP	162 +/- 21
20 μM LSOP	103 +/- 17
200 μM MCPG	190 +/- 9
200 μM PDC	987 +/- 146*
200 μM PDC/MCPG	583 +/- 146*

Data for electrically stimulated increases in glutamate were determined as net changes over baseline values. Control evoked response was 66.5 +/- 7.3 fmol (n = 80 stimulations, 21 rats). Values in the table are expressed as percent of the control levels, mean +/- SEM. For additives, n = 16, 4 rats.
* indicates significantly different from control ($p < 0.02$)

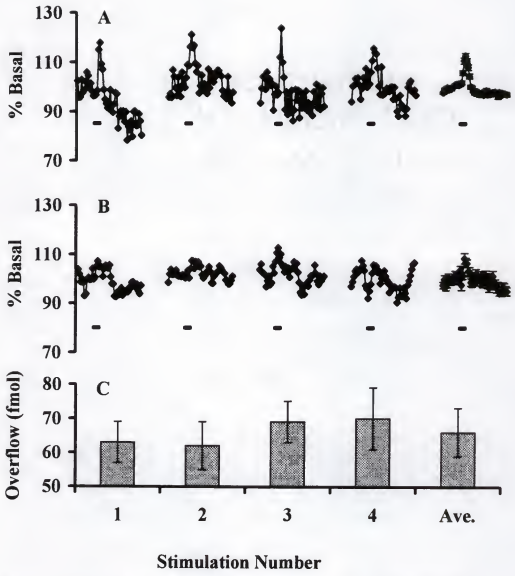

Figure 4-1. Electrical stimulation of the perforant path. Traces represent four consecutive stimulations spaced 20 min apart followed by the averages trace +/- SEM. A) Glu, B) Asp. C) Bar graph representing the average Glu overflow for consecutive stimulations followed by the overall average overflow (n = 20). Bars in A and B denote stimulation and represent 20 s.

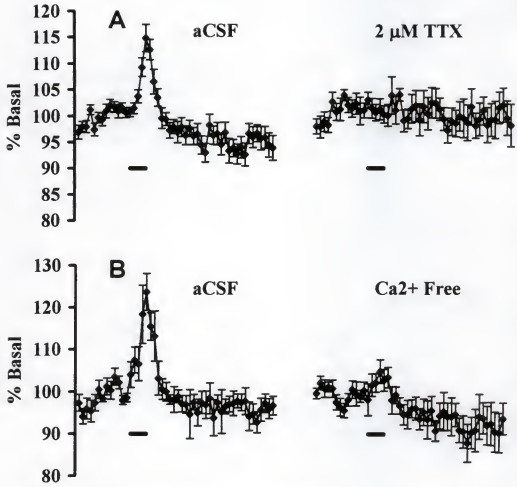

Figure 4-2. Evidence for neuronal origin of electrically stimulated Glu. A) Blocking sodium channels with 2 μM TTX or B) Removing calcium with 2 mM EGTA in calcium free aCSF obolishes stimulated overflow but does not alter basal levels. Bars indicate stimulation and correspond to 20 s. (4 rats, n = 16)

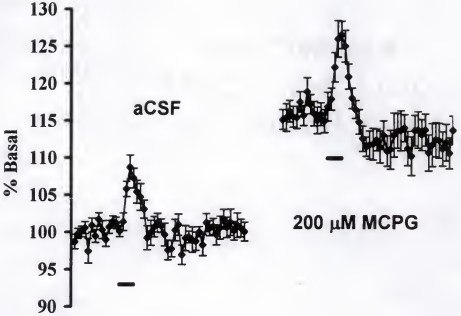

Figure 4-3. Effect of metabotropic receptor blockage on electrically stimulated Glu. Addition of 200 μM MCPG to the perfusion medium results in a 116% increase in basal levels and 190% increse in stimulated overflow of Glu. Bars indicate stimulation and correspond to 20 s.

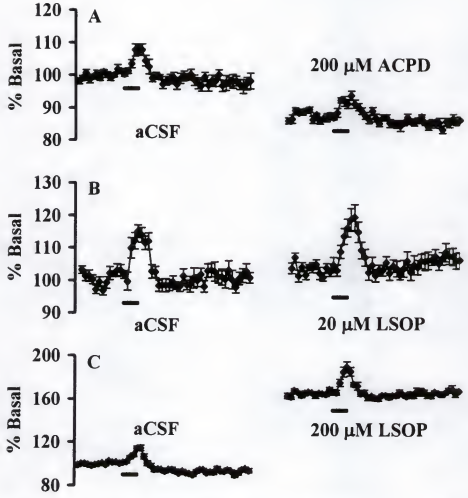

Figure 4-4. Effect of metabotropic receptor activation on electrically stimulated Glu A) Activation by 200 μM ACPD. Basal levels increased to 87 % of control while stimulated overflow did not change B) Activation by 20 μM ACPD. elicited no change in either basal or stimulated overflow of Glu. C) Activation by 200 μM LSOP. caused an increase in basal and stimulated overflow by 166% and 162%, respectively. Bars indicated stimulation and correspond to 20 s.

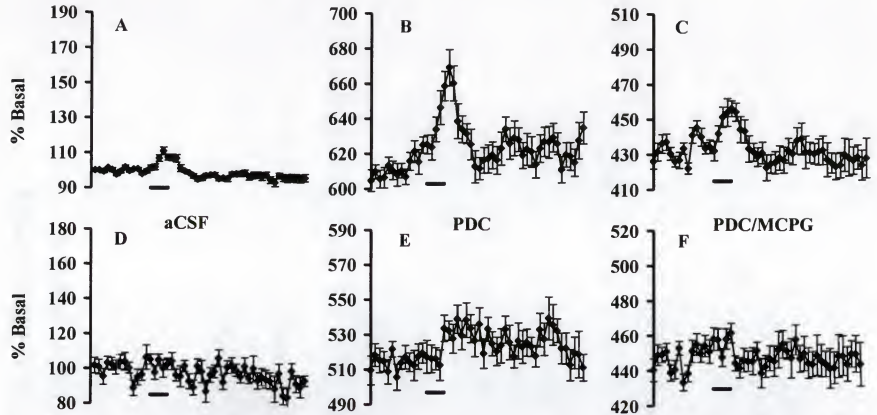

Figure 4-5. Effect of uptake inhibition on electrically stimulated Glu and Asp. A and D) control stimulation. B and E) Inhibition of uptake with 200 μM PDC added to the perfusion medium results in a 614% increase in basal levels of Glu and a 987% increase in stimulated overflow. Asp basal levels increases by 510%. C and F) 200 μM PDC and 200 μM MCPG decreases Glu and Asp relative to PDC only to 430% and 450% of original basal. Stimulated overflow of Glu decreases to 580% of control. Bars indicate stimulation and correspond to 20 s.

CHAPTER 5
REGIONAL DIFFERENCES BETWEEN STRIATUM AND HIPPOCAMPUS: EVIDENCE FOR VOLUME TRANSMISSION

Introduction

There are two types of synaptic transmission, volume or wire transmission (see ZOL96, ZOL98, ZOL99 for reviews). In the first, a neurotransmitter can diffuse out of the synaptic cleft and interact with neighboring cells. Dopamine is considered the model transmitter for this type of communication (VIZ91, BUN99). In wire transmission a synapse is completely insulated and once a neurotransmitter is released it cannot escape the synaptic cleft to interact with other neurons. The glutamatergic system is thought to use this type of transmission because Glu neurons are typically ensheathed in glial cells (CLE92, MEN95). This line of evidence has been used to discount the ability of microdialysis to make a meaningful measurement of Glu (TIM97). However, recent studies have demonstrated the possibility that Glu can escape from the cleft and perhaps participate in limited volume transmission (RUS98, MIT00, KUL96, KUL98). Additionally, in results presented in the previous chapter and elsewhere (LAD98), we have demonstrated that Glu and Asp can diffuse into the extracellular space under electrically stimulated conditions in both the hippocampus and striatum.

In view of these observations, a further examination of the previous data is warranted. In this chapter the characteristics of electrically stimulated release and their modulation by mGluR active drugs in both regions are compared with respect to volume

vs. wire transmission. To further elucidate the transmission properties in each region addition experiments were conducted to determine the extent of extracellular transport and diffusion.

Experimental

Chemicals and Reagents

All chemicals were purchased from Sigma Chemical (St. Louis, MO USA). All fused silica capillary tubing was from Polymicro Technologies (Phoenix, AZ, USA) and had a 360 μm outer diameter (o.d.) unless noted otherwise.

Capillary Electrophoresis and Laser-Induced Fluorescence Detection

The CE-LIF system for monitoring dialysate was the same as described in Chapter 2. Dialysate was derivatized on-line by pumping 10 mM *o*-phthaldialdehyde/40 mM β-mercaptoethanol (OPA/BME) in 35 mM borate at pH 10.5 at 0.60 μL/min via a syringe pump (Harvard apparatus, Holliston, MA, USA) into a tee attached to the outlet of the dialysis probe. The dialysate and OPA/BME were allowed to mix and react for 50 s as they flowed out of the tee and through a 16 cm long by 75 μm i.d. fused silica reactor capillary. Derivatized dialysate was pumped from the reactor capillary into a flow-gated interface which allowed automatic injection onto the electrophoresis capillary. Dialysate was electokinetically injected for 40 ms at the separation voltage every 3.5 s. Electrophoresis was carried out inside a 5 cm long (3.5 cm from injection point to detector) by 10 μm i.d. capillary. Voltage was applied by grounding the flow-gated interface and applying −14.5 kV to a buffer reservoir that was connected to the outlet of the separation capillary by 20 cm long by 150 μm i.d. linker capillary. The

electrophoresis buffer was 40 mM carbonate adjusted to pH 9.5 with NaOH.

Fluorescence detection was performed on the electrophoresis column with an epillumination fluorescence microscope (Carl Zeiss, Hanover, MD, USA). Fluorescence was excited with 1.3 mW of the 354 nm line of a He-Cd laser (Liconix, Carlsbad CA, USA). Emission over 400 nm was collected with a 40x objective and detected by a PMT (CRG Instruments, Austin, TX, USA). Data was collected via a personal computer (Gateway, Sioux City, SD, USA) and data acquisition board (AT-MIO-16F-5, National Instruments, Austin, TX, USA) at 1 kHz and low-pass filtered at 200 Hz. All collection and analysis software was written in house in Lab Windows (National Instruments).

Microdialysis

Side by side microdialysis probes were constructed as described in Appendix 2. Probes consisted of 9 cm of 20 μm i.d. x 100 μm o.d. fused silica capillary as the inlet and 7 cm of 20 μm i.d. and 100 μm o.d. as the outlet. The dialysis membrane was regenerated cellulose (Spectrum, Houston, TX, USA) with 18 kD cutoff and the tip sealed with polyimide sealing resin (Alltech Associates, Deerfield, IL, USA). Active areas were 200 μm o.d. and 2 mm in length. Before use, all probes were perfused with 70% ethanol in water for 30 min at 1.2 μL/min followed by perfusion with artificial cerebrospinal fluid (aCSF) that consisted of 145 mM NaCl, 2.68 mM KCl, 1.01 mM $MgSO_4$, and 1.22 mM $CaCl_2$, for a minimum of 30 min. Unless otherwise stated, perfusion flow rate was 0.60 μL/min and was driven by a syringe pump (Harvard apparatus, Holliston, MA, USA) for all experiments. Calibration and *in vitro* recovery was performed before implantation by placing the probe in Glu and Asp standards dissolved in aCSF held at 37 °C. For calibration and *in vivo* experiments, the outlet

capillary of the probe was connected to the reactor tee described above for on-line CE-LIF analysis.

Surgical Procedures

Male Sprague-Dawley rats (250-350 g) were anesthetized with 100 mg/ml in H_2O chloral hydrate by an initial subcutaneous injection of 400 mg/kg followed by booster injections of 100 mg/kg at 30 min intervals until the rat no longer exhibited a withdrawal reflex to limb pinch. Additional injections were given as needed. Microdialysis probes were stereotaxically implanted in the dentate gyrus at AP – 3.8 mm, ML –3.0 mm, DV = -4.7 mm (from dura) from bregma. Concentric bipolar stimulating electrodes (Rhodes Medical Equipment, Woodland Hills, CA, USA) were stereotaxically implanted in the lateral perforant path at AP 0.0 mm, ML –4.4 mm, DV –3.5 mm (from dura) from lambda. Both probe and electrode were implanted over a period of 15 to 20 min in order to minimize tissue damage. Recordings were made at least 1 h post implantation and after basal levels were found to stabilize.

All experimental uses of laboratory rats in the present study were reviewed and approved by the University of Florida Institutional Animal Care and Use Committee and conform with policies and procedures set forth by U.S. Public Health Service Policy on Humane Care and Use of Laboratory Animals.

Infusion of D-Asp

For comparison of EAA clearance between the hippocampus and striatum, exogenous D-aspartate was microinjected into the brain region of interest. For these experiments, a 75 μm i.d. fused silica capillary was co-implanted with the dialysis probe. The microinjection capillary was clamped to the same holder as the dialysis probe so that

its outlet was at the dorsal-ventral center of the 2 mm dialysis probe active area and approximately 350 μm medial of the dialysis probe, see Figure 5-1. The outlet tip of the microinjection capillary was ground to a fine point with a Dremel tool so that its o.d. was approximately 90 μm. The inlet of the injector capillary was connected to a 10 μL glass microsyringe (Hamilton). For infusions, 200 nL of 1 mM D-Asp in aCSF was manually injected as recordings were made with the CE-LIF system. To minimize inter-animal variability measurements were performed in the hippocampus and striatum in each rat when possible.

Data Analysis

Electropherograms were analyzed using a statistical moments program written in house (Lab Windows). Glu and Asp peaks were marked manually and dialysate concentration determined by *in vitro* calibration. The 100 % basal level was measured as the average concentration of neurotransmitter (NT) in 10 electropherograms immediately prior to stimulation. Elevated or reduced concentrations due to chemical additives were determined by comparison to the NT concentration before application of the additive. Stimulated overflow was calculated as the total mass of NT collected by the microdialysis probe above the average pre-stimulus level. A two-tailed student's t-test was used to determine all statistical differences.

Results

Comparison of Electrically Stimulated Release in the Striatum and Hippocampus

Striatal stimulations from Chapter 3 and hippocampal stimulations from Chapter 4 are replotted in Figure 5-2. In contrast to the results in the hippocampus, we observed

large changes in Glu in the striatum flowing electrical stimulation of the PFC. Like the results in the hippocampus, the increase began immediately with the stimulation and began to decrease following end of the stimulation. The levels returned to baseline within 40 s. We have also previously characterized the effects of TTX, Ca^{2+} removal, ACPD, MCPG, PDC, and PDC with MCPG on this overflow and basal levels (LAD98). The results from this prior study are summarized in Figures 5-3 and 5-4 for efficient comparison to the data from the hippocampus from Chapter 4.

A striking difference between the electrically stimulated overflow in the hippocampus and the striatum is the magnitude of the responses. Using similar dialysis probes, the average amount collected during a 10 s stimulation in the striatum was 328 ± 31 fmol (n = 17 stimulations from 7 rats) which is 490% of the hippocampus signal (difference significant to $p < 0.001$). Furthermore, the maximal increase was 176 ± 13% for the striatum and 112 ± 3 % in the hippocampus ($p < 0.0001$). The net amount of stimulated Glu overflow is a reflection of Glu release, both synaptic and extrasynaptic, and Glu elimination by active (Glu transport) and passive (diffusion) processes; therefore, it is not possible to discern whether the differences in the electrically stimulated release in the two brain regions are mediated by differences in release or elimination.

Microinjection of D-Asp

To better distinguish the differences in elimination in the two brain regions, we carried out complimentary studies in which a fixed amount (200 pmol) of D-Asp was rapidly infused from a micropipette that was positioned 350 μm from the microdialysis probe and followed the kinetics of D-Asp recovery. D-Asp was selected as the analyte for these experiments in view of the following: (1) it is a chemically stable compound

that is resistant to enzyme-catalyzed degradation and exhibits little or no pharmacological activity at the concentrations used here; (2) D-Asp interacts with EAA transporters in a manner similar to L-Glu insofar as it binds to and is transported by all known classes of EAA transporters with low micromolar affinity; and (3) D-Asp possesses charge characteristics and diffusion properties that are similar to L-Glu.

Dialysate basal levels in the hippocampus were 690 ± 100 nM for Glu and 260 ± 60 nM for Asp and in the striatum 330 ± 120 nM for Glu and 120 ± 40 nM for Asp. This difference in concentrations is consistent with other results (TOS86). Relative recoveries were 37.9 ± 2.2 % for Glu and 42.8 ± 1.8 % for Asp. Infusion results are shown in Figure 5-5. In the striatum 7.4 ± 1.2 pmol (n = 20) was recovered in the dialysis probe from an infusion which was significantly more ($p < 0.0001$) than the 2.2 ± 0.5 pmol (n = 14) recovered in the hippocampus. In the presence of PDC, the amount collected in the striatum was increased to 11.8 ± 1.8 pmol (160% of the control, $p < 0.05$). In the hippocampus, the PDC had a larger effect increasing the amount collected to 4.8 ± 1.3 pmol (218% increase, $p < 0.02$). To further characterize the tissue clearance of D-asp in the two brain regions, we analyzed the decay rate of D-Asp level in the dialysate following the direct infusion as shown in Figure 5-6. Linear decay rates were seen for all conditions in both brain regions. In striatum, clearance rate was $0.189 \pm 0.001\ s^{-1}$ and $0.140 \pm 0.007\ s^{-1}$ for control and PDC conditions respectively while in the hippocampus the clearance rates were $0.146 \pm 0.01\ s^{-1}$ and $0.089 \pm 0.003\ s^{-1}$. Thus, the clearance rate in the striatum was significantly higher for the striatum than for the hippocampus ($p < 0.005$) and addition of PDC significantly decreased the clearance rate in both brain regions ($p < 0.001$). The data also indicate however that PDC had a greater effect on the

decay rate in the hippocampus than in the striatum.

Discussion

Comparison of Electrically Stimulated Overflow in Hippocampus and Striatum.

The electrically stimulated overflow of Glu in the hippocampus provides an interesting comparison to results for overflow in the striatum following electrical stimulation of prefrontal cortex. As shown in Figure 5-2, in both cases a rapid rise in Glu was detected that was well correlated with the stimulus in that the rise began immediately after the stimulus and began to decrease at the termination of the stimulus. As in the hippocampus, the stimulated overflow of Glu in striatum was TTX-sensitive and Ca^{2+}-dependent. These results suggest a neuronal origin for the electrically stimulated signal in striatum as well as the hippocampus. In contrast to the rather weak and complex mGluR effects observed in the hippocampus, we have previously observed a strong autoinhibition of electrically stimulated Glu overflow in the striatum mediated by mGluR (LAD98). As shown in Figure 5-4, ACPD could drastically inhibit release, an effect that was antagonized by MCPG. When glutamate levels were elevated by PDC, overflow was not increased because release was strongly autoinhibited as evidenced by the large increase in overflow by addition of MCPG (see Figure 5-4). These results led to the conclusion that increasing agonist availability activated mGluR to suppress Glu release in a classical autoinhibitory fashion. We also did not observe any switching of the effect of mGluR at different agonist concentrations in the striatum unlike in the hippocampus. Thus, from the electrical stimulation results it is apparent that overflow is regulated differently in the striatum and hippocampus. In the hippocampus, overflow is dominantly regulated by uptake as indicated by the strong effect of PDC. mGluR autoreceptors do

not strongly restrict overflow and in fact, at high agonist availability actually seems to promote release. In the corticostriatal pathway, transporters and autoreceptors appear to work together to restrict and regulate overflow. The importance of autoreceptors can be seen in that with uptake inhibited, no strong overflow occurs because of activation of autoinhibition.

Roles of Diffusion and EAA Transporters in Shaping Glu Overflow

An obvious difference in the stimulated overflow is that hippocampal responses are considerably smaller and of shorter duration than the response evoked in striatum (Figure 5-2). To discern whether the differences in overflow magnitude are mediated by differences in release or elimination we examined the time course of microinjections of fixed amounts of D-Asp in the two brain regions. This experiment allows the elimination and transport processes to be studied in isolation of release processes. As shown in Fig. 5-5, recovery of D-Asp in a microdialysis probe positioned 350 μm from the injection site was reduced by more than 70% in hippocampus relative to striatum. Factors that could give rise to the marked reduction in hippocampal peak amplitude and duration include more efficient transport of D-Asp into hippocampal neurons and glia or a decreased rate of D-Asp diffusion in hippocampal tissues. Studies with the competitive EAA transport inhibitor PDC lead us to conclude that both factors contribute to the diminished recovery of D-Asp in hippocampus relative to striatum. While pretreatment with a high concentration of PDC (200 μM) enhances D-Asp recovery by the probe in both regions, the impact of EAA transport inhibition is two-fold greater in the hippocampus (118 ± 36% vs. 59 ± 15% increase for hippocampus and striatum, respectively) (Fig. 5-5B). This *in vivo* evidence for greater EAA transporter activity

within the hippocampus is consistent with results from *in vitro* studies, including evidence for a greater density of sodium-dependent high-affinity D-[^{3}H]Asp binding sites, a useful marker for EAA transporters, throughout the hippocampal formation relative to striatum (AND90, GRE90, SEI91).

Further examination of the data suggests differences in the diffusional properties of D-Asp between hippocampus and striatum as well. Plots of concentration decay rates in both tissues are shown in Fig. 5-6. Inspection of these data reveals linear rates of decay as a function of concentration in hippocampus and striatum in both the absence and presence of PDC. The signal decays because of both reuptake by the tissue and diffusion away from the probe. The response does not show saturation, which would be indicated by non-linearities at higher concentrations, that would be expected for Michaelis-Menton kinetic control of the decay as expected for reuptake. This may be because diffusion, which would be linear under any condition, is participating in the decay or because the concentrations necessary for saturation were not reached by this experiment. Nevertheless, the results show that the decay rate is significantly lower in the hippocampus than in the striatum, even in the presence of uptake inhibitors. A slower decay rate is due to less reuptake or slower diffusion away from the probe. Since the curve areas suggest greater reuptake in the hippocampus, the lower decay rate must be due to more restricted diffusion. This conclusion is consistent with the expected effective diffusion coefficients (D_{eff}) in the striatum and hippocampus. $D_{eff} = D/\lambda^2$ where D is the diffusion coefficient in buffer and λ is the tortuosity factor of the tissue (HAR49). In the striatum λ is 1.54 (RIC91) leading to an expected D_{eff} of 4.8×10^{-6} cm^2/s. In the hippocampus, the tissue is anisotropic with an average $\lambda = 1.61$ (MAZ98) giving rise to a

D_{eff} of 4.4 x 10^{-6} cm^2/s. (D for glutamate is 1.14 x 10^{-5} cm^2/s which was used for D-Asp in this estimation) (NIC81).

To summarize, direct infusion of D-Asp into the hippocampus and striatum reveals greater reuptake and slower diffusion for EAAs in the hippocampus than in the striatum. This result indicates a greater restriction on the spread of an extracellular concentration pulse of Glu in the hippocampus than in the striatum. This observation helps explain the large difference in stimulated overflow that was observed in the two brain regions. Even with the magnitude of these effects taken into account, it appears that the electrically stimulated hippocampal Glu signals are weaker than those observed in the striatum suggesting less release as well. It is difficult to conclude anything significant from this observation however because the amount released could be affected by the number of neurons in the tract, their relative density at the site of measurement, and the effectiveness of the stimulation.

Implications for EAA Mediated Volume Transmission

Glutamate is generally considered to be a point-to-point neurotransmitter (HIL92); however, many recent studies have evaluated the possibility of synaptic cross-talk or volume transmission in the hippocampus by modeling the mass transport of Glu, observing the architecture of the synaptic region, and local electrophysiological events (RUS98; ASZ97, BAR97, KUL98). These reports have supported the notion of cross-talk that is limited to short distances and nearest neighbor synapses. An interesting observation is that frequency dependent Glu overflow can occur under conditions of high-frequency stimulation to activate receptors outside the synapse using electrophysiological techniques in slice preparations (SCA97). Our *in vivo* results would

be consistent with this observation in that with high frequency stimulation, it is possible to detect synaptic overflow of Glu that is tonically inhibited by autoreceptors; however, the striatum appears to be more suited for volume transmission involving Glu. As shown above, Glu signals spread easier in the striatum than in the hippocampus because of freer diffusion and less effective uptake. These differences are manifested in larger signals in the striatum due to electrical stimulation or direct infusion. In contrast, electrically stimulated overflow is strongly inhibited by mGluR autoreceptors in the striatum whereas this control is relatively weak, even becoming ineffective (or facilatory) at high agonist levels, in the hippocampus. In this case, the autoreceptor is viewed as necessary in the striatum to sense the spread of glutamate and control further release. While volume transmission of glutamate in the striatum has not been evaluated before, the observation that Glu receptors are found on cells which do not have synaptic connections to Glu neurons is supportive of a role for glutamate volume transmission (OLE98). Indeed, mismatch of receptors and release sites is often given as an important criteria for volume transmission (ZOL98).

In conclusion, we have demonstrated that high frequency stimuli can cause synaptic overflow of glutamate in both the hippocampus and striatum. In hippocampus, such overflow is restricted by uptake and diffusion through the tissue suggesting a relatively small circle of influence of glutamate. Such a result is consistent with point-to-point transmission or restricted volume transmission. These results contrast sharply with prior results from the striatum which revealed large overflows that were regulated primarily by autoreceptors and relatively less restricted by diffusion and uptake. These results suggest the potential for more significant volume transmission in the striatum.

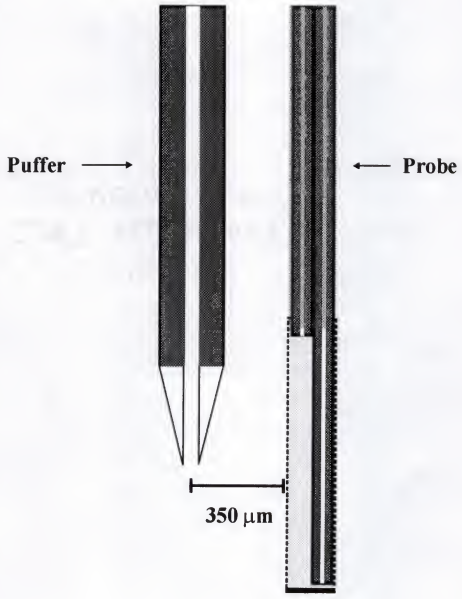

Figure 5-1. Puffer and probe geometry. Puffer is constructed from a 75 μm i.d., 360 μm o.d. Fused silica capillary ground to a point with a diameter at the tip of approximately 90 μm.

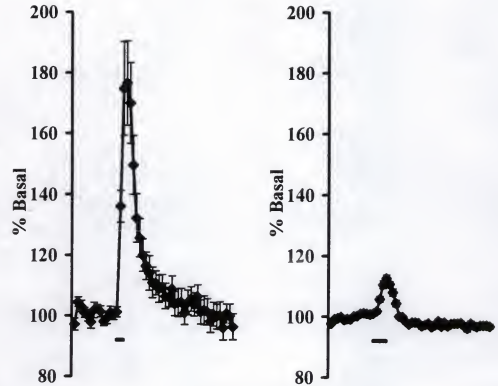

Figure 5-2. Comparison of Glu response to electrical stimulation in different brain regions. A) Striatum, stimulation parameters, 10 s, 20 Hz, 0.5 ms pulse, 80 V (7 rats, n = 17). B) Hippocampus, stimlation parameters, 20 s, 20 Hz, 0.1 ms pulse, 10 V (20 rats, n = 80). Bars indicate stimulation.

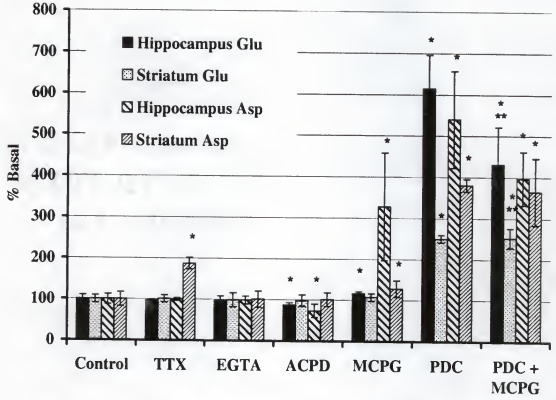

Figure 5-3. Comparison of chemical addifives on hippocampus and striatum extracellular concentrations. Basal Levels of glutamate and aspartate were 310 +/- 40 and 87 +/- 11 nM respectively (n = 21) in hippocampus. Values are expressed as percent of control levels, mean +/- SEM flollowing a 30 min infusion of the drug (n = 4 for additives). Striatum data is taken from LAD98

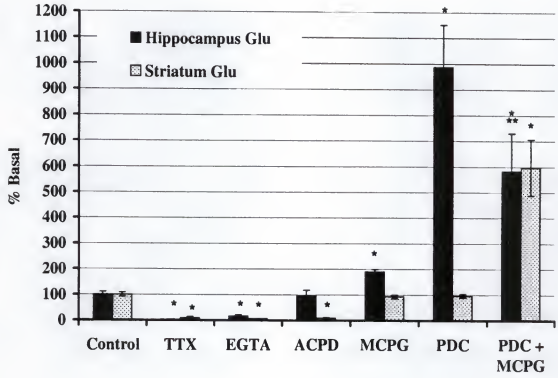

Figure 5-4. Comparison of chemical addifives on hippocampus and striatum Electrically Etimulated Overflow. Control evoked response was 66.5 +/- 7.3 fmol (n = 80 stimulations, 21 rats) in hippocampus. Values are expressed as percent of control levels, mean +/- SEM (n = 16, 4 rats). Striatum data is taken from LAD98.

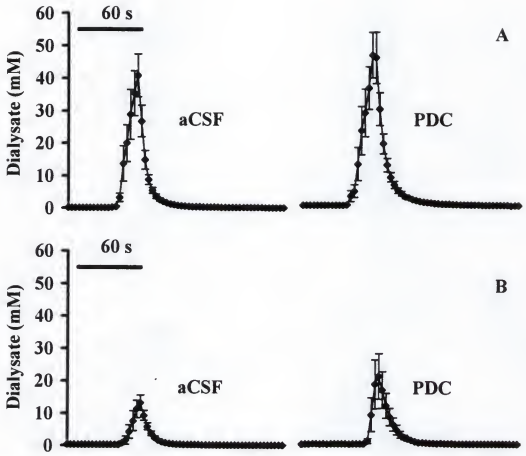

Figure 5-5. Introduction of exogenous 200 pmol D-Asp. 200 nl of 1 mM D-Asp was microinjected approximately 350 μm medial from the probe. A) Striatum. 7.4 +/- 1.2 pmol were collected in the control puff, 11.8 +/- 1.8 pmol collected in the presence of 200 μM PDC via reverse dialysis. B) Hippocampus 2.2 +/- 0.5 pmol colected in control, 4.8 +/- 1.3 pmol in the presence of 200 μM PDC.

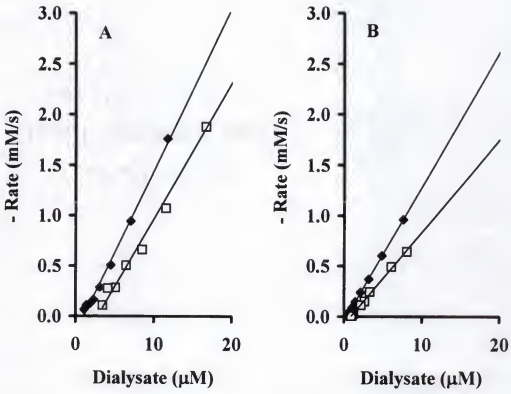

Figure 5-6 Clearance rates for exogenous D-Asp. A) Striatum. calculated slopes are: control (diamond) = 0.189 +/- 0.001 s^{-1}; PDC (square) = 0.140 +/- 0.007 s^{-1}. B) Hippocampus. calculated slopes are: control = 0.146+/- 0.010 s^{-1}; PDC = 0.089 +/- 0.003 s^{-1}. Values for concentration and rate are taken from the averaged puffs in Figure 5-5.

CHAPTER 6
THE ROLE OF GLUTAMATE IN THE PILOCARPINE MODEL OF SEIZURE

Introduction

Cholinomimetics are a class of compounds that affect cholinergic processes in the brain often resulting in an epileptic-like seizure and death. Because of this effect, cholinomimetics are used as chemical warfare agents, so called weapons of mass destruction. Most of the chemicals used in this manner, sarin, soman, and VX (TAY96), are acetylcholinesterase (AChE) inhibitors. AChE is the enzyme in the brain that removes acetylcholine from the synaptic cleft by conversion to choline. Through an as yet not fully understood process, a rise in acetylcholine eventually results in seizures. There is evidence, however, that these agents also have direct effects on other systems in brain such as GABAergic and glutamatergic neurons (CHE99, IDR86, MCD97).

A different, less potent cholinomimetic, pilocarpine (PILO), a muscarinic cholinergic agonist, produces similar seizures to AChE inhibitors and is used as a substitute for warfare agents in the laboratory for safety reasons. It is also used to produce model seizures for the study of epilepsy (for review see TUR89). PILO induced seizures, via intramuscular or intravenous injection, in awake rats are behaviorally characterized by tremors and gustatory and olfactory automatisms followed by limbic seizures and status epilepticus. The seizures result in altered pH, blood gas, and glucose concentrations in the brain (FIJ86, CLI87). Neurological effects can be seen electroencephalographically a few minutes after injection and include high voltage

spiking and low voltage fast activity. These effects are first seen in the hippocampus, followed by the amygdala and cortex (TUR83). Brain damage associated with seizure is greatest in the forebrain and hippocampus and resembles damage observed in the excitotoxic reaction to Glu (OLN86). Lethality can be as high as 85%, usually occurring in the first 24 hr during an episode of status epilepticus (JOP86). Spontaneous recurrent seizures occur for the remainder of the animal's life (TUR83A).

With a pretreatment of lithium, usually between 2 to 24 hr prior to PILO administration (CHA99), the seizure threshold can be greatly reduced. A 10 fold lower dose of PILO after Li pretreatment produces identical pathologies to high PILO treatments only (CLI87). It is suggested that the mechanism for this effect is inhibition of inositol phosphatase activity which in turn depletes the supply of myo-inositol, a second messenger system that is utilized by the glutamatergic system in the brain (TRI91).

Even though PILO directly acts on acetylcholine receptors, most of the evidence pertaining to seizure generation does not point to a cholinergic mechanism for generation. Most notably, anticholinergic agents are not effective anticonvulsants once a seizure has been initiated (MAY75). In addition to its direct effect on acetylcholine, PILO has been shown to modulate both levels of GABA (FRI99, HOU96, TRE92) dopamine (GEO97, ALA96, STA96), and Glu (HAL96, MIL93, MEL94, SMO97) and their receptors, any of which may have a role in either seizure generation or maintenance.

Glu has long been believed to be responsible, at least in part, for the generation and long term effects of seizures mostly because of its excitotoxic effects. Glu's role in seizures is supported by several lines of evidence (see SHE99, CHA00, URB98 for recent reviews) including an increase in Glu and Asp in humans or animals with chronic

seizures. Perhaps most studied as of late, is the activity of Glu receptors before, during, and after seizure.

Of particular interest here is the effect of metabotropic Glu receptors on seizure activity. Several studies have been performed to understand how each group of mGluR participates in seizures. The application of a group III agonist had no effect on kindled seizures in the rat dentate gyrus and therefore it was concluded that this group has no effect on seizure generation (FRI99). In a similar experiment it was found that a group II mGluR selective agonist attenuates kindled seizures, so activation of mGluR II inhibits seizure activity (KEE99). It has been shown in several studies that group I receptors have pro-convulsant actions (BOR99, MER97). In particular the mGluR agonist ACPD has been found to induce seizure activity measured by electrographic activity in hippocampal slices (TEB97) and *in vivo* (SAC92).

Unfortunately, the effect of PILO on extracellular Glu does not appear to be as clear-cut as Glu receptor activity seems to be. There are conflicting published reports on its effects including, no change, an increase, a decrease, or even a temporary decrease followed by an increase. Most of these differences may arise from different experimental protocols, such as introduction method, injection or direct infusion and whether the animal is awake or anesthetized.

In the awake rat, via intravenous injection, PILO was shown to have no effect on extracellular Glu in the hippocampus via microdialysis with LC/EC detection (MIL93). By intramuscular injection, Glu decreased during status epilepticus, remained low for 24 h, then increased and maintained an elevated level for at least 45 days (CAV94). In another report with intramuscular injection, Glu increased after status epilepticus

(LIU97). Direct infusion through a microdialysis probe immediately decreased Glu in both striatum (SMO97) and hippocampus (KHA99). In the striatum, once PILO was removed Glu returned to basal levels while in the hippocampus, Glu increased to an elevated level approximately 200% of the original pre-PILO level. Only one paper has reported PILO's effect on Glu in anesthetized rats. In this case Glu increased immediately with PILO infusion via a microdialysis probe in the hippocampus and then returned to basal 20 min after PILO was removed (MIL93). Behavioral or physical effects of PILO were seen in all experiments with awake animals while there was no mention of any effects in anesthetized rats.

In the work presented earlier (Chapters 4 and 5) we demonstrated the ability to measure neuronal Glu and Asp in the hippocampus (the region suspected to generate seizures (TUR89)) via microdialysis with on-line capillary electrophoresis. The regulation of both Glu and Asp via mGluR under normal conditions was demonstrated by the application of receptor agonists and antagonists. In this chapter, we will apply these methods to determine the effects of pilocarpine on seizure generation and extracellular Glu and Asp in the hippocampus of anesthetized rats. Seizure generation was monitored by physiological changes as well as by electroencephalographic recording at the site of microdialysis.

Additionally, because electrical stimulation elicits a response in extracellular Glu and Asp that is completely neuronal in origin it can be used to explicitly study the effect of PILO on glutamatergic neurons in the hippocampus. In anesthetized rats, stimulation of the perforant path, similar to the stimulation used in Chapter 4, was shown to evoke seizure-like high voltage spikes in the dentate gyrus (WAL94). In awake animals,

prolonged stimulation, up to 60 min, has been used to evoke sustained epileptic activity (SLO83, HAL96). This type of stimulation results in brain damage similar to that found in other seizure models.

Experimental

Chemicals and Reagents

All chemicals were purchased from Sigma Chemical (St. Louis, MO USA). All fused silica capillary tubing was from Polymicro Technologies (Phoenix, AZ, USA) and had a 360 μm outer diameter (o.d.) unless noted otherwise.

Capillary Electrophoresis and Laser-Induced Fluorescence Detection

The CE-LIF system for monitoring dialysate was the same as that described in Chapter 2. Dialysate was derivatized on-line by pumping 10 mM *o*-phthaldialdehyde/40 mM β-mercaptoethanol (OPA/BME) in 35 mM borate at pH 10.5 at 0.6 μL/min via a syringe pump (Harvard Apparatus, Holliston, MA, USA) into a zero dead volume tee (described in Chapter 2) attached to the outlet of the dialysis probe. The dialysate and OPA/BME were allowed to mix and react for 50 s as they flowed out of the tee and through a 16 cm long by 75 μm i.d. fused silica reactor capillary. Derivatized dialysate was pumped from the reactor capillary into a flow-gated interface which allowed automatic injection onto the electrophoresis capillary. Dialysate was electokinetically injected for 40 ms at the separation voltage every 5 s. Electrophoresis was carried out inside a 5 cm long (3.5 cm from injection point to detector) by 10 μm i.d. capillary. Voltage was applied by grounding the flow-gated interface and applying –13 kV to a buffer reservoir that was connected to the outlet of the separation capillary by 20 cm long

by 150 μm i.d. linker capillary. The electrophoresis buffer was 40 mM carbonate adjusted to pH 9.5 with NaOH.

Fluorescence detection was performed on the electrophoresis column with an epillumination fluorescence microscope (Carl Zeiss, Hanover, MD, USA). Fluorescence was excited with 1.3 mW of the 354 nm line of a He-Cd laser (Liconix, Carlsbad CA, USA). Emission over 400 nm was collected with a 40x objective and detected by a PMT (CRG Instruments, Austin, TX, USA). Data was collected via a personal computer (Gateway, Sioux City, SD, USA) and data acquisition board (AT-MIO-16F-5, National Instruments, Austin, TX, USA) at 1 kHz and low-pass filtered at 200 Hz. All collection and analysis software was written in house in Lab Windows (National Instruments).

Microdialysis

Side by side microdialysis probes were constructed as described in Appendix 2. Probes consisted of 9 cm of 20 μm i.d. and 100 μm o.d. fused silica capillary as the inlet and 7 cm of 20 μm i.d. and 100 μm o.d. as the outlet. The dialysis membrane was regenerated cellulose (Spectrum, Houston, TX, USA) with 18 kD cutoff and the tip sealed with polyimide sealing resin (Alltech Associates, Deerfield, IL, USA). Active areas were 200 μm o.d. and 4 mm long. Before use, all probes were perfused with 70% ethanol in water for 30 min at 1.2 μL/min followed by perfusion with artificial cerebrospinal fluid (aCSF) that consisted of 145 mM NaCl, 2.68 mM KCl, 1.01 mM $MgSO_4$, and 1.22 mM $CaCl_2$, for a minimum of 30 min. Perfusion flow rate was 0.6 μL/min and was driven by a syringe pump (Harvard apparatus, Holliston, MA, USA) for all experiments. Calibration and *in vitro* recovery was performed before implantation by placing the probe in Glu and Asp standards dissolved in aCSF held at 37 慢. For

calibration and *in vivo* experiments, the outlet capillary of the probe was connected to the reactor tee described above for on-line CE-LIF analysis.

Surgical Procedures

Male Sprague-Dawley rats (250-350 g) were anesthetized with chloral hydrate by an initial subcutaneous injection of 100 mg/ml H_2O at a dose of 400 mg/kg followed by booster injections of 100 mg/kg at 30 min intervals until the rat no longer exhibited a withdrawal reflex to limb pinch. Additional injections were given as needed. Microdialysis probes were stereotaxically implanted in the dentate gyrus of the hippocampus at AP = -3.8 mm, ML = -3.0 mm, DV = -4.7 mm relative to bregma. For experiments in which electrical stimulations were performed, a concentric bipolar stimulating electrode was implanted in the lateral perforant path (AP = 0.0 mm (from lambda), ML = -4.4 mm, DV = -3.4). Both probe and electrode were implanted over a period of 15 to 20 min in order to minimize tissue damage. Recordings were made at least 1 h post implantation and after basal levels were found to stabilize.

Electroecephalography

Brain activity at the microdialysis probe was monitored on a Grass Medical Instruments (Quincy, MA, USA) encephalograph, model 8-10C electroecephalographic instrument. The recording electrode consisted of a 150 μm diameter stainless steel wire sleeved inside a 250 μm i.d. fused silica capillary. Two mm of wire were exposed past the capillary with the insulation removed from the last 1 mm. The electrode was co-implanted 350 μm lateral to the microdialysis probe and situated dorsal ventrally to be in line with the center of the active area of the probe. The isolated ground and reference electrode were from Grass Instruments (E2B) and were placed in the scalp and front limb

respectively. EEGs were recorded on a personal computer (Gateway, Sioux City, SD, USA) with an AT-MIO-16 data acquisition board at 100-500 Hz. Fourier transforms of the electroencephalograms were calculated by the TS-find software provided by Dr. R. Mark Wightman (University of North Carolina-Chapel Hill).

All experimental uses of laboratory rats in the present study were reviewed and approved by the University of Florida Institutional Animal Care and Use Committee and conform with policies and procedures set forth by U.S. Public Health Service Policy on Humane Care and Use of Laboratory Animals.

Pharmacological Treatments and Electrical Stimulation

Animals to be treated with a PILO injection were first given a methyl atropine pretreatment (10 mg/kg in 20 mg/kg H_20, subcutaneous) at least 30 min prior to PILO to minimize peripheral effects. PILO was administered via intravenous injection at 50 mg/kg (delivered in 100 mg/ml in H_2O) in the tail vein.

PILO was also administered by direct infusion to the hippocampus via reverse dialysis. Perfusion media was changed from aCSF to 10 mM pilocarpine in aCSF via liquid switch (SciPro, North Tonawanda, NY, USA). In some cases, animals were pretreated with LiCl (125 mg/kg, in 125 mg/ml H_2O, subcutaneous) 4 to 6 hr before application of PILO. The mGluR agonist (1S,3R)-1-aminocyclopentane-trans-1,3-dicarboxylic acid (ACPD) (Tocris Cookson, Ballwin, MO, USA) (200 μM in 10 mM PILO in aCSF) was administered via reverse dialysis.

Electrical stimulation of the perforant path were the same as in Chapter 4 and consisted of application of a 20 s train of 0.1 ms, 20 Hz, 10 V square wave pulses (Grass Medical Instruments). Prior to treatment, 4 control stimulations were recorded in each

rat, with 20 min between each stimulation. 20 min after the last control stimulation, the dialysis media was switched to 10 mM PILO. Four additional stimulations were applied in approximately 20 min intervals in the same manner as above.

Data analysis

Electropherograms were analyzed using a statistical moments program written in house (Lab Windows). Glu and Asp peaks were marked manually and dialysate concentration determined by *in vitro* calibration. The 100 % basal level was measured as the average concentration of NT in 10 electropherograms immediately prior to stimulation. Elevated concentrations due to AA were determined by comparison to the NT concentration before application of the additive. Stimulated overflow was calculated as the total mass of NT collected by the microdialysis probe above the average pre-stimulus level. A two-tailed student's t-test was used to determine all statistical differences. All values are reported as mean ± one standard error, n is given as the number of rats for basal concentrations or number of stimulations for overflow.

Results

Intravenous Injection

Basal levels of Glu and Asp were 240 ± 70 nM and 96 ± 5 nM (n = 4) respectively, microdialysis recoveries were 31.5 ± 0.6 % and 33.4 ± 2.6 %. Physical effects of intravenous injection of PILO with methyl atropine pretreatment consisted of the classic seizure response. Symptoms appeared 1-5 minutes after injection and were characterized by twitching of whiskers and limbs and excessive salivation. Within 20 minutes involuntary muscle contractions occurred over the entire body and discharge of

bodily fluids was heavy. Two of the 4 animals died 40 to 60 min after injection, the two surviving animals exhibited a gradual dissipation of symptoms over 120 min. Without methyl atropine, the dose of PILO was fatal to all animals (n = 3) within 20 min.

Continuous monitoring of Glu and Asp every 5 s after intravenous injection of PILO following a pretreatment of methyl atropine (10 mg/ml) showed no effect on extracellular levels of Glu or Asp over 40 min (Figure 6-1). Of the 2 animals that survived the course of the experiment, no further change in Glu or Asp was observed over 120 min.

Electroecephalography at the dialysis probe showed a change in brain activity immediately following injection of PILO, see Figure 6-2A and C. This change was primarily characterized by the generation of periodic high frequency components as seen in representative Fourier transforms of the EEGs in Figures 6-2 B and D. There is also a small amplitude increase as seen in Figure 6-2 A and C. The largest change in activity occurred within the first 2 minutes after injection and gradually returned to near basal activity over the course of the experiment but never returned to pre-injection levels.

Direct Infusion

Basal levels of Glu and Asp were 360 ± 50 nM and 120 ± 20 nM (n = 8) respectively and associated recoveries were 34.4 ± 2.2 % and 36.5 ± 2.9 %. There were no physical effects observed due to direct infusion of 10 mM PILO in the hippocampus. The concentration of PILO used has previously been shown to cause an increase in Glu in anesthetized animals (MIL93) and cause changes in Glu and induce seizures in behaving animals (KHA99).

Glu and Asp were monitored continuously for 30 min followed by measurements

every 5 min for an additional 30 min. Figure 6-3 illustrates the change that occurred in half (4 of 8) the animals. Both Glu and Asp immediately decreased and reached a minimum after 5 min of perfusion (Glu 75 ± 4 %, Asp 48 ± 5 %) after which Glu began to increase, returning to basal after 15 min of infusion and stabilizing to an increased level at about 30 min (170 ± 20 %). Asp, on the other hand, increased only slightly and returned to only 80 ± 10 % of original basal levels. Monitoring for up to 180 min showed no additional change in either Glu or Asp. In less than half (3 of 8) of the animals, neither Glu nor Asp returned to or above basal as seen above (Figure 6-4). At 5 min of PILO infusion Glu was 55 ± 8 % of basal while Asp was 60 ± 8 %, after thirty minutes, both Glu and Asp decreased slightly, but not statistically significant, to 50 ± 10% and 50 ± 7 % of basals respectively. Additional monitoring to 120 minutes showed no further change in either transmitter. In one case, both Glu and Asp decreased slightly, followed by a return to basal levels within 10 min (data not shown).

Electroecephalographic changes were slight and identical in all animals. A representative EEG is shown in Figure 6-5; in this particular experiment, Glu did not increase after the initial change. A small frequency shift was observed immediately with perfusion of 10 mM PILO and did not change over the course of the experiments. There was no associated change in amplitude or appearance of high voltage spiking.

Infusion with Lithium Pretreatment

Lithium is known to enhance the susceptibility to seizures and requires the use of 10 times less PILO via injection. In these experiments, LiCl (125 mg/kg) was injected subcutaneously between 4 and 6 hr prior to infusion of PILO. Increasing the time between LiCl and PILO had no effect on either Glu and Asp or EEG changes (up to 26

hr). Basal Glu and Asp in dialysate were 350 ± 50 nM and 110 ± 20 nM respectively for these rats (n = 6). Relative recoveries for the microdialysis probes were 29.6 ± 1.6 % and 34.0 ± 2.6 % for Glu and Asp. There were no physical symptoms of seizure due to infusion of 10 mM PILO with lithium pretreatment.

Effects of this treatment on Glu and Asp were similar to the second observed change with PILO only and occurred in all animals (n = 6) (Figure 6-6). Both Glu and Asp immediately decreased with infusion of 10 mM PILO, Glu reached a minimum of 65 ± 4 % of basal in 5 min and Asp a minimum of 55 ± 10 % in 10 min. After 60 min Glu decreased to 60 ± 5 % of basal and Asp rose to 73 ± 10 %. Further monitoring showed no additional change in either transmitter up to 150 min. Removal of PILO resulted in a return to basal level for Glu within 5 min and an increase in Asp to 150 ± 20 % (n = 2) (Figure 6-7). The addition of 200 μM ACPD to the perfusion medium (with PILO) results in an increase in both Glu and Asp to 140 ± 20 % and 130 ± 15 % after 15 min of perfusion (n = 3); there is no further change up to 60 min after addition of ACPD. Again, Asp does not reach a stable level until after Glu.

For 4 of 6 animals, electroencephalographic recordings showed identical changes to those seen in Figure 6-5 namely no amplitude change with a shift to higher frequency. However, in 2 of the 6 animals tested classic seizure activity, characterized by both high voltage spikes and low voltage frequency shifts, was observed with a latency of 40 min following PILO perfusion (Figure 6-8). At 40 min, individual high frequency spikes appeared followed by trains of spikes lasting 5 to 10 s. By 1 hr this activity was continuous and lasted approximately 40 min (Figure 6-8C).

To determine if this activity could be correlated to a rapid change in either Glu or

Asp, both were monitored simultaneously with EEG and can be seen in Figure 6-8. A comparison of pre-PILO (Figure 6-8A) to PILO without seizures (Figure 6-8B) and PILO with seizures (Figure 6-8C) does not present a change in Glu or Asp associated with either PILO only or PILO during seizure. There also does not appear to be a fast Glu or Asp change that correlates to the train of spikes seen in Figure 6-8C at approximately 1 min. An interesting effect of PILO infusion is an improvement in the reproducibility of Glu measurement. The standard deviation of pre-PILO Glu is 8.4 % (Figure 6-8A), compared to 7.8% with PILO but without seizure (Figure 6-8B) and 6.7% with PILO during seizure (Figure 6-8C). This trend was observed in every rat but there is no clear explanation at this point.

The addition of 200 μM ACPD to the perfusion medium after 100 min of PILO infusion results in an increase in Glu and Asp but no change in EEG activity. It must be noted that the frequency of EEG spiking had already decreased to the level observed in Figure 6-8D before ACPD perfusion. The standard deviation of Glu increased to 8.5%, the same as pre-PILO Glu.

In another experiment, 200 μM ACPD with 10 mM PILO was added soon after electroencephalographic seizure-like activity was observed. Instead of a single EEG recording electrode, 3 were implanted at various locations in the hippocampus while one was used as a reference in the opposite hemisphere (Figure 6-9). Immediately upon addition, a train of high voltage spikes was observed with the electrode nearest the probe. The next closest probe showed a decreased amplitude of the spikes while the third electrode and reference electrode showed no sign of spiking. Only one set of recurrent spikes were observed approximately 30 s after the first set.

Electrical Stimulation of the Perforant Path with PILO Infusion

Basal levels for Glu and Asp during these experiments were 280 ± 30 nM and 150 ± 30 nM respectively (n = 4) and relative recoveries were 30.5 ± 1.6% for Glu and 33.2 ± 1.0 % for Asp. The maximum increase in Glu due to stimulation was 109 ± 1% (n = 16) and the mass collected was 63 ± 5 fmol without PILO infusion, both in good agreement with the results presented in Chapter 4. There was no significant change in Asp during stimulation.

Figures 6-10 and 6-11 show the response of Glu and Asp respectively to electrical stimulation of the perforant path in the presence of PILO. The first stimulation with PILO infusion was given at 18 ± 1 min after start of PILO treatment with Glu at 61 ± 5 % of basal ($p < 0.0002$). There was no immediate response to stimulation as seen in control, but a statistically significant ($p < 0.05$) increase to 71 ± 3% in Glu was observed beginning 20 s after termination of stimulation and continuing through the end of the measurement. Asp decreased to 35.1 ± 3.0% ($p < 0.00001$) of basal and showed a similar but further delayed response to stimulation. The increase became statistically significant ($p < 0.05$) 55 s after termination of stimulation (47.3 ± 3.7) and returned to below significance after 20 s. Successive stimulations were administered 39 ± 1 min, 59 ± 1 min, and 80 ± 2 min after PILO infusion. Basal levels of Glu immediately prior to stimulation were 66 ± 6 %, 66 ± 4 %, and 60 ± 5 % respectively and were not statistically different from each other. The response diminished and became more delayed with each consecutive stimulation. Each trace had only one point statistically different from prestimulus levels at 40 s, 50 s, and 70 s respectively.

The electroencephalographic response to stimulation of the perforant path in the

dentate gyrus is seen in Figure 6-12 with the corresponding Glu concentration overlaid. Application of the electrical stimulus resulted in 20 Hz spikes during stimulation followed by approximately 10 s of high voltage spikes in control experiments. Glu increased during the stimulus and returned to basal levels within 15 s, as seen in Chapter 4. Following 16 min of PILO infusion, electrical stimulus resulted in a similar EEG response. There was a slight change in the shape of activity both during and after stimulation. Post stimulation spikes were seen for the same length of time in both control and PILO stimulation but the pattern of spikes changed. In the control stimulation, individual spikes can be discerned but in the PILO stimulation the spikes occurred in groups of 3 or 4. Significant inter-animal variability in both the number and duration of post stimulus spikes was seen but intra-animal differences were minimal.

Discussion

Pilocarpine Induced Seizures in Anesthetized Animals

The intravenous injection of 50 mg/kg PILO in chloral hydrate anesthetized rats results in convulsions and loss of body function strong enough to be fatal without a pretreatment of methyl atropine to reduce muscular seizures. This treatment was only sufficient to induce some of the altered brain activity associated with PILO induced seizures in awake animals (TUR89). While the observed frequency shift and small amplitude change in EEG activity is similar to that seen in seizures, the high voltage spiking typically used to identify a seizure was absent. Direct infusion of 10 mM PILO in the hippocampus resulted in low voltage frequency shift only in EEG, though to a lesser extent than i.v. injection, with no physical effects. In animals pretreated with

lithium, a chemical known to increase seizure susceptibility, PILO infusion induced seizures characterized electrographically by both low voltage frequency shift and high voltage spikes in one third of the animals (2 of 6). The remaining 4 rats exhibited only a low voltage frequency shift while none of the 6 exhibited any physical symptoms of seizure.

From this evidence and the paucity of literature (only one publication, MIL93) it can be concluded that the levels of PILO used to generate seizures in awake animals (both infusion and injection) do not do so in chloral hydrate anesthetized animals. It is unknown if the infused PILO in the study by Millan et al. actually induced a seizure. No electrographic recordings were performed nor was there a mention of any physical symptoms of seizure. In the case of Li pretreated animals, EEG changes associated with seizures were seen in 2 of 6 animals. It may be possible that a higher concentration of PILO will consistently induce seizures, but this experiment was not attempted.

It appears that a very high, widespread concentration of PILO is required to generate a seizure in an anesthetized rat. Assuming an equal distribution (not likely), density of 1 g/ml for a rat, and correcting for the extraction efficiency of the microdialysis probe, to achieve the equivalent concentration as a 10 mM PILO infusion in the hippocampus an intravenous injection of 815 mg/kg would be required. This increase is 16 times more than the original near lethal dose. If Li pretreatment is to be accounted for, an injection of 8.15 g/kg is required, well above a lethal dose.

Effect of Pilocarpine on Glutamate and Aspartate

Again, it appears that a very high concentration of PILO is required to alter the extracellular level of Glu or Asp in anesthetized rats. Intravenous injection had no effect

on either transmitter while direct infusion gave varied results. It is expected that direct infusion of a chemical via reverse dialysis would result in a very reproducible response, and is seen with the addition of other chemicals in the manner (see Chapter 4). By increasing the efficacy of PILO with a Li pretreatment, results were consistent with a decrease in both Glu and Asp. This decrease in Glu is consistent with several previous studies in awake rats by infusion from Michotte's group (SMO97, SMO97a, SMO97b, KHA99) or injection (CAV94). The removal of PILO in the Li pretreated rats caused Glu to return to basal levels and Asp to reach an elevated level, also similar to Michotte's work.

Role of Glu in Seizure Generation

From the variability in the response of Glu to PILO and inconsistent generation of seizures, it is difficult to make a definite conclusion on the direct link between cholinomimetic induced seizures and Glu. A PILO induced seizure does not appear to require an increase in extracellular Glu. Such an increase in Glu was seen in only 4 of 22 experiments (all treatments pooled) while the only experiments that resulted in full electroencephalographic seizures occurred when Glu and Asp were reduced.

The evidence for the role of elevated Glu in seizure generation is indirect. The first such line of evidence is that damage associated with a seizure is similar in appearance to damage caused by excitotoxic levels of Glu (OLN86). Additionally, in human epileptic patients Glu increases during spontaneous seizures (DUR93, WIL96). Finally, the injection of Glu ionotropic receptor agonists can induce seizures (SCH78, TRI89) while antagonists can inhibit seizures (DIN90, MEL92). Attempts to measure a direct link between elevated Glu and seizure generation have shown no relationship

(MAS95, OBR96). Increasing extracellular Glu by addition of the uptake inhibitor PDC does not induce seizure (MAS95) nor does it facilitate a seizure coupled with PILO application (MIL93).

The addition of ACPD, a mGluR agonist demonstrated to increase seizure activity (TEB97, SAC92) did however increase both Glu and Asp to greater than basal levels. In one experiment, ACPD caused immediate high voltage spikes but did not result in any prolonged seizure activity. This result is consistent with the proconvulsive action reported in the literature in which the frequency of high voltage spikes increased with application of ACPD (TEB97).

Electrical Stimulation with Pilocarpine Infusion

Even though the PILO initiated change in Glu does not cause a seizure, it appears that the glutamatergic system is altered under these conditions. The apparent lack of consistent results correlating Glu levels and seizures have lead to the development of an increased glutamate-mediated excitation theory (OBR96). In this theory seizure is induced or at least maintained by the overactivation of Glu receptors, both ionotropic and metabotropic. Evidence includes the ability of receptors (both ionotropic and metabotropic) to control a seizure (see introduction) and that receptor concentrations and mRNA expression are altered by seizure (acute or chronic) (CHA00, GED90, GRO99, MAT98, especially CHA98). The EEG data presented here offer support for this theory. Cellular signaling creates a potential in the extracellular space with each cell adding to the net potential. The electroencephalogram measures the extracellular voltage in the vicinity of the electrode. The high frequency shift seen in every experiment indicates that overall cellular activity increases. The high voltage spikes occur only when the cells fire

synchronously and were not observed in most cases. The decrease in basal levels of both Glu and Asp could also be accounted for by overactive inhibitory receptors.

As seen in the control stimulations (Figure 6-10), the synchronous firing of Glu neurons causes an increase in extracellular Glu. In the presence of PILO introduced by reversed dialysis, electrical stimulation of the perforant path resulted in an altered response in Glu that varied with infusion time. None of the four consecutive stimulations showed an immediate response to stimulus and only the stimulation administered 20 min after PILO infusion demonstrated a significant response, a delayed and prolonged increase in Glu. Asp also changes in similar fashion to the infusion of PILO with only the first stimulation after perfusion leading to a significant change. EEGs changed only slightly with PILO infusion.

In conclusion, the data presented here indicate that PILO either by injection or direct infusion into the brain does not generate neuronal seizures in chloral hydrate anesthetized rats. A pretreatment with Li followed by direct infusion of 10 mM PILO can generate seizures in a fraction of the animals. Even though seizures are not generated, direct infusion of PILO only does have an effect on glutamatergic neurons as evidenced by a limited EEG change and altered response of Glu to electrical stimulation of the perforant path. These results are consistent with the theory that seizures are induced by an overly active neurological system, not elevated Glu (OBR96).

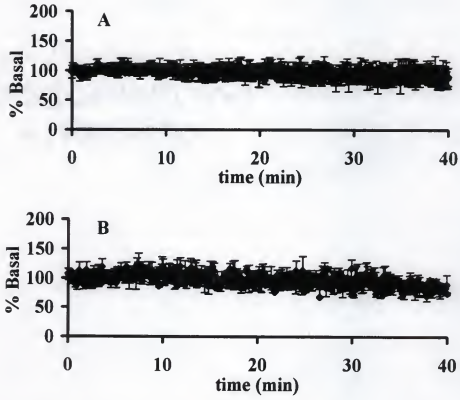

Figure 6-1. Effect of pilocarpine intravenous injection on hippocampal Glu (A) and Asp (B). 10 mg/kg pilocarpine was injected in the tail vein at time = 0. Continuous monitoring showed no change in either Glu or Asp over 40 min.

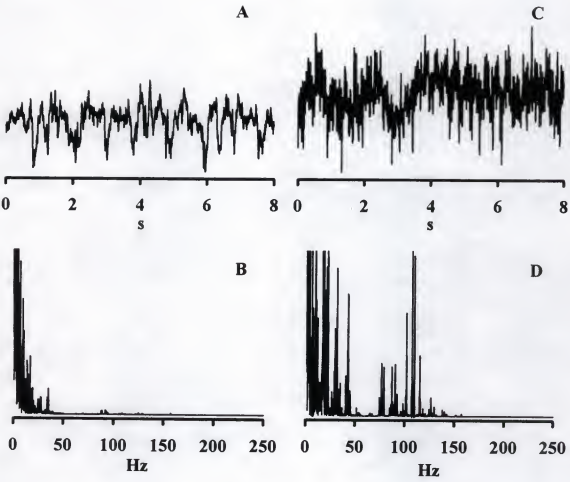

Figure 6-2. Electroencephalography during pilocarpine injection. A) Basal EEG before pilocarpine injection. B) Fourier transform of A. C) EEG 2 minutes after pilocarpine injection. D) Fourier transform of C. Note high frequency shift in Fourier transforms after pilocarpine injection.

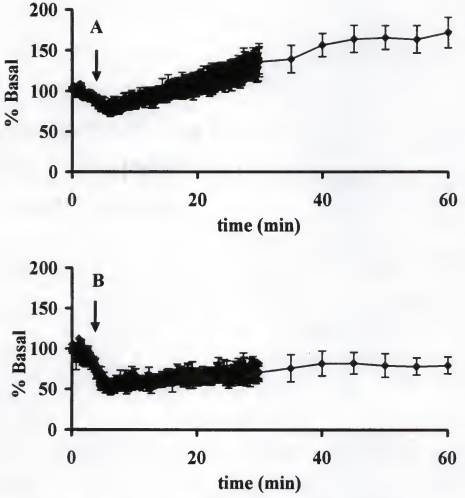

Figure 6-3. Effect of pilocarpine infusion on hippocampal Glu (A) and Asp (B). Perfusion fluid was switched to 10 mM pilocarpine in aCSF at the arrow. Continuous monitoring was performed for 30 min followed by monitoring at 5 min intervals for an additional 30 min. This increase in Glu was was seen in 4 of 8 rats.

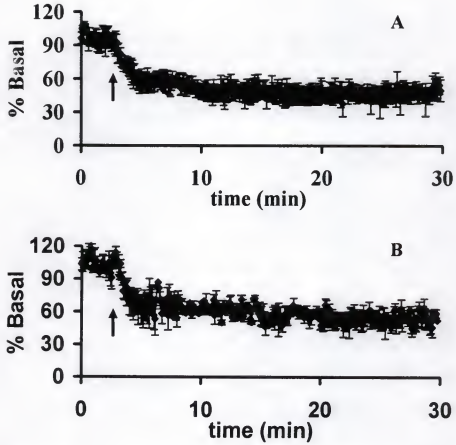

Figure 6-4. Effect of pilocarpine infusion on hippocampal Glu (A) and Asp (B). Perfusion fluid was switched to 10 mM pilocarpine in aCSF at the arrow. Continuous monitoring was performed for 30 min, no further change was observed. This decrease in Glu was was seen in 3 of 8 rats.

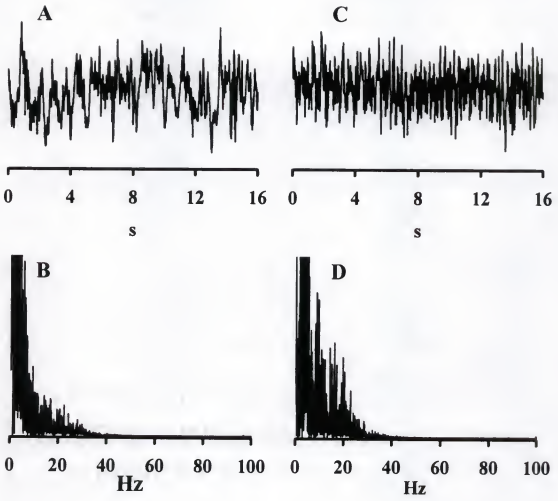

Figure 6-5. Electroencephalography during pilocarpine infusion. A) EEG before infusion. B) Fourier transform of A. C) EEG immediately following switch to 10 mM pilocarpine in perfusion fluid. D) Fourier transform of C.

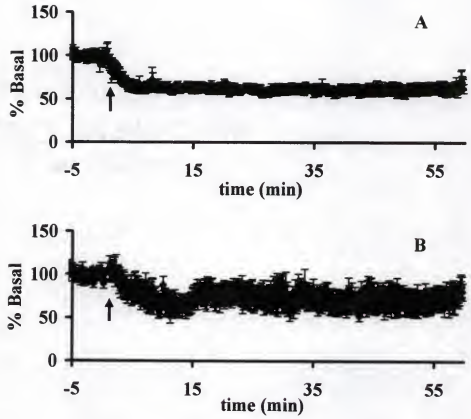

Figure 6-6. Effect of pilocarpine infusion with Li pretreatment on hippocampal Glu (A) and Asp (B). Animals were treated with 125 mg/kg LiCl subcuetaneously 4-6 hr before infusion of 10 mM pilocarpine, indicated by the arrow. 6 of 6 rats demonstrated this response.

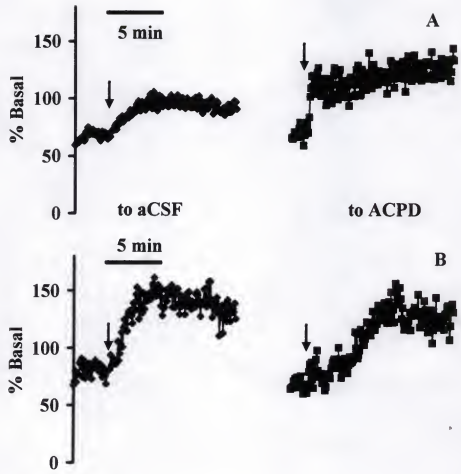

Figure 6-7. Return to aCSF and addition of 200 μM ACPD after pilocarpine infusion in Li pretreated rats. A) Glu, B) Asp. Removal of pilocarpine from the perfusion medium resulted in an increase in Glu and Asp (n = 2). Addition of 100 μM ACPD to 10 mM pilocarpine increased both Glu and Asp but with different time courses (n = 3). Arrows indicates change of medium. Error bars are removed for clarity.

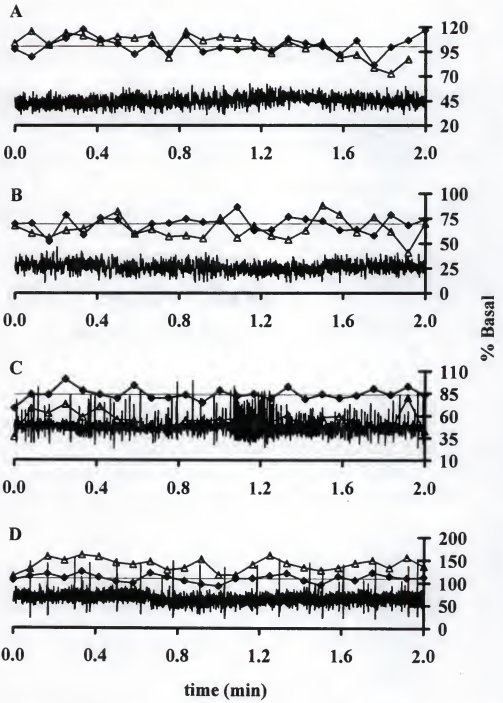

Figure 6-8. Electroencephalographic and Glu and Asp changes during seizure induced by pilocarpine infusion with Li pretreatment. A) Basal EEG activity and Glu (diamond) and Asp (triangle) fluctuations. B) Depressed Glu and Asp levels with 20 min pilocarpine infusion. C) High voltage spikes associated with seizure. D) 15 min after ACPD infusion with pilocarpine. EEG activity had already decreased before ACPD was added to the perfusion medium.

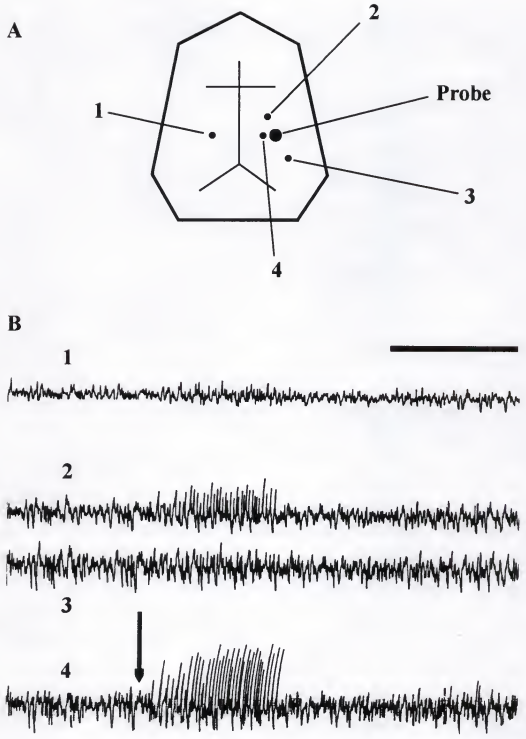

Figure 6-9. Effect of ACPD infusion on Li-PILO treated rats. A) Position of probe and implanted recording electrodes 1. dentate gyrus in opposite hemisphere 2. CA1/CA3. 3. CA1/CA3. 4. DG/CA1. B) Recorded EEGS. Arrow denotes ACPD infusion. Bar corresponds to 10 s.

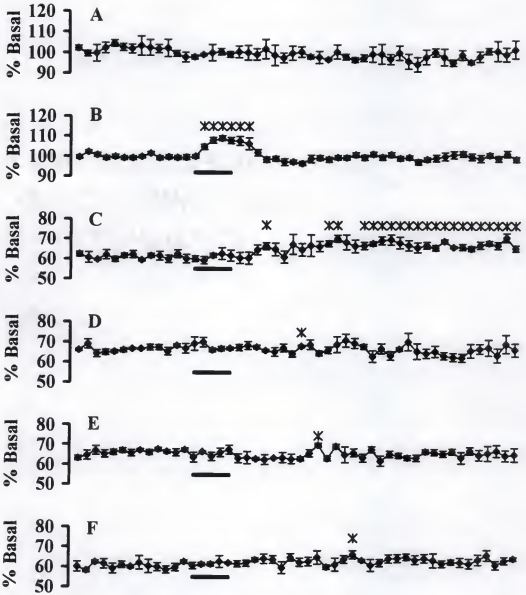

Figure 6-10. Response of Glu to electrical stimulation of the perforant path with pilocarpine infusion. A) Basal Glu, no applied stimulus. B) Control stimulation (n = 16 stimulations, 4 rats). C) Stimulation after 19 min of pilocarpine infusion. D) After 39 min. E) After 59 min. F) After 80 min. Bars indicate stimulation and correspond to 20 s. * indicate statistically different from pre stimulus levels ($p < 0.05$). n = 4 for C-F.

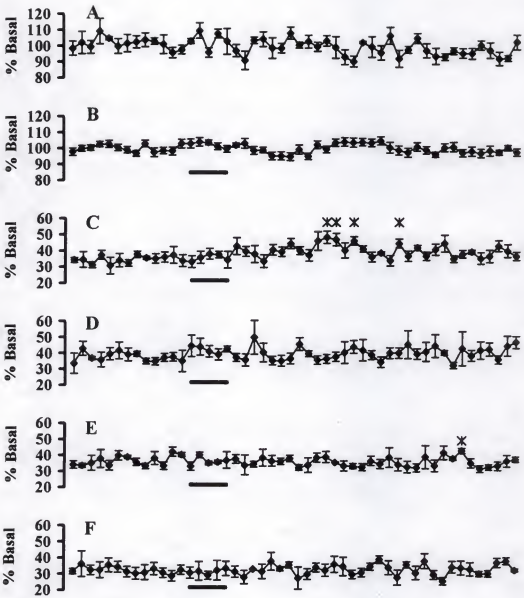

Figure 6-11. Response of Asp to Electrical Stimulation of the Perforant Path with Pilocarpine Infusion. A) Basal Asp, no applied stimulus. B) Control stimulation (n = 16 stimulations, 4 rats). C) Stimulation after 19 min of pilocarpine infusion. D) After 39 min. E) After 59 min. F) After 80 min. Bars indicate stimulation and correspond to 20 s. * indicate statistically different from pre stimulus levels ($p < 0.05$). n = 4 for C-F.

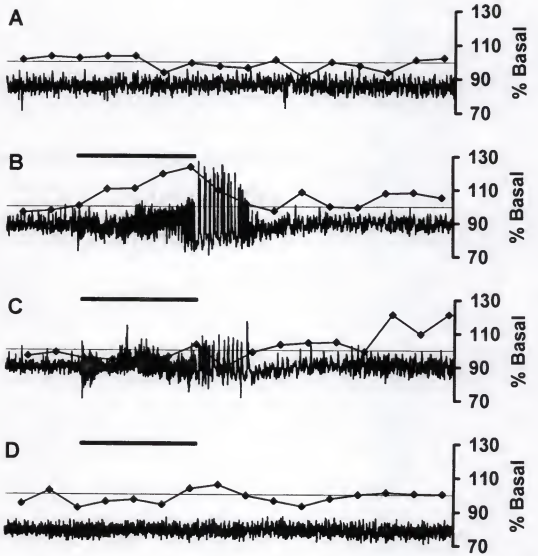

Figure 6-12. Glu concentration and electroencephalographs during electerical stimulations. A) Basal Glu and EEGs, no stimulation applied. B) Control stimulation, perfusion of aCSF only. C) Stimulation 16 min after the start of perfusion with 10 mM PILO. D) Experiment with no response to stimulation. Note: A, B, and C are from the same rat, B and C are concecutive stimulations. Bar indicates stimulation and represents 20 s. See text for conditions.

CHAPTER 7
DEVELOPMENT STRATEGIES FOR HIGH-SPEED CHROMATOGRAPHIC SEPARATIONS

Introduction

In the introductory chapter, liquid chromatography was briefly discussed with respect to microdialysis. While LC separations are used extensively with microdialysis high-speed separations compatible with on-line analysis are relatively rare (CHU87, CHE95, NEW94). Nevertheless, high-speed LC separations are still highly desirable. As seen in the basal electropherogram in Chapter 3 the majority of the components in dialysate are neutral and therefore can not be resolved by CE but could be resolved by a reversed phase LC separation. This chapter presents a review of the strategies used to develop high-speed LC separations.

The speed of liquid chromatographic separations has been steadily increasing over the past 30 years due to advances in column technology, which directly follow the well-developed theories of band broadening. Separations which took over an hour in the 1970s and 1980s can now be performed in minutes or even seconds. Excellent reviews of high-speed chromatographic separations have recently appeared (CHE95, PAL96). At the time of these reviews, improvements in separation speed were shown to be largely the result of production of particles with diameters down to 1-2 μm, non-porous particles, superficially porous particles, and perfusion particles. In addition, elevated temperatures were illustrated to be effective in decreasing analysis times (CHE93). In the years since

these reviews, the potential for fast separations has further increased with the use of even smaller particles (< 1μm) packed into capillaries with flow controlled by either ultra-high pressure pumps or electroosmosis. In addition, several other experimental systems such as monolithic columns, open tubular columns, and small diameter packed capillaries have been explored with some success for fast separations.

Theory

Before considering the recent advances in rapid technology and separations, it is useful to briefly consider the band broadening theory which has been used as the basis for the advances. The speed with which a chromatographic separation can be performed is limited by the sources of band broadening which become dominant at high mobile phase velocities. A useful method of evaluating band broadening is based on the Knox equation:

$$h = A\upsilon^{0.33} + B/\upsilon + C\upsilon \qquad (1)$$

where h is the reduced plate height and υ is the reduced velocity (KNO69). A, B, and C are system constants which are determined by the magnitude of band broadening due to eddy diffusion, longitudinal diffusion, and resistance to mass transfer respectively. The use of reduced parameters, defined as:

$$H = H/d_p \text{ and } \nu = u \bullet d_p/D_m \qquad (2, 3)$$

where H is plate height, d_p is particle diameter, u is linear velocity, L is column length, and D_m is the diffusion coefficient of the analyte in the mobile phase, allows comparison of columns with different stationary phases, analytes, column lengths and particle sizes. The Knox equation shows that increasing mobile phase velocity, while decreasing

the analysis time, will also increase the plate height and yield lower resolution. This well-known problem is of course distinct from the situation with CE.

For well-packed columns using porous supports and unretained solutes, it is expected that A = 1, B = 2, and C = 0.10 (CHE93). For a column with these figures of merit, the C term will dominate the band broadening at high mobile phase velocities. For example, at υ of 150, the resistance to mass transfer accounts for over 60% of the total plate height. The C-term is dependent upon the capacity factor and can become even more dominant for retained compounds. The C-term is an aggregate term that includes effects of slow desorption-sorption kinetics, inhomogenous flow, and slow diffusion out of the stagnant mobile phase in porous particles. It is frequently observed that the majority of the C term, especially for large compounds like proteins, arises from slow diffusion in and out of stagnant mobile phase in pores. In cases where the C-term is sufficiently reduced, the A term can dominate band broadening, even at high flow rates (COL93). As discussed below, certain capillary column configurations can reduce or eliminate the A term for improved performance at high flow rates. Since the A and C terms both increase with increasing particle diameter, it is also apparent that smaller particles will aid performance at high flow rates. This necessitates the use of higher pressures. These considerations will also be discussed in more detail below.

Non-Porous and Superficially Porous Particles

One of the most common ways of obtained improved performance at high flow rates in chromatography is the use of pellicular or non-porous particles. In non-porous particles, the stationary phase is coated on the outside of a solid microsphere thus

eliminating any stagnant mobile phase in the column. With no stagnant mobile phase, the C-term is significantly reduced compared to porous particles resulting in flat van Deemter curves and high efficiency at high flow rates compared to porous particles of the same size. Pellicular glass beads with large diameters (>40 μm) were used as stationary phase supports early in the development of liquid chromatography but they lost favor with the advent of porous silica particles with much smaller diameters <10 μm which provided high surface area (and therefore high capacity) and higher efficiency. Recent improvements in synthetic methods for pellicular particles have allowed production of monodisperse beads with diameters <3 μm (UNG85). This improvement, coinciding with increased demand for higher speed separation has sparked renewed interest in non-porous particles.

Preparation of Non-Porous Particles

The synthesis of non-porous particles has been reviewed for a variety of supports (HAN97, LEE97). The most common synthetic method for non-porous silica involves hydrolysis of alkyl silicates and subsequent condensation of silicic acid in alcoholic solutions to produce highly monodisperse (2% variation in diameter) particles (STO68, UNG85). The production of non-porous zirconia beads coated with reversed-phase stationary phase has also been described (DUN94). These particles, with diameters <3 μm, were found to yield rapid, high efficiency separations for a variety of analytes including polycyclic aromatic hydrocarbons, alkylbenzenes, oligosaccharides, amino acids, peptides, and proteins. With appropriate end-capping and use of polymeric surface coverage with stationary phase, the particles had little metallic interactions and yielded quasi-homoenergetic interactions. Alternative approaches to producing monodisperse,

non-porous chromatographic supports include filling in the pores of porous particles with polymer (HJE91) and rendering porous particles non-porous by sintering at high temperatures (GER87). Non-porous supports based on organic polymers are produced by suspension polymerization techniques which allow control of particle diameter (MAA88, SIN95).

Characterization of Non-Porous Particles

Unger's group performed an in depth evaluation of non-porous particles with 1.5 μm diameter for the separation of proteins and peptides in a series of papers (UNG86, JIL87, JAN87, JAN87A). In a comparison of pellicular and porous particles for reversed-phase chromatography of peptides and proteins several differences were observed. One difference was that the capacity factor of an analyte was much less sensitive to changes in the percentage of organic solvent modifier compared to porous particles (UNG86). Plots of log(k') versus organic phase ratio yielded slopes 10 times more shallow than would be expected with porous particles. This effect requires adjustment of gradient development (see Snyder) and was attributed to the proteins having free access to the stationary phase on the surface rather than being required to diffuse into pores. We note however, that for small molecules non-porous columns have been reported to be more sensitive to organic content with the slope of log(k') vs. organic content is twice as steep for non-porous reversed-phase columns (JEN96).

The main observable difference between non-porous and porous particles was an increase in peak capacity for small, non-porous beads compared to columns packed with porous particles (JIL87). For example, in one comparison, columns with the same surface area to volume ratio revealed peak capacities, defined as gradient time/peak width

(4σ), that were typically 3 times greater on non-porous beads than porous beads for a given analysis time. Peak capacities as high as 94 were achieved for proteins with 10 min gradients on the 1.5 μm non-porous particles. Alternatively, peak capacities that were the same as that achieved on porous particles could be achieved in shorter times on the non-porous particles. A potential drawback of non-porous columns is the reduced amount of stationary phase resulting in reduced capacity. Unger's work showed a decreased capacity with non-porous columns; however with a sample capacity of 1 mg protein per column volume (column dimensions 36 long x 8 mm i.d.), the column was considered suitable for "micropreparative" and analytical work. Thus, it appears that the capacity issue is moot for analytical scale separations on non-porous particles. Some workers however, have investigated the use of fimbriated phases and tentacle gels, these are "fuzzy" polymeric stationary phases that can increase the capacity 10-fold for a given surface area, as a way of improving the performance of non-porous particles (VAR93).

Studies comparing pellicular and porous particles with a variety of stationary phases and analytes have supported the initial observations made by Unger (KAL90, BAR97, JEN96, LOM93). Many of these studies have emphasized the analysis speed possible with pellicular particles and consistently have shown equivalent resolution with 200 to 400% reductions in analysis time (HUR98, JEN96). Several researchers have observed the need to use weaker solvents to obtain retention in non-porous materials that is similar to porous particles as a result of the lower capacity of the pellicular supports (ITO93, LOM93).

Small Non-Porous Particles and Ultra High Pressure

It is apparent from chromatographic theory that the surest approach to achieving

faster separations with high efficiency is to decrease the particle size. Over the past 30 years decreases in the particle size have indeed resulted in impressive decreases in the analysis time while maintaining comparable efficiencies. Decreasing the particle size requires increased pressures and at present, most chromatographic equipment has approximately a 6,000 psi limit. With this pressure limit, it is difficult to further improve separation speed by going to particles less than 2 μm because of the extremely high pressures required to achieve high flow rates. Another factor that limits the utility of smaller particles is the high temperatures generated due to the friction associated with flow through a packed bed. It is calculated that a 1 ml/min flow rate on a typical 4.6 mm column at 3,500 bar (50,000 psi) will generate over 5 W of power, much more than could be dissipated (MAC97).

The temperature problem can be solved by using packed capillaries due to their small diameter and excellent ability to dissipate heat. A 30 μm i.d. capillary operated at 4,100 bar (60,000 psi) is expected to generate approximately 0.4 mW of power, which can easily be dissipated across the capillary. A route to increasing the pressure limit has recently been reported with the development of high pressure pumping equipment compatible with HPLC solvents consisting of a modified, three-stage pneumatic amplifier pump that can supply 4,500 bar (65,000 psi). Special high-pressure fittings to connect capillary columns to the high pressure system were also described. The pump was used with 50-70 cm long by 30 μm i.d. capillary columns packed with 1.5 μm non-porous particles. The optimum flow rate required 1,300 bar (19,000 psi) of pressure for 30 minute analyses and generated up to 330,000 plates (52 cm column) for a lightly retained compound. At 4,100 bar (59,000 psi) analysis times were less than 10 min and still

produced 190,000 plates. More recently, the use of 1 μm particles yielded efficiencies of 200,000 plates in 6 min for a small solute with k' ~1 (MAC99). Using an exponential dilution method to form a gradient, a different type of high-pressure pump (syringe design with maximum pressure of 130,000 psi) was used to generate a peak capacity of 300 in a 30 min analysis time on a 27 cm long column.

While emphasis of these initial reports using ultra-high pressure LC was on high efficiency and not speed, it is apparent that the availability of such high pressures could be used for very fast separations in shorter, packed capillaries. Also, while all work published so far with ultra-high pressure columns has utilized non-porous particles, it is clear that similar equipment could be used with small, porous particles to achieve high flow rates and fast analysis.

Superficially Porous Particles

Although non-porous particles are gaining popularity, some disadvantages can be noted. Most importantly is the lower capacity. Furthermore, the use of very small particles, which is typical with the non-porous material, requires high-pressures (which are still not commonly available) and the resulting shear forces between particles can harm delicate macromolecules. As a way to take advantage of the short diffusion paths associated with very small particles (porous or non-porous), but at lower pressures and with higher capacity, Kirkland developed superficially porous particles (KIR92). These particles consist of a solid 5 μm core coated with a layer of porous microspheres (1 μm diameter with 300 A pores). The particles are produced by spray drying a mixture of silica sol and pellicular particles. The efficiency of the columns were equivalent to columns packed with 1-2 μm totally porous particles but had the back pressure of 7 μm

particles.

Capillary Columns

Packed Capillary Columns

In the past, capillary columns were not considered to be compatible with rapid separations; however, this was largely due to two factors. The first, was that initial columns were not well-packed and exhibited rather high A and C-terms. The second reason was that a perceived advantage of capillary columns was the ease of preparing long columns for generating high theoretical plates, even if at the expense of analysis time, thus most work initially emphasized producing columns >50 cm long. In 1988 however, Karlsson and Novotny demonstrated that by decreasing column diameter from 250 μm down to 44 μm resulted in improved performance with decreasing column diameter including reduced A-terms (as small as 0.49) and C terms (KAR88). As a result, the 44 μm column, packed with 5 μm particles, was able to generate 226,000 plates in 33 minutes for a lightly retained compound. This work was confirmed and extended to columns as small as 21 μm i.d. (KEN89) and 10 μm (HSI96) where it was shown that A terms as small as 0.15 could be achieved.

The potential benefits of reduced column diameters for fast separations was evaluated in a study of columns with 50-250 μm i.d. packed with non-porous and perfusion particles (COL93). This work was based on the idea that with non-porous and perfusion media the C-term becomes so small that the A-term is the dominant form of band broadening, even at high flow rates. In fact, using typical values of A and C for conventionally-sized, non-porous columns, the A term can contribute as much as 90% of the total plate height even at high velocities; therefore, reductions in the A term

associated with packed capillaries may have substantial benefit. This study confirmed a combined reduction of A and C terms with the non-porous particles. This allowed generation of ~700 plates/s for unretained species using 8 μm particles packed into a 75 μm capillary. With this column, 4 catechol compounds were resolved in ~40 s isocratically.

Open Tubular Liquid Chromatography (OTLC)

Another type of capillary column, the open tubular column, may also offer a route to fast separations. In this type of chromatography, the stagnant mobile phase and eddy diffusion terms are eliminated. Without these band broadening effects, the potential exists for fast separations; however, numerous difficulties arise from the need to have columns with inner diameters of 10 μm or less to achieve reasonable results. Difficulties with implementing OTLC with such small columns include injection, detection and fabrication of columns with good phase ratios and stability.

Research on the fabrication of open tubular columns, such as use of sol-gel technology for production of superficially porous capillaries (GUO95), continues to improve the state-of-the-art. These new procedures, combined with optical gating or other injection techniques used for fast separations in miniaturized CE systems, may ultimately allow practical, rapid separations by OTLC.

In addition to the properties mentioned above, capillary columns have been used with ultra-high pressure and small particles because of their heat dissipation properties, CEC for heat dissipation purposes, and with temperature gradients because of their low thermal mass. Thus, for a variety of reasons capillary columns are part of the future of fast separations.

Monoliths

In a monolithic or continuous bed column, the separation path consists of a network of pores defined by a continuous polymeric network of support instead of a bed of discrete particles. Three distinct approaches to the preparation of monolithic columns have been described: 1) polymerization of a rigid stationary phase support within a separation tube, 2) polymerization of a compressible gel network within a tube followed by compression, and 3) sintering of discrete particles packed into a tube. (Microfabricated "monoliths" have also been described; however, they will be considered under electrochromatography). Monolithic columns are more frequently used with electrochromatography than pressure driven chromatography because frequently the small pores prevent flow; however with sufficient control in the formation of the monolith, large pores are available to allow flow at reasonable back-pressures.

Rigid Polymer Monoliths

Rigid polymer networks have been formed from both organic polymers (XIE97, MOO98, CIO98, TEN98, VIK97, PET96, PET96A and silica networks (ISH98, FUJ97, MIN95, MIN98, CAB96) with both having advantages. Organic polymer networks offer selectivity and relatively simple preparation because the separation characteristics of the column are due to the functional groups and backbone of the polymer itself. A change in monomer composition will change the separation performance. Silica based monoliths allow the use of previously developed derivatization chemistry for conventional particles and can handle higher pressures than most polymers.

Hjerten's group has explored the preparation of microcolumns based on monolithic media for reversed-phase and ion-exchange chromatography. Reversed phase

columns as small as 25 μm i.d. were prepared by (1) synthesis in the column tube of a continuous bed matrix from a monomer solution (piperazine diacrylamide, methacrylamide) containing allyl glycidyl ether and 2-hydroxyethyl methacrylate and (2) linking of C-18 ligands by reacting 1,2-epoxyoctadecane with the epoxy and hydroxyl groups in the matrix (LIA96). This continuous network showed good performance in the separation of proteins and peptides and analysis times as short as 100 s for the resolution of 5 standard proteins. Ion exchange columns as small as 10 μm i.d. were prepared by a similar fashion (LI94). With this synthetic procedure, the porous rod is attached directly to the walls obviating the need for frits and results in a stable bed. Interestingly, it was also claimed that the covalent linkage of the bed to the tube wall also suppresses the zone-broadening "wall effect" which can occur with columns in the 100 to 300 μm i.d. range.

Sintered Packed Beds

Another approach to preparing silica-based monoliths is based on sintering porous particles into a 75 μm capillary. Columns prepared in this fashion with 6 μm particles had improved column stability compared to a normal packed bed capillary; however no improvement at high flow rates was noted (ASI98). It did not appear however, that these columns had a fundamentally different performance than the packed bed.

Compressed Monolithic Beds

A third approach to forming monolithic columns, described by Hjerten's group, involves compressed gel porous networks as separation media (HJE92, ERI96, LIA96, HJE93). Such columns have been prepared with reversed phase, ion-exchange, and affinity stationary phases. In an early disclosure of this approach (LIA96) the procedure

for column synthesis was described as polymerization of an agarose support within the column to form a network that could be compressed with either pressure or a plunger in the column. The compressed bed had flow through channels that formed a continuous porous network. Several impressive examples of rapid separations were shown including reversed phase separation of 5 proteins in 3 min, cation exchange separation of 6 proteins in 30 s and resolution of an enantiomeric pair in 40 s. Subsequent work has shown continued improvement in column fabrication as well as a number of applications of the technique. This technology also evolved into the rigid polymers for microcolumns described above.

Summary of Monoliths

The results presented so far suggest that monolithic columns may hold promise for rapid, pressure-driven separations. By far the most activity has been with rigid polymer networks and it appears that a great deal of versatility and control are possible in terms of pore design, skeleton thickness, and stationary phase attachments. At present however, a well-developed theory to guide experimenters in devising the appropriate properties of the porous network is lacking. In addition, while several groups have compared the performance of the monolithic columns to columns packed with conventional porous particles, more relevant comparisons would be with perfusion, pellicular, and superficially porous packed beds. Comparisons to these types of columns allow better evaluation of the true benefits of these types of columns for fast separations.

Temperature

Temperature control is an underused variable in LC separations as evidenced by the paucity of commercial chromatographs equipped with temperature control units;

however, it has been established that elevated temperatures improve separation speed in several ways. Increasing the temperature decreases the mobile phase viscosity which decreases the pressure required for high flow rates, potentially allowing smaller particles to be used, and increases the diffusion coefficient of the analyte in the mobile phase. In addition, increasing the temperature can accelerate the sorption-desorption kinetics of the analyte thus reducing this band broadening effect. In a demonstration of utilizing higher temperature for fast separations, four standard proteins (ribonuclease A, cytochrome C, lysozyme, and β-lactoglubulin B) were separated in 12 s at 120 °C with a 10-90 % acetonitrile gradient (flow rate 5 ml/min) on a 2 μm ODS-silica column (3 cm x 4.6 mm). An important feature of this system was that the mobile phase was pre-heated prior to pumping into the column eliminating the problems associated with poor heat transfer through the packed bed that would result in uneven temperature profiles and associated band broadening (CHE93).

Precisely controlled temperature is important if highly reproducible chromatograms are to be obtained, especially when dealing with steep gradients, which is often required for fast analyses. In one example, it was found that a water bath provided a much more stable temperature than a convective air heater for the separation of proteins and oligonucleotides (HUB93). Seven test proteins were studied with respect to retention and resolution over a range of temperatures from 30 to 80 °C on a 2.1 μm diameter non-porous poly(styrene-divinylbenzene) 50 x 4.6 mm column. It was found that most of the proteins' chromatographic behavior changed equally as temperature increased. One protein (catalase) however was slightly more sensitive to temperature. It coeluted with β-lactoglobulin A at 30 °C but was baseline resolved at 80 °C. The same study was carried

out for the separation of oligonucleotides which reached it maximum resolution at 40 to 50 °C.

The temperature change does not have to be a drastic one in order to see significant improvements in the separation. A 5 minute gradient separation of 11 hydrazones at 20 °C did not allow for the complete resolution of all the components however, by increasing the column temperature by just 10 degrees allowed all the components to be baseline resolved (PAA97).

The good heat transfer properties of small diameter fused silica capillaries make them more amenable to temperature controlled LC and can even be used with temperature programming. This concept has been demonstrated with separations of mixtures of alkylbenzenes (AB) and PAH on a fused-silica column (50 cm x 180 μm i.d.) packed with 6 μm ZorbaxSB ODS-silica. The retention of the alkylbenzenes was evaluated as function of acetonitrile concentration at a fixed temperature and as function of temperature at a fixed acetonitrile level (POP83, POP81). These studies showed that a 5 °C temperature change had the same effect on retention as a 1 % change of acetonitrile concentration. Thus, it was possible to perform mobile phase programming and temperature programming to achieve identical separations. Temperature programming was also used for separating simple protein mixtures. Finally, a combination of temperature and mobile phase programming was found to be effective for optimizing separations in less than 2 minutes (CHE97). The results from these studies show that packed capillaries with elevated temperatures may offer a convenient route to faster separations. Limitations of this approach include the instability of stationary phase and the stability of delicate analytes at elevated temperatures.

One potential drawback of using high temperatures for fast separations is that columns become less stable at higher temperatures, resulting in changes in capacity factor and loss of resolution. A way to avoid this problem is to use a stationary phase or support material that is more stable than regular silica. This has been addressed by using 2.5 or 4.5 μm polybutadiene coated zirconia particles (LI97). The columns (100 x 4.6 mm) were evaluated for stability at temperatures up to 200 °C and were found to have a constant k' for at least 1,300 column volumes at the highest temperatures. An isocratic separation of test compounds at 100 °C maintained baseline resolution of all the compounds with a 5 fold increase in flow rate and 18 fold reduction in separation time.

The effects of temperature on efficiency and speed in open tubular columns have also been studied in the separation of steroids (RYA96). Air convection was used to thermostat commercially available OTLC columns of 50 or 100 μm diameter. As a result of pressurization, temperatures well above the normal boiling point for the solvent could be used. Increasing the temperature of the column from 100 to 150 °C gave a 3 fold improvement in plates. Both step and linear gradients were applied during the separation. With a linear gradient of 60 °C (90-150 °C) the analysis time decreased by 40 % compared to an isothermal run at 90 °C and maintained baseline resolution of the 6 model compounds.

Electrochromatography

In capillary electrochromatography (CEC), mobile phase is pumped electroosmotically instead of by pressure as is typical for HPLC. While the concept of CEC was introduced many years ago, it has recently received an explosive growth in interest. Several reviews of CEC (COL97, CRE96) have appeared in the past few years

as well as a series on the practical aspects of CEC (DIT98, DIT97, DIT96, DIT95). Given the presence of these reviews, this work will emphasize CEC from the vantage point of fast separations.

Principles of CEC for Fast Separations

CEC is an attractive possible route to fast separations. The plug flow profile associated with EOF decreases band broadening associated with resistance to mass transfer in the mobile phase allowing flat van Deemter curves as demonstrated in several studies (KNO91, SEI97, ZHA98, YAM92, YAN95). The flat curves could potentially allow high efficiency at high flow rates and short times. Electroosmosis may also enhance intraparticle mass transfer due to flow within particles; however, this is still under investigation (VAN96, CHO97, SEI98). In addition, pressure differentials are not used to drive flow; therefore, it should be possible to use particles smaller than 2 μm without the problems associated with the pressure limits of current instrumentation. Flow rates of 1-3 mm/s are typical and can be easily obtained with 30 kV power supplies.

An instrumental advantage of CEC is that it can be carried out on most commercial CE instruments so no additional equipment must be purchased. The "short end injection" technique common in CE can be applied to CEC (EUE98). Commercial CE instruments typically require at least 30 cm of capillary, 8-10 of which is post detection. For "short end injection" the portion that is normally after the detector is used as the inlet end giving separation distances 8 to 10 cm. In CE, this arrangement "wastes" most of the voltage that is applied; however, in CEC since the resistance is greater across a packed bed than open tube, it is possible to drop the majority of voltage across a short portion of the capillary that is packed so that only a small portion of the applied voltage is

wasted across the empty tubing. A 4-fold reduction in analysis time was demonstrated by decreasing the separation length from 25 cm to 7.5 cm while maintaining a constant applied voltage.

A significant issue in fast CEC separation is control of EOF and obtaining EOF that is fast compared to what may be obtained by high-pressures. EOF was studied according to type and percentage of organic modifier and demonstrated that as percent organic increases, electroosmotic flow decreases until very near 100% when the flow drastically increases (WRI97). Acetonitrile gives the fastest EOF followed by water and then methanol. These results suggest potential difficulties in developing mobile phase gradients. The ability to apply a gradient to CEC would allow fast separations of analytes with widely different hydrophobicities. Yan, et al have used two computer-controlled high voltage power supplies to form gradients for CEC (YAN96). Potentials are applied to two separate reservoirs connected by a tee with a common ground at the outlet of the capillary. By maintaining the overall voltage and changing one voltage relative to the other a gradient is produced. Huber, Choudhary, and Horvath (HUB97) describe a gradient system in which the mobile phase (0.1-0.2 ml/min) was input from two reciprocating displacement pumps via a 10-µl mixer and a 17 ml cavity housing the column inlet and an electrode. This system provided reproducible gradient profiles.

Column design is still being actively explored in CEC. Designs have included packed columns, monolithic columns, open tubular columns, microfabricated open tubular columns (KUT98), and microfabricated monoliths (HE98). No particular design seems to have a theoretical advantage in terms of speed of separation; however, the microfabricated columns do provide a convenient means for rapid injection which may be

useful for separation times <10 s.

In the present work, we examine band broadening for unretained solutes in small bore columns (<50 μm) packed with non-porous particles to evaluate their applicability to fast separations. For comparison, we also examine electroosmotically driven flow in the same columns.

CHAPTER 8
COMPARISON OF PRESSURE AND ELECTROOSMOTICALLY-DRIVEN FLOW IN CAPILLARIES PACKED WITH NON-POROUS PARTICLES FOR HIGH-SPEED SEPARATIONS

Introduction

The previous chapter presented a review of the parameters affecting the speed of a chromatographic separation. This chapter will utilize three of those parameters to improve the separation efficiency of packed capillary columns especially at high flow rates. Improving the speed of chromatographic separations requires suppression of band broadening effects that dominate at high flow rates. The most important effects can be identified by measuring the reduced plate height (h) as a function of reduced velocity (v) and fitting the data to the Knox equation:

$$h = A \bullet v^{0.33} + B/v + C \bullet v \qquad (1)$$

where A, B, and C are coefficients describing the magnitude of eddy diffusion, longitudinal diffusion, and resistance to mass transfer, respectively.

A well-packed HPLC column containing porous particles is expected to have Knox coefficients of A = 1, B = 2, C = 0.10. With these coefficients, the resistance to mass transfer term will dominate at high flow rates. For example, at a reduced velocity of 50, 57% of the total plate height would be contributed by the C term; consequently most efforts to improve chromatographic performance have focused on reducing the resistance to mass transfer effects. One effective approach has been to utilize non-porous particles which eliminate the stagnant mobile phase resulting in much reduced C terms.

Knox estimated that C = 0.003 for unretained solutes in a well-packed column of non-porous particles (KEN72). With non-porous particles the A term will dominate the band broadening over a wide range of flow rates. For example at a reduced velocity of 50, with A = 1 and C = 0.003, the A term would account for 95% of the total plate height.

It has been shown that Eddy diffusion can be reduced by using small columns and column to particle diameter ratios (ρ) (KNO69, KAR88, KEN89, COL93, HSE96) due to wall effects on packing; therefore, small bore columns packed with non-porous particles should have reduced A and C terms and be suitable for rapid separations. When ρ is greater than 100, as in conventional columns, there are no wall effects and ρ is unimportant. From ρ = 20 to ρ = 6 wall effects become more important until below 6 when no additional effects improve.

Another potential route to reduced plate heights at high flow rates is the use of electroosmotic flow (PRE74, JOR81, KNO91). In capillary electrochromatography (CEC), the plug shaped flow profile improves efficiency over all flow rates while flow inhomogeneties are reduced causing significant reductions in plate height as the flow rate increases.

Experimental

Packing Procedures-Reversed-Phase Particles

The packing procedure was similar to previously described methods (KEN89, BOU95). Fifteen mg of 3.0 μm ODS non-porous particles (Micra Scientific, Northbrook, IL) were weighed into a clean glass vial and 3 ml of HPLC grade acetonitrile (Fisher Scientific, Pittsburgh PA) added as slurry solvent. The mixture was placed in an

ultrasonic bath for a minimum of 30 minutes to ensure a well-dispersed slurry. Fused silica capillaries (Polymicro, Phoenix, AZ) (50 or 20 μm i.d., 365 μm o.d.) were cut approximately 10 cm longer than the desired packing length and a retaining frit of borosilicate glass beads (Duke Scientific, Palo Alto, CA) (8.2 μm diameter for 50 μm and 2.5 μm beads for 20 μm capillaries) was sintered into one end of the capillary with a flame. The capillary was packed at an initial pressure of 70 bar which was stepped up 35-75 bar every 5 minutes to a final pressure of 3450 bar. In this manner 7-12 cm of the capillary could typically be packed in 20 to 45 minutes. Once a sufficient length of capillary was packed, the pump was turned off and the pressure was allowed to bleed through the capillary for at least 30 minutes. Glass beads for a second frit were then tapped into the inlet end of the capillary, the solvent changed to methanol, the capillary flushed with the same pressure steps as the packing procedure, and the final pressure held for 2 h. During this procedure, the length of the packed bed would decrease up to 0.5 cm. While under pressure, the beads for the second frit were sintered into place by applying an electric arc. Typical columns had a total length of approximately 15 cm with 7 to 10 cm of packed bed. For chromatographic testing, the packed end was used as the inlet.

Packing Procedure - Bare silica particles

Slurries of bare silica particles (4.5 μm diameter) were prepared by sonication of 20 mg of particles in 3 ml of 20 mM (N-tris[Hydroxymethyl]methyl-3-aminopropanesulfonic acid) (TAPS) and 20 mM 2-amino-2-methyl-1,3-propanediol (AMPD) (Sigma) (TAPS/AMPD) at pH 8.0, sonication in 3 ml dilute nitric acid, and finally additional sonication in 3 ml TAPS/AMPD as final slurry solvent for at least 30 minutes to disrupt aggregates. Omission of any sonication steps resulted in frequent

capillary clogging during packing. Fifty μm i.d. by 365 μm o.d. capillaries were packed with the same pressure gradient as above while simultaneously applying an electric field of + 100 to 750 V/cm to the capillary with the packing bomb as ground. Packing was initially performed without the applied voltage which resulted in unstable columns, giving rise to gaps after only a few chromatographic runs. Electrokinetic packing as described by Yan (YAN) was attempted but was extremely slow. The combination of pressure and electrokinetic packing provided good bed stability in an acceptable packing time. A 20 cm capillary would pack in less than 2 h after which both the pressure and electric field were held for an additional 2 h. The electric field was then removed, the pump turned off, and the pressure allowed to bleed for at least 30 minutes. The capillary was dried by pumping through nitrogen, a second frit sintered into place by flame, and a detection window made with hot sulfuric acid.

The minimum total length of capillary that could be easily handled during chromatographic runs was 15 cm while the minimum length to the detector was 7 cm. Packing bare silica columns at least 15 cm could be routinely done; however, packing with ODS particles often stalled at approximately 12 cm. Instead of spending additional time increasing the packed length, frits were simply made in the middle of the ODS columns once sufficient lengths were packed.

Instrumentation and Experimental Parameters

ODS columns were tested using 100 nM Rhodamine RG as the analyte and 100% methanol as mobile phase. Detection was accomplished using an LIF detector similar to that described elsewhere (YEU92) (Figure 8-1.). Rhodamine was excited by the 543 nm line of a He-Ne laser (Melles-Griot, Carlsbad CA) and emission collected after a 580 nm

long pass (Melles-Griot) and spatial filter by a PMT (Hamamatsu R 647, Japan). Columns packed with bare silica particles were tested using 50 μM anthracene as the analyte and a mobile phase of 60% acetonitrile, 40% 20 mM TAPS/AMPD. Detection was accomplished using UV absorbance at 251 nm (Spectraphysics, Anaheim, CA). Test analytes were dissolved in mobile phase. In both cases, detection was performed on-column, 2-5 mm before the outlet frit of the column.

For all experiments, electrokinetic injections were used. To ensure that injection did not contribute to the observed plate height, injections were performed with successive reductions of voltage and time until no improvement in plate height was observed. Typically injections were 1-2 kV for 2 s with a Spellman CZE 100R high voltage power supply (Plainview, NY).

For LC, flow from a Varian 2510 HPLC pump (Palo Alto, CA) was split after a Rheodyne six port valve (Cototi, CA) and maintained during injection with a dummy column of approximately equal length. Pressure was applied to the column by switching the valve at the start of the run. After the run was completed, the flow rate was stepped down in ~35 bar increments over several minutes so that the column was not damaged by a sudden pressure drop.

Diffusion coefficients were determined by the stopped flow method (MOO93) in their respective mobile phases and were $10.0 \pm 0.3 \times 10^{-6}$ cm^2/s (n = 5) and $7.2 \pm 0.3 \times 10^{-6}$ cm^2/s (n = 5) for anthracene and rhodamine RG respectively. Both anthracene and rhodamine were determined to be nearly unretained by comparison of retention times to the migration of an intentionally injected air bubble in LC mode. The air bubble was assumed to move with the solvent front and its migration closely matched

that of the analytes.

Data were low pass filtered by a variable passive RC filter (τ = 0.01 to 0.2 s) and collected on a personal computer (Gateway 2000, Sioux City SD) with an AT-MIO-F5 data acquisition board (National Instruments, Austin TX) at 2-5 times the filter rate. Plate heights were calculated by statistical moments software written in house (Lab Windows) and data fit to the Knox equation by non-linear regression using Systat (Systat, Inc.).

Results

Column Packing

Capillaries generally packed smoothly, with the first 2 to 3 cm packing in a few minutes and the remaining length packing at a constant rate for both ODS-modified and bare silica particles. Occasionally packing would stop but could often be restarted by an increase in pressure up to 354 bar or by a sudden release of pressure. Visual inspection of a stalled capillary usually showed a small plug of particles at the capillary inlet which could be cut off and packing resumed. Packing at higher pressures was attempted but gave no decrease in packing time and plugged the capillary more often.

Column-to-Column Reproducibility

All columns packed were tested over as a wide a flow velocity range as possible using pressure and EOF. For pressure-driven tests, the flow rate range was limited by the fittings which were not reliable above 275 bar. For EOF, the flow rate was limited by the power supply and column length (maximum field = 4 kV/cm). Figure 8-2 shows the Knox plots for each of the three types of columns tested for both pressure and

electroosmotic pumping. Each point is the average of all the columns tested (2 to 4 columns tested with 5 measurements at each velocity per column) at a given velocity and error bars represent ± one standard deviation. The solid lines are obtained from the best fit of the data to the Knox equation. Column-to-column reproducibility was good for all dimensions, with plate heights varying by 2 to 6% at most flow rates tested.

In some columns, poor performance was observed with pressure-driven flow which was invariably associated with gaps that developed in the packed bed. The gaps could be removed by sonicating the column while under pressure, which would close the gap and leave a void at the column inlet. The void at the inlet could be removed by cutting off the tip of the column and installing a new frit. The reconditioned column would then have plate heights equal to those before gap formation. Only columns confirmed not to have voids were used for data in the plots.

Performance of Pressure-Driven Flow

The best-fit lines from Figure 8-2 are replotted in Figure 8-3A for the pressure-driven flow only for comparison of the different ρ's. In addition to the data collected here, we have added a plot for a column from previous work (COL93) which had a 50 μm i.d. column and 8.0 μm non-porous particles ($\rho = 6.2$) for comparison. Data from all of the columns show that performance improves with decreasing ρ. For example, h_{min} decreases from 1.97 for the column with the largest ρ to 0.96 for the column with the smallest ρ. The latter value corresponds to 370,000 plates/m.

The good performance of the 20 μm i.d. column suggests that decreasing column i.d. may also be beneficial; however, a comparison with a larger column with slightly smaller ρ (50 μm i.d. with 8 μm particles for $\rho = 6.2$) shows that the larger column

actually had slightly better performance. These data indicate that decreasing ρ is more important than decreasing the column diameter for achieving good performance in capillary columns with pressure-driven flow. This is in agreement with our conclusion reached previously for columns from 50-150 μm i.d. packed with larger non-porous particles (COL93).

The improved performance with decreasing ρ can be attributed to decreasing A terms. This trend is shown in Table 3-1 which shows the calculated Knox coefficients for the different columns tested. The small A terms and their decrease with ρ are in agreement with previous results in columns in this size range (KNO69, UNG85). Although performance improved for columns with decreasing ρ, the results at high flow rates were somewhat worse than expected for all columns. In particular the C-terms, as calculated from best fits to the Knox equation, were higher than what could be expected in the best case. The C-terms actually increased with smaller ρ, an unexpected trend not previously observed. For the 20 μm i.d. columns, the C term was equal to 0.04 whereas a value as low as 0.003 might be expected for a well-packed column (KNO87). In previous work with larger non-porous particles, it had been possible to achieve C-terms that were as low as 0.007 (COL93). A number of possible explanations exist for these relatively large C-terms. One is that the flow rates achieved were not large enough to actually measure the C-term accurately. Supporting this possibility, we have observed that small changes in the plate heights at high velocities can drastically change the calculated values for the A and C terms. Another possibility is that the performance was adversely affected by aggregates of particles. It is well known that 3 μm particles are considerably more difficult to pack without aggregation than particles that are >5 μm.

Thus, improvements in the packing procedure may be expected to improve the results of the columns in the pressure-driven mode, especially at high velocities.

Performance of EOF

The performance of the same columns operated in CEC mode is shown in Figures 8-2 and 8-3B. The data clearly show that EOF performance is superior to pressure-driven for all column sizes tested. In most cases the plate height is approximately one-half that achieved with pressure-driven flow with the difference becoming more pronounced at high velocities. Minimum reduced plate heights were between 0.3 and 0.5 (670,000 to 1,000,000 plates/meter) for the same columns in CEC mode. Although columns operated in CEC mode always performed better than in pressure-driven mode, the difference was less with columns with small ρ (20 μm with 3 μm particles) as seen by comparing Figure 8-2A and C.

Columns with EOF were relatively unaffected by column diameter or ρ as shown by the plots in Figure 8-3B. These results corroborate those obtained for 75 and 100 μm columns reported previously (KNO87, REB96, FER98). The effect of ρ on pressure-driven chromatography has been attributed to a reduction of flow inhomogeneties (CHE97). With EOF, flow inhomogeneties are masked by the plug-flow profile and the independence of flow velocity on channel diameter. Interestingly, we also observed that columns driven by EOF were less susceptible to problems with packing. For example, as mentioned above, columns with gaps had noticeably poorer performance during operation in pressure-mode; however, the presence of gaps had virtually no effect with EOF. This observation illustrates further independence from packing quality gained by using EOF. This effect has been previously suggested (SEI98).

Discussion

Prospects for Fast Chromatography

In the 20 μm i.d. columns, the reduced plate height was ~2 at a reduced velocity of 30 with pressure-driven flow. For a 7.5 cm long column, this corresponds to 12,500 plates with a dead time of 10.4 s or 1,200 plates/s. As mentioned above, the relatively high C-term hurt the value for plates/s and may be improved with better packing. For the same column operated in the CEC mode, at the same flow rate, the reduced plate height is 0.85 corresponding to 29,400 plates or 2,830 plates/s. At the maximum reduced velocity achieved (41), the efficiency was 25,200 plates or 3,310 plates/s. Sample chromatograms for unretained test solutes under high flow rates conditions are shown in Figure 8-4. Similar values of plate heights and plates/s have recently been achieved using CEC with smaller (1.5 μm) non-porous particles (DAD98).

The results show that by using columns with small ρ, small particles, and non-porous particles it is possible to achieve simultaneous reductions in the A and C term for fast separations. The CEC mode is clearly capable of producing high plates in short times while improvements in packing will be required to allow better performance in the pressure-driven mode. For the best columns tested here, if we extrapolate to $\nu = 300$, (highest velocity achieved in reference 147) we could expect $h = 13.5$ for pressure-driven and $h = 3.65$ for EOF driven columns. These h values correspond to 1,850 and 6,850 plates respectively in 1.0 s. Analysis times this fast will require the ability to pump the mobile phase faster. For pressure-driven chromatography, recent advances in fittings and pumping mechanisms make this feasible (MAC97, MAC98). For CEC, higher E will be required.

Table 8-1. Calculated Knox Terms for cLC

Column/Particle diameter (μm)	ρ	A	B	C
50/3.0	16.7	0.88	2.86	0.009
50/4.5	11.1	0.22	1.95	0.05
20/3.0	6.7	0.22	2.02	0.04
50/8.0[a]	6.2	0.37	2[b]	0.085

[a] values from reference (COL93), [b] assumed

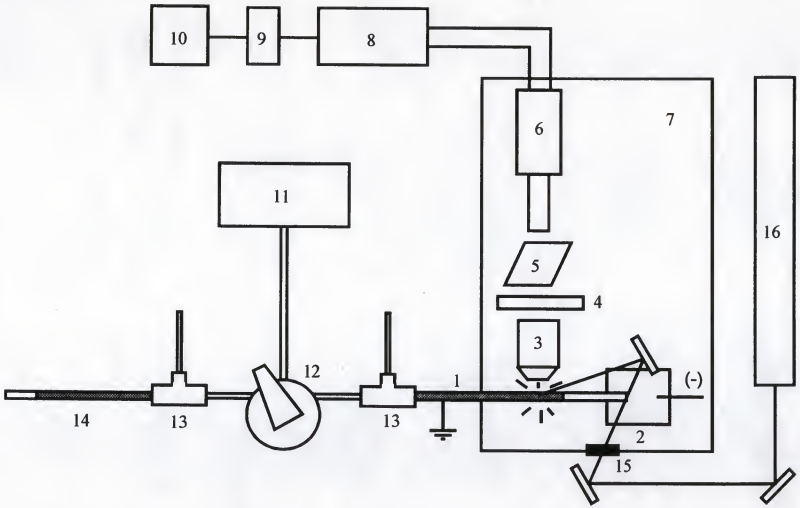

Figure 8-1. System diagram for LC-LIFD. 1) capillary column 2) buffer reservoir 3) microscope objective 4) long pass filter 5) spatial filter 6) photomultiplier tube 7) light tight box 8) power supply/current amplifier 9) passive RC filter 10) computer 11) HPLC pump 12) injection valve 13) splitter 14) dummy column 15) band pass filter 16) He-Ne laser

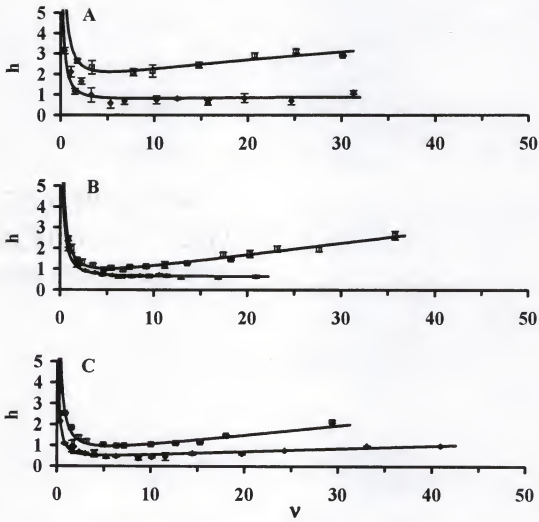

Figure 8-2. Knox plots for tested columns. Each set of data points are the average of at least 2 columns at each velocity, error bars represent +/- 1 standard deviation. Diamonds represent CEC and squares represent LC. A) $\rho = 16.7$, B) $\rho = 11.1$, C) $\rho = 6.7$.

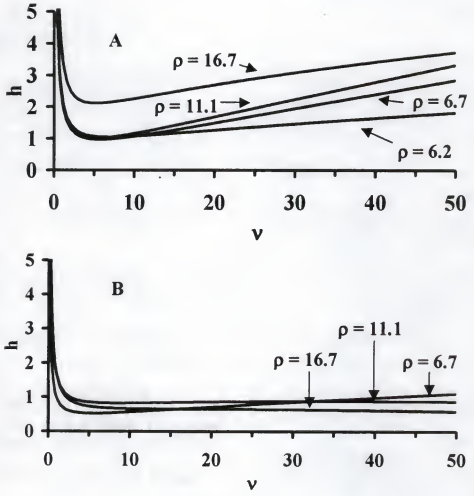

Figure 8-3. Fitted Knox curves for A) Pressure driven flow and B) Electroosmotic flow. For ρ = 16.7, i.d. = 50 μm dp = 3.0 μm ; ρ = 11.1, i.d.= 50 μm dp = 4.5 μm; ρ = 6.7, i.d = 20 μm dp = 3.0 μm; ρ = 6.2, i.d. = 50 μm dp = 8.0 μm.

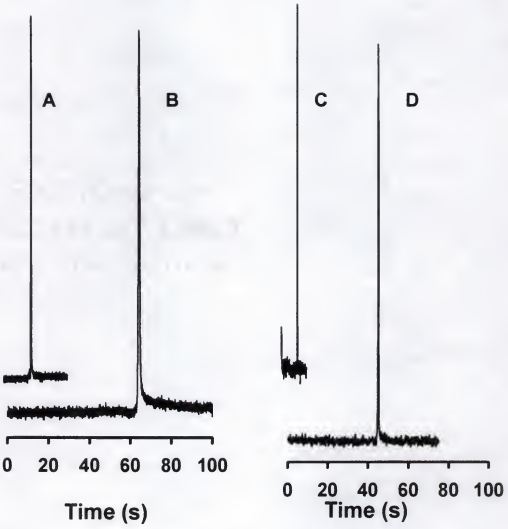

Figure 8-4. Chromatograms (A and B) and electrochromatograms (C and D) demonstrating plate heights at ν_{opt} and vmax for 20 μm i.d., 3.0 μm ODS packed columns. See text for conditions. A) ν_{max} = 29, h = 2.14 B) ν_{opt} = 7.3, h = 0.96 C) ν_{max} = 41, h - 0.98, N/s = 3350 D) ν_{opt} = 19, h = 0.27, 1.2 x 10^6 N/s.

CHAPTER 9
SUMMARY AND FUTURE DIRECTIONS

Summary

The use of *in vivo* microdialysis has enabled researchers to study many different classes of biologically interesting compounds from drugs and their metabolites to neurotransmitters. Conventional analysis methods such as HPLC with electrochemical or fluorescent detection allows samples as small as a few microliters to be analyzed, resulting in temporal resolution down to the minute time scale. These methods do not, however, allow observation of short-lived processes such as neurotransmission. We have developed an on-line capillary electrophoresis system that allows monitoring of the excitatory amino acid neurotransmitters glutamate (Glu) and aspartate (Asp) in 3.5 s intervals.

In order to fully realize the temporal resolution possible with on-line CE-LIF, it was first necessary to determine the resolution of the microdialysis probe itself. The study revealed that the time taken to clear the active area of the probe was the limit to temporal resolution of the microdialysis probe. By eliminating system dead volumes, it was possible to eliminate all measurable sources of temporal broadening in the CE analysis system. The main contributor to system broadening was the commercial tee used to mix dialysate with derivatization fluid, which held a dead volume equal to that of the active volume of a 2 mm tip probe. By replacing the tee with a custom built zero dead volume

tee, the system contributed no measurable time to the overall temporal resolution.

With a completely optimized system, focus was shifted to the in vivo analysis of the neurotransmitter amino acids Glu and Asp. Even though the presence of ascorbic acid (AA) in the brain has been well characterized, its function is not completely known. It is believed that AA heteroexchanges with Glu during transport of Glu out of the extracellular space following release (REB97, GRU93). Direct infusion of 500 μM AA into the striatum caused Glu to increase to 360 % of the original basal level. Electrical stimulation of the prefrontal cortex in the presence of 500 μM AA resulted in the increase of Glu overflow to 500% of control values. This effect was not due only to an antioxidant effect because the infusion of iso-ascorbic acid had no significant effect on either basal or overflow levels. These results are the first to show the direct modulation of Glu by AA and are consistent with the heteroexchange model.

Continuing the theme of characterizing synaptic release in the brain, the effect of mGluR and Glu transporters on Glu release were characterized in the rat hippocampus. High frequency electrical stimulation of the perforant path caused an increase in extracellular Glu in the dentate gyrus. Asp exhibited a response that was only apparent after signal averaging. The Glu overflow was Ca^{2+} and TTX sensitive, suggestive of a neuronal origin for stimulated Glu. The selective application of mGluR agonists and antagonists showed that the receptors were weakly active under basal conditions. The application of electrical stimulation for the measurement of neuronal Glu is crucial because it bypasses the factors that make basal levels apparently non-neuronal. Extracellular Glu comes from different pools in the brain. Glu is used in several metabolic processes including protein, peptide, and GABA synthesis and carbohydrate

metabolism (FIL95). Second is the contribution from glial cells (KOR85) and third is the contribution from neurons. The electrical stimulation will only stimulate Glu neurons and therefore will be both TTX and Ca^{2+} sensitive. Additionally, the detection of autoreceptors by modulation of Glu with the application of agonists and antagonists is a criterion for neuronal measurements. Again this criterion has been demonstrated here. Inhibiting uptake resulted in a 600% increase in basal Glu and almost 1000% increase in stimulated overflow. From these results, it appears that regulation of extracellular Glu is mainly due to a highly active transport system as opposed to autoreceptor control as seen in the striatum (LAD98).

The differences in electrically stimulated overflow and autoreceptor control between the striatum and hippocampus warranted an in-depth study to determine the source of this difference. By introducing exogenous D-Asp it was possible to determine the relative differences in both uptake and diffusion between the two regions. The striatum allowed for a higher recovery of D-Asp than the hippocampus as well as a faster rate of decay. However, the hippocampus showed a much larger response to uptake inhibition. These results were interpreted to mean that the striatum had faster diffusional properties but less uptake than the hippocampus. Taken together with strong autoreceptor control, these results indicate that the striatum is more likely to utilize volume transmission than the hippocampus.

Glu has long been believed to be responsible, at least in part, for the generation of seizures mostly because of its excitotoxic effects (SHE99, CHA00, URB98). In order to study this role, the effects of the cholinomimetic pilocarpine (PILO) on both Glu and Asp in anesthetized rats were monitored. PILO was administered via intravenous injection

and direct infusion into the hippocampus and electroencephalographic (EEG) monitoring provided indication of seizure generation in the brain. Injection of PILO produced physical signs of seizure but did not produce the full spectrum of brain activity associated with seizure nor did it produce a change in either Glu or Asp. Direct infusion of PILO produced varied Glu responses and little change in EEGs. With pretreatment with lithium, consistent decreases in both Glu and Asp were seen as well as full seizure activity via EEG in some animals. Electrical stimulation in the hippocampus with PILO infusion showed a delayed response in only the first stimulation after 20 min of PILO infusion. Subsequent stimulations showed little or no response. Because of the variability in response to PILO, it was determined that a change in extracellular Glu, either increase or decrease, does not induce a cholinomimetic seizure. The combination of EEGs and electrical stimulation of the perforant path suggests that PILO causes over activation of Glu receptors (OBR96).

Because fast LC separations would be able to separate different types of components in dialysate (specifically, neutral amino acids) the applicability of non-porous particles with both pneumatic and electroosmotic flow was determined in packed capillary columns with respect to high-speed separations. The chromatographic performance of capillaries with 20 and 50 μm inner diameter packed with 4.5 and 3.0 μm non-porous particles was evaluated under conditions of pressure and electroosmotically driven flow (EOF) for unretained analytes. Decreasing column diameter and column diameter to particle diameter ratio (ρ) enhanced performance for pressure-driven flow but not for electroosmotically-driven flow. It was concluded that decreasing column bore and ρ in pressure-driven columns enhances the uniformity of the column allowing for

improved performance; however, the use of electroosmotic flow masks heterogeneous flow and thus does not benefit from these effects.

Future Directions

Analytical Applications

The analytical challenges that lie ahead take their cues from the biology. The first area for improvement comes from the hippocampal stimulations, better system reproducibility. In its present state, the system has an *in vitro* peak height reproducibility around 2%. When in vivo measurements are performed reproducibility becomes 4-5%. This increase may be due to either system related problems (on-line reaction) or biology. An improvement in reproducibility will allow for smaller changes to be measured and may let changes in hippocampal Asp be studied. The second area for improvement is in separation time. Even though 3.5 or 5 s separations are fast, higher sampling will result in better profiling of the fast changes observed in hippocampal electrical stimulations. It is known that cultured hippocampal astrocytes show Ca^{2+} oscillations that may be related to Glu changes (PAS97). A faster, more reproducible instrument may be able to observe these changes. The poorer reproducibility in *in vivo* measurements may be a result of these oscillations.

The instrument in its present state does not offer much room for improvement. Shortening the separation capillary or using higher voltages will give baseline resolution between Glu and Asp down to 2 s. Unfortunately, the switching valve used can not inject more often than every 3.2 s or switch faster than 30 ms.

One possible solution to both reproducibility and separation time is to construct as much of the system on a microfabricated chip. A chip with a mixing tee, reaction

chamber, and flow-gated interface would greatly improve several aspects of the system. First, a microfabricated mixing tee would remove the labor intensive fabrication of the tee and eliminate possible sources of clogs and leaks due to the Teflon connectors. A fixed distance in the flow-gated interface would make day-to-day reproducibility in peak height much more consistent. For optimal injection reproducibility in the current system the reaction and separation capillaries must be cut as flat and smooth as possible. With a microfabricated interface this source of irreproducibility would be eliminated. Currently separation efficiency on chips does not compare to efficiency in capillaries, but if a satisfactory separation could be performed, the entire instrument could be on a single chip, making commercialization a more likely possibility.

Another obvious area for improvement is the detection limit. As it currently stands, Asp is near the limit of quantitation for the system. Either a more powerful laser or a different derivatization reaction would improve the limit of detection. Over the course of this research the laser tube of the HeCd laser was replaced twice. The first tube had approximately 4.5 mW of power at 354 nm and a limit of detection for Glu of approximately 10 nM. The present laser tube has 1.3 mW or power at 354 nm and a limit of detection of approximately 30 nM. The use of NDA as a derivative reagent could improve the detection limits significantly. The derivatization chemistry of NDA is nearly as fast as OPA and may be a viable alternative (ZHO95a). The improvement with NDA would be two fold. Laser power now severely limits the detection limit of the instrument. The 442 nm line (excitation wavelength of NDA) is much stronger than the current 354 nm line (perhaps as much as ten times higher). Also, the quantum efficiency of NDA is better than that of OPA, providing more emission at the same excitation power.

An improvement in detection limit would offer many advantages. First, flow rates and probe sizes that would result in prohibitively low recovery would no longer be prohibitive. A ten-fold improvement in detection limit could make possible the use of ultra-small probe lengths (100's of μm) at equivalent flow rates as used now, resulting in improved spatial and temporal resolution. Theoretically, multicomponent analysis would be possible with resolution easily in the sub-second temporal resolution. Also, with the right separation conditions, it may be possible to simultaneously monitor GABA, dopamine, glycine, as well as Glu and Asp. This would cover the major transmitter systems in the brain.

Biological Applications

The next step for this research is to continue the study of the effects of pilocarpine on Glu and Asp in the hippocampus. The first experiment should be to confirm the TTX and Ca^{2+} sensitivity of the changes seen in Glu and Asp with PILO infusion and electrical stimulation. The reported changes of Glu in the literature have all been confirmed to be either TTX or Ca^{2+} sensitive (SMO97, MIL93). It is expected that the change due to electrical stimulation in Glu will be TTX and Ca^{2+} sensitive.

More interesting will be the effect of PILO on mGluR in the hippocampus. The response of the specific groups have already been determined, mostly all in *in vitro* experiments (BOR99, FRI99, KEE99, MER97). However, the *in vivo* effects have not been specifically addressed. Based on ACPD's role in augmenting seizures, it is likely that the response of Glu to electrical stimulation in the presence of PILO will be enhanced. The effect on EEGs must also be monitored. ACPD should increase the electroencephalographic response to electrical stimulation. A Group II mGluR agonist

also should be tested because this group has been shown to inhibit seizures (KEE99). By characterizing the autoreceptors in response to electrical stimulation in the presence of PILO, the role of the glutamatergic system in seizures can be better understood.

A logical choice for a future direction in biology is the use of awake, behaving rats. With minor modification, mainly elongating the probe outlet length, the system will easily accommodate an awake animal without a significant loss of temporal resolution. As shown in Chapter 2, there is very little broadening due to diffusion in the capillaries. Because of the problems inducing a seizure in the anesthetized rat, the same experiments performed here should be performed on awake animals.

Behavior responses would be an interesting and wide ranging area of research. The hippocampus is responsible for learning and memory and also involves the glutamate system. With real-time monitoring of Glu and Asp it may be possible to observe changes in the neurotransmitters as a rat is performing a maze test. Changes in the response may also occur as the rat learns the maze and the path is transferred to long term memory. In addition, the response of an animal to stress, such as a swim test, may elicit a change in Glu and Asp.

Behavior is a much more complicated activity than an electrical stimulation or the application of a drug. Therefore the analysis of other neurotransmitters (glycine, taurine, GABA as well as dopamine and seratonin) would be much more beneficial than only the excitatory amino acids.

APPENDIX A
TROUBLESHOOTING THE INSTRUMENT*

Problem	Likely Cause	Solution
No current	Clog at sep'n/connector junction	Take apart and reconnect
	Clog in separation capillary	Replace
	Air bubble	Flush capillary
High current, EOF slow	Clog at gating interface	Take apart, flush interface
High current, peaks large and broad	Rxn and sep'n capillaries too close	Adjust distance
	Leak in CSF	Replace connectors
High current, peaks broad, regular to small size	Leak in OPA/BME	Replace connectors
Low current	Clog at gating interface	Take apart, flush interface
	Cracked sep'n capillary	Replace
	Ground/HV not connected	Connect
Current normal, no/small peaks	Rxn and sep'n capillaries too far apart	Adjust distance
	Leak at reaction tee	Tighten/Replace connectors
	Cracked sep'n capillary near inlet	Replace
	Laser not aligned	Align laser
Current normal, small peaks, large OPA/BME peaks	Clog in CSF before tee	Replace connector
EOF slow	Water not completely flushed from connector capillary	Flush with buffer
	Material in sep'n/connector interface	Take apart and flush
Poor injection reproducibility	Rxn/sep'n capillaries not at ideal distance	Adjust distance
	Material in interface	Take apart and flush
	Material in reaction tee	Take apart and flush
	Switching valve dirty	Take apart and clean
	Rotor old/scratched	Replace rotor

This dissertation was submitted to the Graduate Faculty of the Department of Chemistry in the College of Liberal Arts and Sciences and to the Graduate School and was accepted as partial fulfillment of the requirements for the degree of Doctor of Philosophy.

December, 2000

Dean, Graduate School

Problem	Likely Cause	Solution
Poor injection reproducibility	Switching gas too low (less than ~ 200 psi)	Replace tank/adjust regulator
	Cross flow syringe too full	Use no more than 30 ml in 50 ml glass syringe
High background fluorescence	Too much oil on objective	Remove excess oil
	Rxn/sep'n capillaries too close	Adjust distance
	Air bubble/material in oil	Replace oil
Continuous injection	Rxn/sep'n capillaries too close	Adjust distance
	No cross flow	Check pump for correct flow rate/leaks at syringe
	Clog at interface	Take apart and flush
	Loose wires on switching box	Check wires

*Notes: This guide assumes all solutions are made correctly.
When multiple causes are given, they are in the order of likelihood.
Most problems can be solved by taking apart the interface and separation and connector capillaries. Flush both with buffer and reconnect.

APPENDIX B
MICRODIALYSIS PROBE CONSTRUCTION

Please note that while construction of a microdialysis probe is a fairly straightforward, simple procedure, it does take practice to consistently make reproducible, straight probes. While probe construction takes a total of approximately 15 min per probe, the process requires two days due to the drying time of the polyimide sealing resin. A minimum drying time of 12 hr is required; while 24 hr is suggested. In case of emergency, the resin can be dried in 2 hr at 70 °C, although this is not recommended. A diagram of lengths and materials can be seen in Figure A2-1.

Day 1

Cut dialysis fibers into 1 cm lengths with sharp surgical scissors. Be sure that the end to be sealed is cut at 90°. Then, using a 26 gauge needle as an applicator, seal one end of the cut fiber with polyimide. For a reliable seal, the thickness of the resin when dry should be 50-100 μm. Depending on the viscosity of the resin, the wet polyimide will be anywhere from 200 to 500 μm thick. In general, the more viscous the polyimide, the better the seal. An old bottle of sealing resin that has become too viscous for the remaining steps is ideal. Let the polyimide dry overnight.

Day 2

Assemble the Capillaries

To make a dialysis probe, three pieces of fused silica capillary are required, two probe capillaries (an inlet and an outlet) and a sleeve. The probe capillaries should be

100 μm o.d. by 40 μm i.d. For the instrument described here with a zero dead volume tee, the inlet capillary length is 9 cm and does not have to be exact. The outlet capillary length is 7 cm and must be accurate. The sleeve capillary is 360 μm o.d. by 250 μm i.d. and should be 2.5 cm long. If the difference in length of the inlet and outlet capillaries do not make them readily identifiable, mark one end of the outlet capillary with a blue or black sharpie for identification.

Hold the probe capillaries together with the thumb and forefinger of one hand so that the ends are offset by 3-4 mm. With the sleeve capillary in the other hand, slide both probe capillaries though the sleeve capillary. With some practice this can be done quite easily without the aid of a microscope. Under a stereoscopic microscope, use a mm-graded ruler to adjust the offset of the probe capillaries so that the ends are the desired length apart (2 mm in this case). The inlet capillary must always be the furthest extended capillary (to but against the sealed dialysis fiber). Pressing the offset ends against the ruler, slide the sleeve capillary so that it is 1 cm from the tip of the inlet capillary. Place a drop of cyanoacrylate glue at the other end (away from the offset probe capillaries) of the sleeve capillary. Allow at least 5 mm of glue to be drawn into the capillary. Allow to dry for a few minutes.

Assemble the Probe

For this step a holder is required for the dialysis fiber. The apparatus currently used is generally kept with the bulk dialysis fiber and is a metal inverted "U" shaped piece approximately 2 cm long and 1 cm tall. Scotch tape is affixed to the flat portion, sticky side up to hold the fiber.

Place the sealed fiber on the holder so that the unsealed end sticks halfway over

the edge of the holder. Cut the tip of the fiber at an approximately 20° angle. Under a stereoscopic microscope, sleeve the fiber onto the assembled capillaries so that the inlet capillary touches the sealed end of the fiber. Once both capillaries are inside the fiber, it may be difficult to slide them all the way to the sealed end. Be careful not to bend or fold the dialysis fiber. During this process the fiber usually detaches from the holder; if it does not, carefully remove the fiber from the holder.

Hold the fiber between the thumb and forefinger of one hand and the capillary between the thumb and forefinger of the other. Attempt to push the fiber onto the capillaries, as if to puncture the polyimide seal. If the seal does break, discard the fiber and repeat the above procedure. A good seal will not break, even if a great deal of force is applied. Look to see if the probe is straight. If the probe curves, there are two possible remedies. First, pull the dialysis fiber back a few hundred μm; if the probe straightens, the capillaries were simply pushed too far into the fiber. If the probe still curves, it may be possible to straighten. Holding the fiber in place, twist the capillaries. This procedure will often straighten the probe; if the probe still curves, discard the fiber.

Under the stereoscopic microscope, slide the fiber almost off the capillaries so that the edge of the fiber is ca. 200 μm from the tip of the outlet capillary. With the 26 gauge needle, starting at the sleeve capillary, apply a coating of sealing resin to the capillaries. In this case, the less viscous the resin the better.

NOTE: DO **NOT** allow the resin to be drawn into the outlet capillary. Slowly slide the fiber onto the capillaries, allowing the resin to draw up to but not into the outlet capillary. The inlet capillary should touch the sealed end of the fiber to avoid any unswept volume. Apply an additional coating of sealing resin to the fiber, starting at the

sleeve capillary. Leave uncoated only the desired active area of the probe. Allow to dry approximately 15 minutes. At this point the resin usually collects into beads. With a 26 gauge needle break up the beads and smooth over the probe. Remove any excess resin. Allow to dry overnight.

Day 3 or Before Use

Final Assembly

Even though the probe itself is completely ready for use, two modifications must be made to handle the probe easily.

First, a stainless steal sleeve must be attached so as not to crush the probe on the stereotaxic holder. Cut both ends of a 1½ inch 22 gauge needle with the cut-off wheel attachment on the Dremel tool. The resulting shaft should be approximately 2 cm long. File both ends to remove any burrs or jagged sections. Slide the shaft over the sleeve capillary and attach with cyanoacrylate glue.

Second, sleeve capillaries (360 μm o.d., 150 μm i.d.) must be attached to both the inlet and outlet capillaries. Remove any Sharpie marking from the inlet capillary. Use a 2 cm length of capillary for the inlet and a 1 cm length for the outlet (if using a zero dead volume tee). Affix with cyanoacrylate, making sure that the ends are flush with the sleeve and allow to dry for approximately 10 min.

Construction is now complete, but before use the probe must be conditioned for optimal performance. Perfuse the probe with 70 % ethanol in water for a minimum of 30 min followed by an additional 30 min with aCSF.

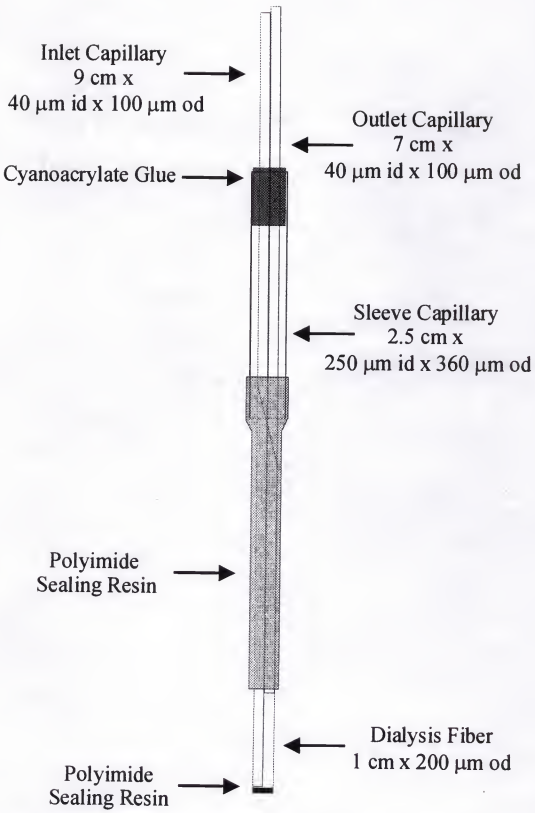

Figure B-1. Diagram of a microdialysis probe. The required material and dimensions are given for the probes used in the bulk of this work.

REFERENCES

ABE92 Abe, T.; Shigemoto, R.; Nakanishi, S. *J. Biol. Chem.* **1992**, 267, 13361.

ALA96 Alam, A. M.; Starr, M. S. *Neuropharm.* **1996**, 35, 159.

AND91 Anderson, K. J.; Bridges, R. J.; Cotman, C. W. *Brain Res.* **1991**, 562, 285.

ASI98 Asiaie, R.; Huang, X.; Farnan, D.; Horvath, C. *J. Chromatogr. A* **1998**, 806, 251.

ARR97 Arriza, J. L.; Eliasof, S.; Kavanaugh, M. P.; Amara, S. G. *Poc. Natl. Acad, Sci. USA*, **1997**, 94, 4155.

ASZ97 Asztely, F.; Erdemli, G.; Kullmann, D. M. *Neuron*, **1997**, 18, 281.

BAR97 Barbour, B.; Hausser, M. *Trends Neurosci.* **1997**, 20, 377.

BAR97a Barder, T. J.; Wohlman, P. J.; Thrall, C.; Dubois, P. D. *LC-GC*, **1997**, *15*, 918.

BAS91 Basse-Tomusk, A.; Rebec, G. V. *Brain Res.* **1991**, 538, 29.

BEY94 Beyer, R. E. *J. Bioenerget. Biomemb.* **1994**, 26, 319.

BUN99 Bunin, M. A.; Wightman, R. M. *Trends Neurosci.* **1999**, 22, 377.

BOR99 Bordi, F.; Ugolini, A. *Prog. Neurobiol.* **1999**, 59, 55.

BOU95 Boughtflower, R. J.; Underwood, T.; Maddin, J. *Chromatographia* **1995**, 41, 398.

BOY00 Boyd, B. W.; Witowski, S. R.; Kennedy, R. T. *Anal. Chem.* **2000**, 72, 865.

BRI91 Bridges, R. J.; Stanely, M. S.; Anderson, M. W.; Cotman, C. W.; Chamberlin, A. R. *J. Med. Chem.* **1991**, 34, 717.

BRO95 Brown, R. E.; Reymann, K. G. *Neurosci. Lett.* **1995**, 196, 17.

BRU98 Bruno, V.; Battaglia, G.; Copani, A.; Casabona, G.; Storto, M.; Gerevini, V.; Ngomba, R.; Nicoletti, F. *In: Prog. Brain Res.*, Ottersen, O. P.; Langmoen, I. A.; Gjerstad, L. eds. **1998**, 116, 209.

BRU94 Bruno, V. Battaglia, G.; Copani, A.; Giffard, R. G.; Raciti, G.; Raffaele, R.; Shinozaki, H.; Nicoletti, F. *Eur. J. Pharmacol.* **1994**, 256, 109.

BUN90 Bungay, P. M.; Morrison, P. F.; Dedrick, R. L. *Life Sci.* **1990**, 46, 105.

BUR89 Burger, P. M.; Mehl, E.; Cameron, P. L.; Maycox, P. R.; Baumertr, M.; Lottspeich, F.; De Camilli, P.; Jahn, R. *Neuron*, **1989**, 3, 715.

BUR88 Burke, S. P.; Nadler, J. V. *J. Neurochem.* **1988**, 51, 1541.

CAB96 Cabrera et al. *Anal. Chem.* **1996**, *68*, 3498.

CAM91 Cammack, J.; Ghasemzadeh, B.; Adams, R. N. *Brain Res.* **1991**, 565, 17.

CAR89 Carlson, M. D.; Kish, P. E.; Ueda, T. *J. Biol. Chem.* **1989**, 264, 7369.

CAV94 Cavalheiro, E. A.; Fernandes, M. J.; Turski, L.; Naffah-Mazzacoratti, M. G. *Epilepsia*, **1994**, 35, 1.

CHA98 Chapman, A. G. *Glutamate receptors in epilepsy in Prog. Brain Res. v 116.* Ottersen, O. P.; Langmoen, I. A.; Gjerstad, L., eds. Elsevier, NY **1998**, 371.

CHA00 Chapman, A. G. *J. Nutr.* **2000**, 130, 1043s.

CHA95 Chaudhry, F. A.; Lehre, K. P. Campagne, M. V.; Ottersen, O. P. Danbolt, N. C.; Storm-Mathisen, J. *Neuron*, **1995**, 15, 711.

CHA99 Chaudhary, G.; Malbotra, J.; Chaudhari, J. D.; Gopinath, G.; Gupta, Y. K. *Meth. Find. Exp. Clin. Pharm.* **1999**, 21, 21.

CHE99 Chebabo, S. R.; Santos, M. D.; Albuquerque, E. X. *Neurotoxicology.* **1999**, 20, 871.

CHE95 Chen, A.; Lunte, C. E. *J. Chromatogr. A* **1995**, *61*, 29.

CHE93 Chen, H.; Horvath, C. *Anal. Methods Instrum.* **1993**, *1(4)*, 213.

CHE95a Chen, H.; Horvath, C. *J. Chromatogr. A* **1995**, *705(1)*, 3.

CHE97 Chen, M. H.; Horvath, C. *J. Chromatogr. A* **1997**, *788*, 51.

CHO96 Choi, S.; Lovinger, D. M. *J. Neurosci.* **1996**, 16, 36.

CHO97 Choudhary, G.; Horvath, C. *J. Chromatogr. A*. **1997**, *781*, 161.

CIO98 Ciovannini, R.; Freitag, R.; Tennikove, T. B. *Anal. Chem*. **1998**, *70*, 3348.

CLE92 Clemments, J. B.; Lester, R. A. J.; Tong, G.; Jahr, C. E.; Westbrook, G. L. *Science*, **1992**, 258, 1498.

CLI87 Clifford, D. B.; Olney, J. W.; Maniotis, A.; Collins, R. C.; Zorumski, C. F. *Neuroscience*, **1987**, 23, 953.

COC97 Coco, S.; Verderio, C.; Trotti, D.; Rothstein, J. D.; Volterra, A.; Matteoli, M. *Eur. J. Neurosci*. **1997**, 9, 1902.

COL93 Cole, L. J.; Schultz, N.; Kennedy, R. T. *J. Microcol. Sep*. **1993**, *5*, 433.

COL97 Colon, L. A.; Guo, Y.; Fermier, A. *Anal Chem*. **1997**, *69*, 461A.

CON94 Conn, P. J.; Winder, D. G.; Gereau, R. W. in: *The Metabotropic Glutamate Receptors*, Conn, P. J.; Patel, J. eds. **1994**, Humana Press, Inc. p 195-229.

CRE96 Crego, A. L.; Gonzalez, A.; Marina, M. L. *Crit. Rev. Anal. Chem*. **1996**, *26(4)*, 261.

DAD98 Dadoo, R.; Zare, R. N.; Yan, C.; Anex, D. S. Anal. Chem. **1998**, *70*, 4787.

DAN90 Danbolt, N. C.; Pines, G.; Kanner, B. I. *Biochemistry*, **1990**, 29, 6734.

DAV99 Davies, M. J.. *Anal. Chim. Acta* **1999**, *379*, 227.

DAV97 Davies, M. I.; Lunte, C. E. *Chem Soc. Rev*. **1997**, *26(3)*, 215.

DAW97 Dawson, L. A. *J. Chromatogr. B Biomed. Sci. Appl*. **1997**, 697, 89.

DIE97 Dietrich, D.; Beck, H.; Kral, T.; Clusmann, H.; Elger, C. E.; Schramm *Brain Res*. **1997**, 767, 220.

DIN90 Dingledine, R.; McBain, C. J.; McNamara, J. O. *Trends Pharmacol*. **1990**, 11, 334.

DIT96 Dittmann, M. M.; Rozing, G. P. *J. Chromatogr. A*. **1996**, *744*, 63.

DIT98 Dittmann, M.M.; Rozing, G. P. *Biomed. Chromatogr*. **1998**, *12(3)*, 136.

DIT97 Dittmann, M. M.; Rozing, G. P.; Rees, G.; Adam, T.; Unger, K. K. *J. of Cap. Electrophor*. **1997**, *4(5)*, 201.

DIT95 Dittmann, M. M.; Wienard, K.; Bek, F.; Rozing, G. P. *LC-GC*, **1995**, *13(10)*, 800.

DUN94 Dunlap, C. J.; Carr, P. W.; Blackwell, J. A. *Biotechnol. Prog.* **1994**, *10(6)*, 561.

DUR93 During, M. J.; Spencer, D. D. *Lancet* **1993**, 341, 1607.

ERI96 Ericson, C.; Liao, J. L.; Nakazato, K.; Hjerten, S. *Anal. Biochem.* **1996**, *241(2)*, 195.

EUR98 Euerby, M. R.; Johnson, C. M.; Cikalo, M.; Bartle, K. D. *Chromatographia.* **1998**, *47*, 135.

EWI82 Ewing, A. G.; Wightman, R. M.; Dayton, M. A. *Brain Res.* **1982**, 249, 361.

FER98 Fermmier, A.; Colon, L. A. *J. Microcolumn Sep* **1998**, 10, 439.

FIJ86 Fijikawa, D. G.; Itabashi, H. H.; Wasterlain, C. G. *Soc. Neurosci. Abstr.* **1986**, 12, 982.

FIL95 Fillenz, M. Behav. *Brain Res.* **1995**, 71, 51.

FIL86 Fillenz, M.; O'Neill, R. D.; Grunewald, R. A. *in: Monitoring Neurotranmsmitter Release During Behaviour*, Joseph, M. H.; Fillenz, M.; MacDonald, L. A.; Marsden, C. A., eds. **1986**, Ellis Norwood, England, p 144.

FLO91 Flott, B.; Seifert, W. *Glia* **1991**, 4, 293.

FRI99 Friedl, M.; Clusmann, H.; Kral, T.; Dietrich, D.; Schramm, J. *Brain Res.* **1999**, 821, 117.

FRI99 Fritschy, J. M.; Kiener, T.; Bouilleret, V.; Loup, F. *Neurochem. Int.* **1999**, 34, 435.

FUJ97 Fujimoto, C.; Kino, J.; Sawada, H. *J. Chromatogr. A* **1997**, *762*, 135.

FUR97 Furuta, A.; Martin, L. J.; Lin, C. L.; Dykes-Hoberg, M.; Rothstein, J. D. *Neuroscience*, **1997**, 81, 1031.

GED90 Geddes, J. W.; Cahan, L. D.; Cooper, S. M.; Kim, R. C.; Choi, B. H.; Cotman, C. W. *Exp. Neurol.* **1990**, 108, 214.

GEO97 George, B.; Kulkarni, S. K. *Method Find. Exp. Clin.* **1997**, 19, 481.

GER84 Gerhardt, G. A.; Oke, A. F.; Nagy, G.; Moghaddam, B.; Adams, R. N. *Brain Res.* **1984**, 290, 390.

GER87 German R. M. *Ceramics and Glasses, Engineered Materials Handbook*, ASM International, **1987**, 260.

GON81 Gonon, F.; Buda, M.; Cespuglio, R.; Jouvet, M.; Pujol, J. F. *Brain Res.* **1981**, 223, 69.

GOT94 Gotz, M. E.; Kunig, G.; Riederer, P.; Youdim, M. B. H. *Pharmacol. Therap.* **1994**, 63, 37.

GRO00 Grooms, S. Y.; Opitz, T.; Bennett, M. V. L.; Zukin, R. S. *Proc. Natl. Acad. Sci. USA*, **2000**, 97, 3631.

GRE90 Greenamyre, J. T.; Higgins, D. S.; Young, A. B.; Penney, J. B. *Int. J. Devel. Neurosci.* **1990**, 8, 437.

GRI94 Griffiths, R.; Dunlop, J.; Gorman, A.; Senior, J.; Grieve, A. *Biochem. Pharmac.* **1994**, 47, 267.

GRU93 Grunewald, R. A. *Brain Res. Rev.* **1993**, 18, 123.

GUN98 Gundersen, V.; Chaudhry, F. A.; Bjaalie, J. G.; Fonnum, F.; Ottersen, O. P.; Storm-Mathisen, J. *J. Neurosci.* **1998**, 18, 6059.

GUO95 Guo, Y.; Colon, L. A. *Anal. Chem.* **1995**, *67*, 2511.

HAL96 Halonen, T.; Nissinen, J.; Jansen, J. A.; Pitkanen, A. *Eur. J. Pharm.* **1996**, 299, 69.

HAN97 Hanson; Unger, K. K. *LC-GC.* **1997**, *15(2)*, 170.

HAR49 Harris, E. J.; Burn, G. P. *Trans. Faraday Soc.*; **1949**, 45, 508.

HE98 He, B.; Tait, N.; Regnier, F. *Anal. Chem.* **1998**, *70*, 3790.

HER90 Hernandez, L.; Marquina, R.; Escalona, J.; Guzman, N. *J. Chromatogr.* **1990**, 502, 247.

HER96 Herrera-Marschitz, M.; You, Z.; Goiny, M.; Meana, J. J.; Silveira, R.; Godukhin, O. V.; Chen, Y.; Espinoza, S.; Pettersson, E.; Loidl, C. F.; Lubec, G.; Andersson, K.; Nylander, I.; Terenius, L.; Ungerstedt, U. *J. Neurochem.* **1996**, 66, 1726.

HER92 Herrero, I.; Miras-Portugal, M. T.; Sanchez-Preieto, J. *Nature*, **1992**, 360, 163.

HJE92 Hjerten, S.; Li, Y. M.; Liao, J. L.; Mohammad, J.; Nakazato, K.; Pettersson, G. *Nature* **1992**, *356*, 810.

HJE91 Hjerten, S.; Mohammad, J.; Eriksson, K.-O.; Liao, J.-L. *Chromatographia*, **1991**,*31(1/2)*, 85.

HJE93 Hjerten, S.; Nakazato, K.; Mohammad, J.; Eaker, D. *Chromatographia* **1993**, *37*, 287.

HOG94 Hogan, B. L.; Lunte, S. M.; Stobaugh, J. F.; Lunte, C. E. *Anal. Chem.* **1994**, 66, 596.

HOU96 Houser, C. R.; Esclapez, M. *Epilepsy Res.* **1996**, 26, 207.

HSI96 Hsieh, S.; Jorgenson, J. W. *Anal. Chem.* **1996**, *68*, 1212.

HU94 Hu, Y.; Mitchell, K. M.; Albahadily, F. N.; Michaelis, E. K.; Wilson, G. S. *Brain Res.* **1994**, 69, 117.

HUB97 Huber, C. G.; Choudhary, G.; Horvath, C. *Anal. Chem.* **1997**, *69*, 4429.

HUB93 Huber, C. G.; Oefner, P. J.; Bonn, G. K. *Chromatographia.* **1993**, *37*, 653.

HUR98 Hurley, M. B.; Rowarth, J. S. *J. Chrom Sci.* **1998**, 36, 345.

IDR86 Idriss, M. K.; Aguayo, L. G.; Rickett, D. L., Albuquerque, E. X. *J. Pharmacol. Exp. Ther.* **1986**, 239, 279.

IMP84 Imperato, A.; Di Chiara, G. *J. Neurosci.* **1984**, 4, 966.

ISH98 Ishizuka, N.; Minakuchi, H.; Nakanishi, K.; Soga, N.; Tanaka, N. *J. Chromatogr. A* **1998**, 797, 133.

ITO93 Itoh, H.; Kinoshita, T.; Nimura, N. *J. Liq. Chromatogr.* **1993**, 16, 809.

JAN87 Janzen, R.; Unger, K. K.; Giesche, H.; Kinkel, J. N.; Hearn, M. T. W. *J Chromatogr.* **1987**, 397, 81.

JAN87a Janzen, R.; Unger, K. K.; Giesche, H.; Kinkel, J. N.; Hearn, M. T. W. *J Chromatogr.* **1987**, 397, 91.

JEN96 Jenke, D. R. *J. Chromatogr. Sci.* **1996**, 34, 362.

JES93 Jessell, A. M.; Kandel, E. R. *Neuron* **1993**, 19, 1.

JIL87 Jilge, G.; Janzen, R.; Giesche, H.; Unger, K. K.; Kinkel, J. N.; Hearn, M. T. W. *J. Chromatogr.* **1987**, *397*, 71.

JOP96 Jope, R. S.; Morrisett, R. A.; Snead, O. C. *Exp. Neurol.* **1986**, 91, 471.

JOR81 Jorgenson, J. W.; Lukacs, J. D. *J. Chromatogr.* **1981**, 218, 209.

KAH93 Kahle, J. S.; Cotman, C. W. *J. Pharmacol. Exp. Ther.* **1993**, 266, 207.

KAL90 Kalghatgi, K. *J.Chromatogr.* **1990**, 499, 267.

KAR88 Karlsson, K. E.; Novotny, M. *Anal. Chem.* **1988**, 60, 1662.

KHA99 Khan, G. M.; Smolders, I.; Lindekens, H.; Manil, J.; Ebinger, G.; Michotte, Y. *Eur. J. Pharmacol.* **1999**, 373, 153.

KEE99 Keele, B. N.; Neugebauer, V.; Shinnick-Gallagher, P. *J. Neurophysiol.* **1999**, 81, 2056.

KEN89 Kennedy, R. T.; Jorgenson, J. W. *Anal. Chem.* **1989**, 61, 1128.

KEN72 Kennedy G. J.; Knox J. H. *J Chrom Sci* **1972**, 10, 549.

KIR92 Kirkland, J. J.; *Anal Chem.* **1992**, 64, 1239.

KIS73 Kissenger, P. T.; Hart, J. B.; Adams, R. N. *Brain Res.* **1973**, 55, 209.

KLA92 Klancnik, J. M.; Cuenod, M.; Gahwiler, B. H.; Jiang, Z. P.; Do, K. *Neurosci.* **1992**, 49, 557.

KNO69 Knox, J. H.; Parcher, J. F. *Anal. Chem.* **1969**, 41, 1599.

KNO87 Knox, J. H.; Grant, I. H. *Chromatographia* **1987**, 24, 135.

KNO91 Knox, J. H.; Grant, I. H. *Chromatographia* **1991**, 32, 317.

KOR85 Korf, J.; Venema, K. *Neurochem.* **1985**, 45, 1341.

KUL99 Kuligina, N. V.; Shankar, L.; Micheal, A. C. *Anal. Chem.* **1999**, 71, 5093.

KUL98 Kullman, D. M.; Asztely, F. *Trends Neurosci.* **1998**, 21, 8.

KUL96 Kullman, D. M.; Erdemli, G.; Asztely, F. *Neuron*, **1996**, 17, 461.

KUT98 Kutter, J. P.; Jacobson, S. C.; Matsubara, N.; Ramsey, M. J. *Anal. Chem.* **1998**, *70*, 3291.

LAD98 Lada, M. W.; Vickroy, T. W.; Kennedy, R. T. *J. Neurochem.* **1998**, 70, 617.

LAD97 Lada, M. W.; Vickroy, T. V.; Kennedy, R. T. *Anal. Chem.* **1997**, 69, 4560.

LAD96 Lada, M. W.; Kennedy, R. T. *Anal. Chem.* **1996**, 68, 2790.

LEE97 Lee, W.-C. *J. Chromatogr. B.* **1997**, 699, 29.

LEM93 Lemmo, A. V.; Jorgenson, J. W. *Anal. Chem.* **1993**, 65, 1576.

LOM93 Lommen, D. C.; Snyder, L. R. *LC-GC* **1993**, 11, 222.

LEV93 Levi, G.; Raiteri, M. *Trends Neurosci.* **1993**, 16, 415.

LI97 Li, J..; Hu, Y.; Carr, P. W. *Anal. Chem.* **1997**, 69, 3884.

LI94 Li, Y. M.; Liao, J. L.; Kakazato, K.; Mohammad, J.; Terenius, L.; Hjerten, S. *Anal. Biochem.* **1994**, 223, 153.

LIA96 Liao, J.L.; Li, Y. M.; Hjerten, S. *Anal. Biochem.* **1996**, 234, 27.

LIA96a Liao, J. L.; Zeng, L. M.; Palm, A.; Hjerten, S. *Anal. Chem.* **1996**, 68, 3468.

LIU95 Liu, J. Moghaddam, B. *J. Pharmacol. Exper. Therap.* **1995**, 274, 1209.

LIU97 Liu, Z.; Stafstrom, X. E.; Sarkisian, M. R.; Uang, Y. L.; Hori, A.; Tandon, P.; Holmes, G. L. *NeuroReport* **1997**, 8, 2019.

MAA88 Maa, Y.-F.; Horvath, C. *J. Chromatogr.* **1988**, 445, 71.

MAC97 MacNair, J. E.; Lewis, K. C.; Jorgenson, J. W. *Anal. Chem.* **1997**, 69, 983.

MAC99 MacNair, J. E.; Patel, K. D.; Jorgenson, J. W. *Anal. Chem.* **1999**, 71, 700.

MAS95 Massieu, L.; Morales-Villagran, A.; Tapia, R. *J. Neurochem.* **1995**, 64, 2262.

MAT98 Mathern, G. W.; Pretorius, J. K.; Mendoza, D.; Lozada, A. *J. Neurosci. Res.* **1998**, 54, 734.

MAY75 Maynert, E. W.; Marczynski, T. J.; Browning, R. A. *Adv. Neurol.* **1975**, 13, 79.

MAZ98 Mazel, T.; Simonova, Z.; Sykova, E. *NeuroReport*, **1998**, 9, 1299.

MCD97 McDonough, J. H.; Shih, T. M. *Neurosci. Biobehav. Rev.* **1997**, 21, 559.

MEL92 Meldrum, B. S. *Epilepsy Res.* **1992**, 12, 189.

MEL94 Meldrum, B. S. *Neurology*, **1994**, suppl 8, s14.

MEN95 Mennerick, S.; Zorumski, C. F. *J. Neurosci.* **1995**, 15, 3178.

MER97 Merlin, L. R.; Wong, R. K. S. *J. Neurophysiol.* **1997**, 78, 539.

MIL82 Milby, K.; Oke, A.; Adams, R. N. *Neurosci. Letters* **1982**, 28, 169.

MIL93 Millan, M. H.; Chapman, A. G.; Meldrum, B. S. *Epilepsy Res.* **1993**, 14, 139.

MIN95 Minakuchi, et al. *J Chromatogr A* **1995**, 716, 107.

MIN98 Minakuchi, H.; Nakanishi, K.; Soga, N.; Ishizuka, N.; Tanaka, N. *J. Chromatogr. A.* **1998**, 797, 121.

MIT00 Mitchell, S. J.; Silver, R. A. *Nature*, **2000**, 404, 498.

MOG93 Moghaddam, B. *J. Neurochem.* **1993**, 60, 1650.

MOO93 Moore, A. W. Jr.; Jorgenson, J. W. *Anal. Chem.* **1993**, 65, 355.

MOO98 Moore, R. E.; Licklider, L.; Schumann, D.; Lee, T. D. *Anal. Chem.* **1998**, 70, 4879.

NAD90 Nadler, J. V.; Martin, D.; Bustos, G. A.; Burke, S. P.; Bowe, M. A. *Prog. Brain. Res.* **1990**, 83, 115.

NAK92 Nakanishi, S. *Science* **1992**, 258, 597.

NEW94 Newton, A. P.; Justice, J. B. *Anal. Chem.* **1994**, 66, 1468.

NIC81 Nicholson, C.; Phillips, J. M. *J. Physiol.* **1981**, 321, 225.

OBR96 Obrenovitch, T. P. Urenjak, J.; Zilkha, E. *J. Neurochem.* **1996**, 66, 2446.

OLE98 Oleshko, N. N. *Neurosci. Behav. Physiol.* **1998**, 28, 397.

OLN86 Olney, J. W. *Excitatory Amino Acids and Seizure Disorders*, Ben-Ari, Y.; Schwarcz, R. eds. **1986**, Plenum Press, NY, 631-645.

ONE82 O'Neill, R. D.; Grunewald, R. A.; Fillenz, M.; Albery, W. J. *Neuroscience* **1982**, 7, 1945.

ONE84 O'Neill, R. D.; Rillenz, M.; Sundstrom, L.; Rawlins, J. N. P. *Neurosci. Lett.* **1984**, 52, 227.

ORR93 Orrego, F.; Villanueva, S. *Neuroscience*, **1993**, 56, 539.

PAL96 Paliwal, S. K.; de Frutos, M.; Regnier, F. E.; *Methods Enzymol.* **1996**, 270, 133.

PAL89 Palmer, A. M.; Hutson, P. H.; Lowe, S. L.; Bowen, D. M. *Exp. Brain Res.* **1989**, 75, 659.

PAS97 Pasti, L.; Volterra, A.; Pozzan, T.; Carmignoto, G. *J. Neurosci.* **1997**, 17, 7817.

PET96 Petro, M.; Svec, F. Frechet, J. M. *J. Chromatogr. A.* **1996**, 752, 59.

PET96a Petro, M. Svec, F.; Gitsov, I.; Frechet, J. M. *Anal. Chem.* **1996**, 68, 315.

PIE93 Pierce, R. C.; Rebec, G. V. *J. Neurosci.* **1993**, 13, 4272.

PIN95 Pin, J-P.; Duvoisin, R. *Neuropharmacol.* **1995**, 34, 1.

PIN92 Pines, G.; Danbolt, N. C.; Bjoras, M.; Zhang, Y.; Bendahan, A.; Eide, L.; Koepsell, H.; Storm-Mathisen, J.; Seeberg, E. K.; Kanner, B. I. *Nature*, **1992**, 360, 464.

POP93 Poppe, H.; Kraak. J. C. *J. Chromatogr.* **1983**, 282, 399.

POP81 Poppe, H.; Kraak, J. C.; Huber, J. F. K.; Van den Berg, J. H. M. *Chromatographia*, **1981**, 14, 515.

PRE74 Pretorius, V.; Hopkins, B. J.; Schieke, J. D. J. *J. Chromatogr.* **1974**, 99, 23.

REB97 Rebec, G. V. in *Metals and Oxidative Damage in Neurological Disorders*, ed. Connor. Plenum Press, New York **1997**, chapter 9, 149.

REB94 Rebec, G. V.; Pierce, R. C. *Prog. Neurobiol.* **1994**, 43, 537.

REB96 Rebscher, H.; Pyell, U. *J. Chromatogr. A* **1996**, 737, 171.

RIC91 Rice, M. E.; Nicholson, C. *J. Neurophysiol.* **1991**, 65, 264.

RIC97 Rice, M. E.; Russo-Menna, I. *Neuroscience*, **1997**, 82, 1213.

ROB91 Robinson, T. E., Justice, J. B. Jr. *Microdialysis in the Neurosciences* **1991**, Elsevier Science, New York.

ROI91 Roisin, M. P. Brassart, J. L.; Charton, G.; Crepel, V.; Ben Ari, Y. *J. Neurosci. Methods* **1991**, 37, 183.

ROS93 Rose, R. C.; Bode, A. M. *FASEB J.* **1993**, 7, 1135.

RUS98 Rusakov, D. A.; Kullmann, D. M. *J. Neurosci.* **1998**, 18, 3158.

RUS98a Rusakov, D. A.; Kullmann, D. M. *Poc. Natl. Acad. Sci.* **1998**, 95, 8975.

ROT92 Rothstein, J. D.; Martin, L. J.; Kuncl, R. W. *New Eng. J. Med.* **1992**, 326, 1463.

RUS96 Ruzgas, T.; Csoregi, E.; Emneus, J.; Goston, L.; Marko Varga, G. *Anal. Chim. Acta* **1996**, 330, 123.

RYA96 Ryan, K.; Djordfjevic, N. M.; Erni, F. *J. Liq. Chromatogr. & Rel. Technol.* **1996**, *19(13)*, 2089.

SAC92 Sacaan, A. I.; Schoepp, D. D. *Neurosci. Let.* **1992**, 139, 77.

SAN99 Sanchez-Carbente, M.; Massieu, L. *J. Neurochem.* **1999**, 72, 129.

SAU94 Saugstad, J. A.; Kinzio, J. M.; Mulvihill, E. R.; Segerson, T. P.; Westbrook, G. L. *Mol. Pharmac.* **1994**, 45, 367.

SCA97 Scanziani, M.; Salin, P. A.; Vogt, K.; Malenka, R. C.; Nicoll, R. A. *Nature*, **1997**, 385, 630.

SCH82 Schenk, J. O.; Miller, E.; Gaddis, R.; Adams, R. *Brain Res.* **1982**, 253, 353.

SCH78 Schwarcz, R.; Zaczek, R.; Coyle, J. *Eur. J. Pharmacol.* **1978**, 59, 209.

SEI98 Seifar, P. M.; Heemstra, S.; Kok, W. Th.; Kraak, J. C.; Poppe, K. H. *J. Microcol. Sep.* **1998**, *10*, 41.

SEI97 Seifar, R. M.; Kok, W. Th.; Kraak, J. C.; Poppe, H. *Chromatographia* **1997**, *46*, 131.

SHE99 Sherwin, A. L. *Neurochem. Res.* **1999**, 24, 1387.

SHI97 Shigemoto, R.; Kinoshita, A.; Wada, E.; Nomura, S.; Ohishi, H.; Takada, M; Flor, P. J.; Keki, Akio, Abe, T.; Nakanishi, S.; Mizuno, N. *J. Neurosci.* **1997**, 17, 7503.

SHU93 Shultz, N. M.; Kennedy, R. T. *Anal. Chem.* **1993**, 65, 3161.

SIN95 Sinibaldi, M.; Castellani, L.; Federici, F.; Messina, A.; Girelli, A. M.; Lentini, A.; Tesarova, E. *J. Liq. Chromatogr.* **1995**, 18, 3187.

SLO83 Sloviter, R. S. *Brain Res. Bull.* **1983**, 10, 675.

SMO97 Smolders, I.; Bogaert, L.; Michotte, Y. *J. Neurochem.* **1997**, 68, 1942.

SMO97a Smolders, I.; Khan, G. M.; Lindekens, H.; Prikken, S.; Marvin, C. A.; Manil, J.; Ebinger, G.; Michotte, Y. *J. Pharm. Exp. Ther.* **1997**, 283, 1239.

SMO97b Smolders, I.; Khan, G. M.; Manil, J.; Ebinger, G.; Michotte, Y. *Brit. J. Pharmacol.* **1997**, 121, 1171.

SMO97c Smolders, I.; Van Belle, K.; Ebinger, G.; Michotte, Y. *Eur. J. Pharmacol.* **1997**, 319, 21.

STA84 Stamford, J. A.; Kruk, Z. L.; Millar, J. *Brain Res.* **1984**, 299, 289.

STA96 Starr, M. S.; *Synapse*, **1996**, 22, 159.

SWA98 Swanson, L. W. *Brain Maps: Structure of the Rat Brain, 2nd ed.* **1998**, Elsevier, NY.

STO69 Stober, W.; Kink, A.; Bohn, E. J *Colloid Interface Sci.* **1968**, *26*, 2.

SZE87 Szerb, J.; O'Regan, P. A. *Synapse*, **1987**, 1, 265.

TAB92 Tabb, J. S.; Kish, P. E.; Van, D. R.; Ueda, T. *J. Biol. Chem.* **1992**, 267, 15412.

TAY96 Taylor, P. *Goodman and Gilman's: Pharmacological Basis of Therapeutics*, Hardman, J. G.; Limbird, L. E. eds., **1996**, McGraw-Hill, NY. 161-176.

TEB97 Tebano, M. T.; Marinelli, S.; Sagratella, S. *Pharmacol. Let.* **1997**, 61, 343.

TEN98 Tennikov, M. B.; Gazdina, N. V.; Tennikova, T. B.; Svec, F. *J. Chromatgr. A* **1998**, *798*, 55.

TIM97 Timmerman, W.; Westerink, B. H. C. *Synapse*, **1997**, 27, 461.

TIZ95 Tizzano, J. P.; Griffey, K. I.; Schoepp, D. D. *Neuropharmacology* **1995**, 34, 1063.

TON99 Tonto, N.; Laurell, T.; Gorton, L.; Marko-Varga, G. *Anal. Chim. Acta* **1999**, *379*, 281.

TOS86 Tossman, U.; Jonsson, G.; Ungerstedt, U. *Acta Physiol. Scand.* **1986**, 127, 533.

TRE92 Treiman, D. M.; Walton, N. Y.; Gunawan, S.; Gale, K.; Engelsen, B. A. *Epilepsy Res.* **1992**, suppl. 8, 283.

TRI89 Tricklebank, M. D.; Singh, L.; Oles, R. J.; Reston, C.; Iversen, S. D. *Eur. J. Pharmacol.* **1989**, 167, 127.

TRI91 Tricklebank, M. D.; Singh, L.; Jackson, A.; Oles, R. J. *Brain Res.* **1991**, 558, 145.

TRO95 Trojanowicz, M.; Krawczyk, T. K. V. *Mikrochim. Acta* **1995**, 121, 167.

TUR83 Turski, W. A.; Czuczwar, S. J.; Cavalheiro, E. A.; Turski, L.; Kleinrok, Z. *Naunyn-Schmiedebergs Arch. Pharmacol.* **1983**, 324, 25R

TUR83a Turski, W. A.; Czuczwar, S. J.; Kleinrok, Z.; Turski, L. *Experientia*, **1983**, 39, 1408.

TUR89 Turski, L.; Ikonomidou, C.; Turski, W. A.; Bortolotto, Z. A.; Cavalheiro, E. A. *Synapse*, **1989**, 154.

UNG85 Unger, K. K.; Giesche, H. *German Patent* DE-3534 143.1, **1985**.

UNG86 Unger, K. K.; Jilge, G.; Kinkel, J. N.; Hearn, M. T. W. *J. Chromatogr.* **1986**, 359, 61.

URB98 Urbanska, E. M.; Czuczwar, S. J.; Kleinrok, Z.; Turski, W. *Restor. Neurol. Neurosci.* **1998**, 13, 25.

VAD92 Vadgama, P.; Crum, P. W. *Analyst* **1992**, 117, 16557.

VAN96 Van den Bosch, S. E.; Heemstra, S.; Kraak, J. C.; Poppe, H.; *J. Chromatogr. A.* **1996**, *755*, 165.

VAN95 Vanstaden, J. F. *Fres. J. of Anal. Chem.* **1995**, 352, 271.

VAR93 Varady, L.; Ning, M; Yang, Y. B.; Cook, S. E.; Afeyan, N.; Regnier, F. E. *J. Chromatogr.* **1993**, 631, 107.

VIK97 Viklund, C.; Svec, F.; Frechet, J. M.; Irgum, K. *Biotechnol. Prog.* **1997**, 13, 597.

VIL90 Villanueva, S.; Fiedler, J.; Orrego, F. *Neuroscience*, **1990**, 7, 23.

VIZ91 Vizi, E. S.; Labos, E. *Prog. Neurobiol.* **1991**, 37, 145.

WAG86 Wages, S. A.; Church, W. H.; Justice, J. B. Jr. *Anal. Chem.* **1986**, 58, 1649.

WAL95 Walker, M. C.; Galley, P. T.; Errington, M. L.; Shorvon, S. D.; Jefferys, J. G. R. *J. Neurochem.* **1995**, 65, 725.

WES87 Westerink, B. H. C.; Tuntler, J.; Damsma, G.; Rollema, H.; de Vries, J. B. *Naunyn-Schmiedeberg's Arch. Pharmacol.* **1987**, 336, 502.

WIG76 Wightman, R. M. *Nature*, **1976**, 262, 145.

WIL96 Wilson, C. L.; Maidment, N. T.; Shomer, M. H.; Behnke, E. J.; Ackerson, L.; Fried, I.; Engel, J. Jr. *Epilepsy Res.* **1996**, 265, 245.

WRI97 Wright, P. B.; Lister, A. S.; Dorsey, J. G. *Anal. Chem.* **1997**, *69*, 3251.

XIE97 Xie, S.; Svec, F.; Frechet, J. M. J *J Chromatogr. A* **1997**, *775*, 65.

YAM92 Yamamoto, H.; Baumann, J.; Erni, F. *J Chromatogr.* **1992**, *593*, 313.

YAN Yan, C. Electrokinetic Packing of Capillary Columns U.S. Patent 5,453,163.

YAN96 Yan, C.; Dadoo, R.; Zare, R. N.; Rakestraw, D. T.; Anex, D. S. *Anal Chem.* **1996**, 68, 2726.

YAN95 Yan, C.; Dadoo, R.; Zhao, H.; Zare, R. N. *Anal. Chem.* **1995**, 67, 2026.

YEU92 Yeung, E. S.; Wang, L.; Li, W.; Giese, R. W. *J. Chromatographr* **1992**, 608, 73.

ZHA98 Zhang, Y.; Shi, W.; Zhang, L.; Zou, H. *J. Chromatogr. A* **1998**, 802, 59.

ZHO95 Zhou, M.; Peterson, C. L.; Lu, Y-B.; Nadler, J. V. *J. Neurochem.* **1995**, 64, 1556.

ZHO95a Zhou, S. Y.; Zuo, H.; Stobaugh, J. F.; Lunte, C. E.; Lunte, S. M. *Anal. Chem.* **1995**, 67, 594.

ZOL96 Zoli, M.; Agnati, L. F. *Prog. Neurobiol.* **1996**, 49, 363.

ZOL99 Zoli, M.; Jansson, A. Sykova, E.; Agnati, L. F.; Fuxe, K. *Trends Pharm. Sci.* **1999**, 20, 142.

ZOL98 Zoli, M.; Torri, C.; Ferrari, R.; Jansson, A.; Zini, I.; Fuxe, K.; Agnati, L. F. *Brain Res. Rev.* **1998**, 26, 136.

ZUI96 Zuiderwijk, M. A.; Veenstra, E.; da Silva, F. H. L.; Ghijsen, W. E. J. M. *Euro. J. Pharm.* **1996**, 307, 275.

BIOGRAPHICAL SKETCH

Steven Richard Witowski was born October 12, 1971, to Richard and Avis Witowski in Munster, Indiana. He has one older and two younger sisters, Carrie, Nicole, and Kelly. As a youngster he and his family moved to Greenville, South Carolina, where he lived until he began his undergraduate study at the Georgia Institute of Technology. His academic career started in the field of chemical engineering but he soon realized the error in his ways. At Georgia Tech, Steven was a cooperative education student, working at Eastman Chemical Company in Kingsport, TN, and performed research under Dr. Thomas Moran of the Chemistry Department. In June of 1995 he graduated with a B.S. in chemistry and a minor in Spanish. In August of that year he began graduate school at the University of Florida and performed research under the advisement of Dr. Robert T. Kennedy. His research became heavily involved in neuroscience as most of his work involved the *in vivo* measurement of neurotransmitters. In July of 2000 Steven R. Witowski gave up his scalpel and received his Doctor of Philosophy in analytical chemistry.

I certify that I have read this study and that in my opinion it conforms to acceptable standards of scholarly presentation and is fully adequate, in scope and quality, as a dissertation for the degree of Doctor of Philosophy.

Robert T. Kennedy, Chairman
Professor of Chemistry

I certify that I have read this study and that in my opinion it conforms to acceptable standards of scholarly presentation and is fully adequate, in scope and quality, as a dissertation for the degree of Doctor of Philosophy.

James D. Winefordner
Graduate Research Professor of Chemistry

I certify that I have read this study and that in my opinion it conforms to acceptable standards of scholarly presentation and is fully adequate, in scope and quality, as a dissertation for the degree of Doctor of Philosophy.

Richard A. Yost
Professor of Chemistry

I certify that I have read this study and that in my opinion it conforms to acceptable standards of scholarly presentation and is fully adequate, in scope and quality, as a dissertation for the degree of Doctor of Philosophy.

Jon D. Stewart
Associate Professor of Chemistry

I certify that I have read this study and that in my opinion it conforms to acceptable standards of scholarly presentation and is fully adequate, in scope and quality, as a dissertation for the degree of Doctor of Philosophy.

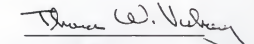

Thomas W. Vickroy
Professor of Veterinary Medicine

This dissertation was submitted to the Graduate Faculty of the Department of Chemistry in the College of Liberal Arts and Sciences and to the Graduate School and was accepted as partial fulfillment of the requirements for the degree of Doctor of Philosophy.

December, 2000

Dean, Graduate School

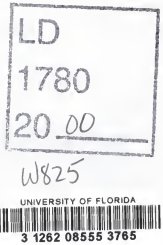
LD
1780
20 00
W825
UNIVERSITY OF FLORIDA
3 1262 08555 3765